Manufacturing By-Products as Partial Replacement in Metakaolin-Based Geopolymer Mortar Production

Ashraf Jihad Awad

Submitted to the
Institute of Graduate Studies and Research
in partial fulfillment of the requirements for the degree of

Doctor of Philosophy
in
Civil Engineering

Eastern Mediterranean University
September 2021
Gazimağusa, North Cyprus

Approval of the Institute of Graduate Studies and Research

Prof. Dr. Ali Hakan Ulusoy
Director

I certify that this thesis satisfies all the requirements as a thesis for the degree of Doctor of Philosophy in Civil Engineering.

Prof. Dr. Umut Türker
Chair, Department of Civil Engineering

We certify that we have read this thesis and that in our opinion it is fully adequate in scope and quality as a thesis for the degree of Doctor of Philosophy in Civil Engineering.

Assoc. Prof. Dr. Beste Çubukçuoğlu
Co-Supervisor

Assoc. Prof. Dr. Tülin Akçaoğlu
Supervisor

Examining Committee

1. Prof. Dr. Özgür Eren
2. Prof. Dr. Burak Felekoğlu
3. Prof. Dr. Nilüfer Özyurt Zihnioğlu
4. Assoc. Prof. Dr. Tülin Akçaoğlu
5. Assoc. Prof. Dr. Ayşe Pekrioğlu Balkis

ABSTRACT

Geopolymer technology is a new, sustainable approach for producing binding materials without using any cement content. Cement production has negative environmental effects in addition to the large amount of energy and nonrenewable resource consumption; therefore, the use of waste-materials is highly valued in geopolymer production. Using waste materials for production has the potential to reduce waste disposal costs and landfills effects on the environment. Within the same context, red mud (RM) is a waste material that is abundantly available in Turkey and around the world. Thus, it is critical to investigate the use of RM and other waste materials that can affect agriculture and groundwater in the construction industry. This study investigates the strength and durability properties of binary and ternary geopolymer mortar composites of metakaolin (MK) and three different waste by-products (RM, rice husk ash, and waste glass powder (GP)), which are abundantly available in Turkey. Further, this dissertation discusses the effects of high temperature on geopolymer mortar properties and the impact of adding two different sizes of glass fibers (GFs) by 0.3% volume to a geopolymer produced using MK and partially replaced by RM and GP. The GFs have been selected due to the cheap price and high flexibility and strength. Moreover, the dissertation explores the strength properties of the produced mortar in sea water and sulphate environments. Finally, the effect of the sand-to-binder (S/B) ratio on the strength and durability properties under different conditions and environments are investigated. The results indicate that the significant strength properties of the geopolymer mortar can be obtained by binary and ternary composites of MK, RM, and GP. The addition of GFs improves the strength properties of the produced mortar; the addition of 12 mm GFs improves the strength more than that

using the 6 mm GFs. However, S/B ratio affects the strength properties significantly, and the results indicated that an S/B ratio of 2.5 is better than that of 2.25. The produced geopolymer is applicable under severe conditions such as high temperature, magnesium sulphate, freezing–thawing, and sea water environment.

Keywords: geopolymer, geopolymer mortar, sustainability, waste materials, strength properties, by-products, glass fiber

ÖZ

Jeopolimer teknolojisi, çimento içermeyen bağlayıcı malzemeleri üretmek için yeni ve sürdürülebilir bir yaklaşımdır. Çimento üretiminde tüketilen yüksek miktarda enerji ve yenilenemeyen kaynak tüketiminin yanı sıra, çimento üretiminin çevresel etkileri nedeniyle, jeopolimer üretim yaklaşımında atık malzemelerin kullanılması oldukça değerlidir. Böyle bir yaklaşım, atık bertaraf maliyetlerini ve çöp depolama alanlarının çevre üzerindeki etkilerini azaltma potansiyeline sahiptir. Aynı bağlamda kırmızı çamur, Dünyada ve Türkiye'de çok miktarda bulunan bir atık maddedir. Bu nedenle, inşaat sektöründe tarımı ve yeraltı suyunu etkileyen kırmızı çamur ve diğer atık maddelerin kullanımının araştırılması kritik önem taşımaktadır.

Bu çalışma, Türkiye'de önemli miktarlarda bulunan metakaolin ve üç farklı atık yan ürünün (kırmızı çamur, pirinç kabuğu külü ve atık cam tozu) ikili ve üçlü jeopolimer harç kompozitlerinin mukavemet ve dayanıklılık özelliklerini araştırmaktadır.

Bu tez ayrıca, jeopolimer harç özellikleri üzerindeki yüksek sıcaklık etkilerini ve kısmen kırmızı çamur ve atık cam tozu ile değiştirilen metakaolin tarafından üretilen bir jeopolimere iki farklı boyutta cam elyafı eklemenin etkisini tartışır. Ayrıca, yapılan harcın deniz suyu ve sülfat ortamlarındaki dayanım özelliklerini araştırır. Son olarak, bu çalışmada kum/bağlayıcı oranının farklı koşullar ve ortamlarda dayanım ve dayanıklılık özellikleri üzerindeki etkileri araştırılmıştır.

Genel olarak sonuçlar, metakaolin, kırmızı çamur ve atık cam tozunun ikili ve üçlü kompozitleri ile jeopolimer harcın önemli mukavemet özelliklerinin elde edilebileceğini göstermiştir. Ayrıca cam elyaf ilavesi üretilen harcın mukavemet

özelliklerini iyileştirir; 12 mm uzunluk boyutu, gücü 6 mm'den fazla artırır. Ancak kum/bağlayıcı oranı dayanım özelliklerini önemli ölçüde etkiler ve sonuçlar 2.5 oranının 2.25'ten daha iyi olduğunu göstermiştir. Ayrıca, üretilen jeopolimer, yüksek sıcaklık, magnezyum sülfat, donma-çözülme ve deniz suyu gibi dayanıklılık koşullarında uygulanabilmektedir.

Anahtar Kelimeler: jeopolimer, jeopolimer harç, sürdürülebilirlik, atık malzemeler, mukavemet özellikleri, yan ürünler, cam elyaf

DEDICATION

I dedicate this thesis to my family in Palestine and Jordan (Duha, Yusuf, Kerem, my parents, and all my relatives).

ACKNOWLEDGMENT

I would like to express my gratitude to Assoc. Prof. Dr. Tülin Akçaoğlu and Assoc. Prof. Dr. Beste Çubukçuoğlu, my PhD supervisors, for all their assistance and guidance. I would also like to express my gratitude to my family, without whom none of this would have been possible.

TABLE OF CONTENTS

LIST OF TABLES

LIST OF FIGURES

Chapter 1

INTRODUCTION

1.1 Background

Ordinary Portland cement (OPC) is one of the most important building materials because of its low price, ease of use, and high mechanical properties. In general, cement demand rises with economic expansion. Thus, many developing economies aim to maintain rapid infrastructure growth as evidenced by the recent increase in cement production (Mishra and Siddiqui, 2014). The cement industry has helped enhance living conditions globally by directly creating millions of jobs and providing various sectors with interconnected economic benefits. Despite its many economic advantages, the cement industry has negative environmental consequences (Johannes, 2012). For example, cement manufacturing can result in negative health and safety consequences because of air and greenhouse gas emissions (Ian and David, 2002). When considering the generation of upstream electricity, the building industry alone has an energy consumption of 36% and a CO_2 emission of 39%, which affects climate change (Global Status Report, 2017).

Many experiments and analysis have been conducted to substitute cement completely or partially for overcoming the disadvantages of OPC production. Many materials are viable alternatives to OPC; however, these materials may not be available in all areas even though they have superior strength and durability. Another approach is using waste materials as a cement substitute material; this is a safe solution to avoid landfill

and other waste disposal options while lowering non-renewable resource usage. Further, using waste materials as cement substitutes is a very cost-effective strategy because of the low cost of these products. Further, replacing natural raw materials in concrete with industrial wastes could be a great approach for solving waste management issues. The use of industrial waste in concrete production is both technically and economically beneficial for many applications, including the manufacture of concrete and mortars. Also, geopolymer concrete which could be produced by these materials represent a sustainable approach.

Many manufacturing by-products like fly ash (FA), bottom ash and rice husk ash (RHA) are rich in aluminosilicates and activated by adding NaOH, Na_2SiO_3, KOH, or K_2O_3Si. Compared to PC manufacturing, the amount of produced greenhouse gas can be reduced by 44 up to 64 percent when industrial-waste ashes are repurposed for geopolymer production. Also, Metakaolin (MK) could be used effectively in geopolymer production (Mclellan et al., 2011).

Recycling and reusing waste have become challenges in the search for a more sustainable world. The most notable of the numerous wastes created by the industrial processes is RM, a residue formed when bauxite minerals are digested with caustic soda during alumina production. A total of 1.6 tons of RM is extracted for each ton of alumina production. Globally, more than 66 million tons of RM is created annually (Ayres et al., 2001; Hind et al., 1999).

In areas where this industry operates, such a large amount of RM poses a dangerous environmental hazard. In addition, the direct dumping of RM into the sea is extremely hazardous to the environment because radioactive metals in RM can scatter faraway.

RM is viewed as a mud that contains 10–30% solids with a pH of strongly alkaline. Several research studies have focused on RM applications in different sectors in the recent decades. Among these studies, those that focus on the use of RM in water and soil treatments are particularly important due to the demand for new materials in these applications (Cengeloglu et al., 2006; Kalkan et al., 2006).

In Turkey, waste glass (WG) remains a major problem. According to the Ministry of Environment and Urban Planning (2017), Turkey produced 878,262 tons of glass in 2014; however, only 17.60% was recycled. There are various types of WG that are generated on the global scale: electronic devices are one of the most significant sources of WG globally; for example, Italy alone has an annual volume of 15,000–16,000 tons of WG (Mugoni et al., 2015).

Turkey is a rice-producing country, and therefore, RHA is a local natural waste material that is obtained in rice production regions after the harvest. Unlike in other countries, these waste materials are only used in a small number of industrial sectors in Turkey. RHA is composed of noncrystalline silica (SiO_2) with a large specific surface area and high pozzolanic reactivity (Karim et al., 2012).

The availability of these by-products in Turkey is both an opportunity and an obstacle, and therefore, this study aimed to find a revolutionary solution using the optimum amounts of these waste materials to achieve the high strength and durability properties of the geopolymer mortar. In addition to MK, waste materials such as RM, GP, RHA, and granulated blast furnace slag (GBFS) have been used to create binary and ternary geopolymer mortar composites.

1.2 Aims and Objectives

This study aims to investigate the strength and durability properties of a MK-based geopolymer mortar when it is replaced partially by waste materials (waste glass powder (GP), red mud (RM), and RHA). The different waste materials are tested in binary and ternary binder composites. The objectives of this study are listed below:

1) To investigate the strength and durability properties of MK-based geopolymer mortar partially replaced by different waste materials (GP, RM, and RHA) and study the microstructural characterization of the produced mortars.

2) To study the effects of changing the river sand-to-binder (S/B) ratio (2.5 and 2.25) on the strength properties, durability, and microstructural characterization of the produced geopolymer mortar.

3) To evaluate the strength behavior of MK-based geopolymer mortar partially replaced by different waste materials (GP, RM, and RHA) under severe conditions such as in a sulphate environment, sea water environment, under high temperatures, freezing–thawing cycles, and to study the changes that occur in the microstructural characterization.

4) To study the effects of adding glass fibers (6 mm and 12 mm) to the MK-based geopolymer mortar partially replaced by different waste materials (GP, RM, and RHA) on its strength and durability properties, fire resistance at high temperatures (400, 600, and 800 °C) and the changes that occur in the microstructural characterization.

5) To compare the mechanical and durability properties of complete MK-based geopolymer mortar to the MK-based geopolymer mortar partially replaced by different waste materials (GP, RM, and RHA).

1.3 Research Outlines

The thesis is presented in six chapters.

Chapter 1 presents a general introduction to the geopolymer industry and explains the main objectives and structure of the thesis.

Chapter 2 provides a literature review of geopolymer concrete (GPC), general properties of the mortar, and use of waste materials in geopolymer technology. It presents the benefits of waste materials in geopolymer production and reviews the literature of the MK-based geopolymer.

Chapter 3 presents the theoretical background about geopolymers and its general concepts.

Chapter 4 includes the methodology, describes the experimental work plan conducted, and briefly introduces the used materials.

Chapter 5 presents the results of the tests performed in the different stages and discusses the obtained results.

Chapter 6 summarizes and concludes the thesis.

Chapter 2

LITERATURE REVIEW

2.1 Background

2.1.1 Introduction

Davidovits (1994) was initially identified GPC as a novel type of inorganic cementitious material that can be utilized as an effective substitute for OPC. Many researchers tried to develop GPC of high mechanical and durability properties. Also, the GPC production method has been studied widely in recent years due the rare of standards in this field.

Aluminosilicate and the activator are the most critical factors that affect the end product because of the reaction process for geopolymer production. Characteristics of the solid aluminosilicate variation affects the dissolution and reaction phases. In the reaction phase, the activator solution dissolves the solid raw material while controlling the breaking up and reconstruction of the aluminosilicate structure, polycondensation, and load balance (Weil et al., 2007; Duxson et al., 2005; Duxson et al., 2007).

This chapter presents the different types of geopolymers and discusses effects of the raw materials on their strength and durability properties.

2.1.2 Geopolymer Matrix Composites Reinforced with Natural Fibers

The addition of fibers to geopolymer composites decreases the development of microcracks and prevents brittle behavior by improving ductility (Korniejenko et al., 2016). Inorganic fibers such as carbon and glass fibers are among the commonly used fiber reinforcements in geopolymers. Natural fibers have gained popularity because of their sustainable nature, low density, and low cost of production (Korniejenko et al., 2016).

The incorporation of metallic fibers increases flexural strength because they control matrix contraction because of their high contact surface (Ranjbar et al., 2016). The size, type, elasticity, aspect ratio (length to diameter ratio, L/D), and volume fraction of the fiber are elements that determine the characteristics of the fiber; further, each fiber type is effective for a certain purpose (Ganesan et al., 2014). Vegetable fibers have several advantages over artificial fibers including lower cost, lower density, biodegradability, sustainable availability, and abundance (Korniejenko et al., 2016).

Alomayri and Low (2013) produced geopolymer samples that include short cotton fibers and reported that the flexural strength of the reinforced composites was considerably higher than that of the pure geopolymer, and concluded that the increased fiber content in cotton causes agglomerations and void spaces, which results in poor fiber dispersion. This results in reduced fiber–matrix interfacial adhesion, and it decreases the strength properties of the materials.

2.2 Use of Metakaolin in Geopolymers

2.2.1 Introduction

Kaolin refers to rocks composed of the mineral Kaolinite ($Al_2Si_2O_5(OH)_4$). Feldspar decomposition produces Kaolinite, which is a hydrous aluminum silicate mineral. China clay is another name for kaolin, Alternate layers of silicate sheets are weakly bonded with aluminum oxide/hydroxide sheets in kaolinite. The cleavage and softness of the mineral are attributed to the poor bonding. The mineral is generally white; however, impurities can give it red, blue, or brown tints. Kaolinite is a rock mineral that is abundantly available in nature (Mitchell and Soga, 2005).

In Turkey, there are a variety of kaolin deposits belonging to different morphological origins. The mineralogical and chemical properties of the raw materials vary owing to the variances in these deposits. Geological formation conditions, location, mineralogical and geochemical features, capability, quality, origin, and economic conditions of kaolin deposits are important considerations in the extraction of raw kaolin (Yank et al., 2010).

In metakaolin (MK), “meta” refers to the hydroxyl ion loss that occurs during the transformation of the kaolinite mineral; this process is called calcination or hydroxylation. The calcination of kaolinite for 4 h at temperatures between 700–800 °C (IS 1344-1981) followed by grinding to a minimum surface area of 20 m^2/g makes the clay extremely reactive (IS 1344-1981). Note that MK is high in alumina and silica, and it can be ground to a particle size of 2 μm, which gives it a specific area of 20 m^2/g (Cheng et al., 2012).

Further, MK is a de-hydroxylated phase of kaolinite, and it has alumina polyhedron layer structures that include 4-, 5-, and 6-coordinated (Al) ions (Duxson et al., 2007). The chemical composition, dosage, concentration, and conditions of curing for the raw materials influence the efficiency of the MK-based geopolymer (Kong et al.2008; Duxson et al., 2005; Roviello et al., 2015; Zhou et al., 2016; Rieger et al., 2015; Muniz et al., 2011).

2.2.2 Metakaolin and GBFS Geopolymer Concrete and Mortar

Huseien et al. (2018) found that the workability is improved when MK is replaced partially (0–15%) instead of GBFS in a GBFS-based geopolymer mortar; a SiO_2:Na_2O ratio of 1.16 achieves the highest early strength after 24 h; and the MK-GBFS geopolymer mortar has a better flexural and tensile strength compared to that of standard OPC mortar. The compressive strength (f_c) of the MK-GBFS geopolymer mortar (62.5, 62.8, and 63.1 MPa) was higher than that of the GBFS geopolymer mortar after 28 d (44.8 MPa). Kumar and Ramesh (2017) found that increasing the GBFS content in MK-GBFS GPC increases the compressive strength. The combination 100GBFS has the highest compressive strength for various proportions of MK and GBFS.

Khater et al. (2016) reported that geopolymer specimens produced from blended MK-GBFS can compete mechanically and physically with fired clay and refractory brick up to 100% slag, whereas using 40% slag results in geopolymer bricks with superior characteristics and compressive strength values exceeding 83 MPa after 28 d.

Basha and Bharath (2018) discovered that the strength of the MK-GBFS based GPC rises with increasing GBFS until 50%; then, this value decreases. Thus, it is

recommended to use the GBFS of optimum 50% in the GPC mixes. The strength of the GPC rises by 2% to 4% in the period of 3–7 d and by 2% to 5% in the period of 7–28 d. MK can perform well because it has a compressive strength of 45 MPa for 3 d; however, GBFS cannot be used because its compressive strength is lower than that of 100MK sample. The results revealed that replacing 60% MK with 40% GBFS resulted in a higher compressive strength. Kumar et al. (2016) found that 25% MK and 75% GBFS produced better results than other ratios; a standard geopolymer acquired a compressive strength of 84.4% and split tensile strength of 86.5% for 7 d. Further, Kumar et al. discovered that although ambient curing was favorable, heat curing and accelerated curing also produced comparable results.

According to Malleswara and Hamantha (2017), the strength of a GPC increases up to 50% of the GBFS content before decreasing. NaOH is an alkaline activator; a higher molarity results in a stronger compressive strength compared to that at lower molarity. Further, the compressive strength appears to be higher in the blend of 50% GBFS and 50% MK than in the other blends. Kchaitanya et al. (2017) found that the maximum f_c of MK-GBFS based GPC can be obtained by 60% MK and 40% GBFS; the compressive strength is 50 MPa (7 d) and 53 MPa (28 d), and f_s is found to be 8.1 and 11.45 MPa after 3 and 7 days, respectively.

Kumar et al. (2017) discovered that GPC workability decreased as the MK content increased relative to GBFS; however, an increase in slag content did not have any effect on workability. With a decrease in MK, mechanical properties such as f_c, f_s, and f_f indicated a growing tendency. The mixture of 30% MK and 70% GBFS appears to have strong f_c and f_f values. Within the first 7 d, nearly 90% of the total geopolymer

strength was reached. Then, compared to 3 and 7 d, the rise in geopolymer strength between 7 and 28 d appeared important, because it implies that a geopolymer reaction occurs after 7 d, albeit at a slower rate.

Sireesha and Madhavi (2018) discovered that at a 50% MK and 50% GBFS ratio of MK-GBFS based GPC achieves the highest compressive strength properties. The f_c increases from 45.0 to 49.56 MPa, while the GBFS content increases up to 50%; the f_s varies from 3.4–4.56 MPa. From 5 to 30 d, the GPC strength rises by 5–7%, which implies there is no significant improvement in strength after 5 d.

According to Kumar et al. (2018), the maximum compressive strengths (37.4 MPa after 7 d and 49.2 MPa after 28 d) of the different combinations of MK-GBFS GPCs were obtained by 20% MK and 80% GBFS; the maximum split tensile strengths (3.11 MPa after 7 days and 3.91 MPa after 28 days) were also obtained with the same combination.

Padmakar and Kumar (2017) found that the f_c, f_f, and f_s of GPC increased with the MK content rising up to 100% MK and 0% GBFS, and it decreased with an increase in GBFS regardless of curing time. Soleimani et al. (2013) found that using 80% phosphorus slag instead of MK resulted in a lesser f_c after curing for 7 d. For curing periods of 14 and 21 days, replacing the slag with MK (10–100%) increased the f_c of the geopolymer samples. Samples cured for 28 d that contain 40 wt.% slag instead of MK achieved an improvement in the value of f_c. When a sufficient amount of slag was applied, it achieved a destructive effect (40–90% of the total weight).

2.3 Use of Red Mud in Geopolymers

2.3.1 Introduction

In the alumina production process, RM is produced by refining bauxite, and it is classified as a waste material. The bauxite refining process produces approximately 35–40% RM waste per ton of bauxite treated. This waste has a detrimental effect on the environment because of storage problems (Kalkan, 2006).

According to Avraanmides et al. (2010), RM includes Si, Al, Fe, Ca, Ti, and Na. Further, RM comprises different composites, and its composition is determined using Bayer's method.

Rai et al. (2012) concluded that the high alkalinity of RM limits the application of this material. Recently, many studies have been focused on utilizing RM in different industrial sectors. The use of RM in the construction sector could be beneficial in from the viewpoint of the mechanical properties and sustainability aspects. Mortaş and Doankuzu bauxite deposits in Turkey have 26.3 million tonnes of high-alumina (55–67% Al_2O_3) bauxite reserve (Öztürk et al., 2002; Horkel, 2010). The only aluminum smelter in the country is supplied by these two bauxite pits in Turkey (Horkel, 2010).

Bauxite obtained from the two mines is combined to provide the Seydişehir plant with the required aluminum composition. Bauxite production yields ~800,000 tons annually, which produces 1.5 million tons of RM. Approximately 10 million tonnes of bauxite are stored in the tailing ponds; the waste material from both bauxite pits is deposited in the tailing ponds as RM (BGS, 2015).

2.3.2 Effect of Red Mud on Geopolymer Strength Properties

Hairi et al. (2015) demonstrated that RM forms geopolymers in a manner similar to MK. Iron (as hematite) in the RM has no effect on geopolymer development. Singh et al. (2017) reported that the mortar f_c and f_f values gradually improve with increasing RM content in the binder until it reaches a maximum strength of 30% RM, when RM is mixed with processed FA and GBFS. With an increase in the RM content from 30% to 50%, the strength drops dramatically.

According to Seabra et al. (2017), the overall compressive strength obtained for RM-FA ash based geopolymers containing 20% RM is significantly higher than that for the ultimate RM-MK based geopolymers. Thus, the use of RM-FA mixture instead of industrial MK for aluminosilicate activation in GPC production is a viable option. Zhang et al. (2010) discovered that higher RM content leads to lower compressive strengths because of the lower reactive silica and alumina content and the tensile behavior afforded by the fine RM particle. Yeddula and Somasundaram (2020) found that the f_c of RM-ferrosialate based geopolymer mortar samples with different percentages of RM increased with an increase in the RM content; it reached an optimal value (30%) and then started to decline. He et al. (2012) investigated geopolymers produced from MK in addition to RM and FA; MK-based geopolymer had a 31 MPa f_c whereas the RM-based geopolymer had 13 MPa f_c. The final products inherited nonreactive crystalline phases from raw materials and had a limited amount of unreacted source materials.

Kumar and Kumar (2013) examined combining RM and FA to create GPC, and they found that adding up to 20% RM to FA increased the reaction and characteristics of

the GPC. He and Zhang (2011) discovered that the f_c of the RM-FA geopolymer mortar varies between 3–13 MPa based on the curing conditions.

Mucsi et al. (2019) found that RM could replace the alkali activator and FA by 10–15% weight. Further, RM addition resulted in a 2.5-fold rise in the compressive strength. The RM and activator ratio affect phase composition changes because zeolite formation is inhibited, which increase f_c.

Lemougna et al. (2017) conducted experiments on the properties of RM-slag geopolymer mortar using a Na2SiO3 solution (modulus range: 1.6–2.2) as an activator, with RM substitutions ranging from 25% to 75%. Only when a sufficient volume of RM was used, the fc was unaffected by the RM presence (up to 25%); a maximum fc of 54 MPa was revealed at 25 °C curing by the 50RM50GBFS sample.

Elson et al. (2016) determined that the strength characteristics of the RM-GBFS geopolymer (f_f and f_s) were superior to those of a standard cement mix. Kulkarni et al. (2018) found that a ternary composite geopolymer concrete composed of RM, FA, and GBFS had a split tensile strength 84.26% higher than that of traditional concrete (3.89 MPa). Geopolymer concrete has a flexural strength of 81.21% compared to that of traditional concrete (4.5 MPa).

He et al. (2014) used RM, RHA, NaOH, and water as raw materials for geopolymer blends. The experiments used an RM/RHA weight ratio of 0.4. They discovered that geopolymer mortar has an optimum f_c of 20.5 MPa, and therefore, it is comparable to OPC.

Ye et al. (2014) found that when silica fume (SF) was added, the properties of a one-part geopolymer mortar produced using Bayer RM as the primary raw material were examined; the long-term strength of the binder was substantially increased by the addition of the 20–30 wt. % SF. The increased strength was attributed to the lower water/solid ratio. The f_c was 31.5 MPa after curing for 28 d.

2.4 Rice Husk Ash

RHA is a value-added commodity because it is extracted from grown crops and can be used as a green mineral additive. Despite its benefits and potential as a cement substitute material, cement and concrete manufacturers in developing countries are concerned about the transportation and production issues of RHA (Baskar et al., 2014).

RHA a by-product of rice production, wherein the thin outer husk is stripped from 20% to 25% of the rice and is normally burned. When these husks are burned, about 18% of them turn to ash. Therefore, 1 ton of rice yields about 45 kg of RHA, which is high in silica (95%) and has significant pozzolanic properties (Gonc et al., 2007). The presence of crystalline SiO_2 in RHA is particularly concerning because crystalline SiO_2 is a serious pollutant. Since rice is the most widely consumed food, a considerable amount of ash is generated each year. China, India, Indonesia, and Bangladesh are top four producers of RHA, and their global rice production potential is over 20 Mt, if RHA represents 3.5% of the total rice weight according to the Rice Federation of the United States of America.

According to Baskar et al. (2014), rice production is a highly localized operation; rice is grown in only two areas in the United States. Such localization increases transportation costs, which affects the economic or environmental viability of the commodity. Although rice is more commonly available in Asia, where the majority of

the world's rice is cultivated, transportation remains a problem. Modern combustion furnaces may not be available in some places, especially in rural areas; thus, only low-quality RHA is generated by simple open-field burning.

2.5 Use of GBFS as Supplementary Cementitious Material

2.5.1 Introduction

Granulated blast furnaced slag (GBFS) has been used to produce cement or cementitious materials in two ways: as a raw material in the manufacturing process and in combination with OPC. GBFS has been used in the manufacture of concrete in several applications (Chi et al., 2012). The addition of a supplementary cementitious material such as GBFS to concrete increases its strength, workability, permeability, durability, and corrosion resistance; further, the f_c of the geopolymer mortar increases as the optimum GBFS component is increased to 70% (Islam et al., 2014; Samson et al., 2017; Zhao et al., 2015, Akcaoglu., 2019).

GBFS can be added as a pozzolanic material in concrete; however, it can be added only after the unground GBFS is processed by crushing or heat treatment. However, these treatments to process unground GBFS incur significant expenses. Many researchers revealed that using GBFS instead of fine natural aggregates improves the consistency of the concrete and allows for the creation of sustainable building materials (Patra and Mukharjee, 2017).

2.5.2 Using GBFS in a Binary and Ternary Cementitious System

Malagavelli et al. (2010) used GBFS and robo sand to produce high-performance concrete. They found that 50% OPC, 25% GBFS, and 25% robo sand increased concrete compressive strength by 11.06 and 17.6% at 7 and 28 d in comparison to 100% OPC.

Luo et al. (2013) investigated the chloride diffusion coefficient and chloride binding capability of OPC with 70% GBFS replacement with or without 5% sulphate in an experimental environment. In blended cement samples, they discovered that the chloride diffusion coefficient decreased and the chloride ion binding potential increased. Oner and Akyuz (2007) found that replacing the OPC with the optimum 55–59% GBFS could achieve the maximum strength.

2.6 Use of Alkaline Activators in Geopolymers

Mixtures of NaOH or KOH and Na_4SiO_4 and K_2O_3Si are the most popular alkaline activators (Davidovits, 1994). The strength characteristics of the GPC increases when the molarity of the solution is increased. Furthermore, based on the observations of the geopolymerization of 16 natural Al-Si minerals, it can be concluded that the NaOH solution caused more mineral dissolution than the KOH solution (Motorwala et al., 2013).

2.7 Microstructure Characterizations of Geopolymer Mortar

Geopolymers are described as amorphous material because the major feature of X-ray diffraction (XRD) patterns is a “featureless hump” at 27–29° (2θ) (Alonso et al., 2002; Barbosa et al., 2000; Palomo, 2001). The XRD diffractograms of several essentially amorphous products including certain silicate gels (Brinker, 1990) and aluminosilicate-zeolite gel precursors before crystallization are nearly equivalent to those of

geopolymers (Yang et al., 2000). These XRD diffractograms are identical because of the characteristic bond distances of inorganic oxide frameworks, and not because of the geopolymers themselves. Many researchers observed the formation of semi-crystalline or polycrystalline phases in some cases, wherein the alkaline activating solution contained little or no soluble silicon (Davidovits, 1991; Rowles, 2003; Palomo, 1992; Jaarsveld et al., 1999; Barrer, 1972; Casci and Cundy, 1982; Baerlocher et al., 2001).

Chapter 3

THEORETICAL BACKGROUND

3.1 Introduction

The production of OPC clinker includes the $CaCO_3$ calcination based on the reaction:

$$5CaCO_3 + 2SiO_2 \rightarrow (3CaO, SiO_2)\ (2CaO, SiO_2) + 5CO_2$$

According to Davidovits (1994), the manufacture of 1 ton of OPC clinker produces 0.55 tons of CO_2 and involves the combustion of 0.40 tons of carbon fuel, which produce more 0.40 tons of CO_2. Thus, 1 ton of OPC production equals 0.95 tons of CO_2. According to Alnahhal et al. (2017), about 2.8 billion tons of OPC products are produced annually, which instigate 5–7% of CO_2 emissions (Schneider et al., 2011; Benhelal et al., 2013). Limestone hills are being harvested widely for cement manufacturing all around the world, and this has resulted in an ecological imbalance (Vermuelen and Tony, 1999).

The CO_2 emissions caused by OPC production represent a challenge that cannot be overcome. Geopolymer does not use calcium carbonate and creates substantially less CO_2 during the manufacturing process, which ranges from 40%–90% (Mclellan et al., 2011).

Davidovits (1993) defined a geopolymer as a new material that can be used in transportation infrastructure, building, and offshore applications as an alternative to OPC. Geopolymer uses minimally processed natural resources or industrial by-

products to cut carbon emissions while avoiding several of the durability related problems that affect OPC. Further, the cure time of the geopolymer cement is faster than that of the OPC. They gained most of their strength within 24 h. However, the geopolymer sets sufficiently slowly to be combined and delivered in a concrete mixer at a batch facility. All types of rock-based aggregates can form a tight chemical bond with geopolymer cement.

3.2 Geopolymer Chemistry

Geopolymers are Al-Si materials with an amorphous three-dimensional microstructure. An alkaline (Na+, K+, Li+, Ca+, etc.) or acidic (phosphoric or humic acid) medium is employed in geopolymer production. The geopolymerization process occurs when Si and Al oxides or aluminosilicates combine with an activator solution to generate a Si-O-Al bond in an alkaline medium. Poly (sialate) type (-Si-O-Al-O-), Poly (sialate-siloxo) type (-Si-O-Al-O-Si-O-), and Poly (sialate-disiloxo) type (-Si-O-Al-O-Si—Si-O-) are the three types of structures (Davidovits, 1991). Here, silicon-oxo-aluminate is represented by the abbreviation sialate. A sialate network composed of SiO_4 and AlO_4 becomes tetrahedrally interrelated by sharing an oxygen atom. (+) ions are required in the framework cavities to equalize the (-) charge of Al ion in the IV-fold coordination (Davidovits, 1991).

3.3 Effect of Curing Temperature on Geopolymer Strength Properties

The f_c of the MK-based geopolymer decreases because of the high temperature used during curing. The effect of high curing temperature can be discussed from two different viewpoints:

1) The f_c of the material diminishes as it transforms from the amorphous to the crystalline phase as the temperature rises above 60 °C. Since the crystalline phase has

considerable porosity and voids, the increase in temperature lowers the compressive strength. The rate of crystalline phase generation is affected by the curing temperature, which transforms the geopolymer gel from the amorphous to the crystalline phase rapidly, and therefore, there is no trace of the crystalline process when curing the MK geopolymer concrete at room temperature (Tosheva and Valtchev, 2005).

2) Increasing the curing temperature of MK GPC causes the mixture to lose water, which increases the voids in the structure of the GPC and decreases its compressive strength (Rovnank, 2010). The geopolymerization process accelerates with an increase in the curing temperature. Thus, although the early compressive strength increases, the later compressive strength decreases. The compressive strength is low despite the presence of only the amorphous phase because the geopolymerization process is slow at low temperatures (10 °C).

3.4 Geopolymer Microstructure

Many researchers have attempted to identify the microstructural characterization of geopolymers and concluded it can be detected using a variety of methods such as scanning electron microscopy (SEM), XRD, and thermogravimetric analysis (TGA) (Belmokhtar at al., 2017; Du et al., 2016; Tho-In et al., 2018; Tian at al., 2017; Tuyan et al., 2018).

Several methods were used to investigate the internal structural properties of the MK-based geopolymer. The current study characterizes the manufactured mortar using SEM, XRD, and TGA techniques to explain the phase composition and structure of MK-based geopolymeric materials when MK is partially replaced by by-product materials.

SEM is used to examine the microstructural characteristics of geopolymers subjected to high temperatures and those that were not. Hoa et al. (2002) investigated the microstructure of an aluminosilicate inorganic polymer in detail using SEM. They discovered that the geopolymer has a nonporous microstructure. The attributed this structure to the extensive aluminosilicate species dissolution prior to polycondensation, which resulted in the convergence of the shapes of the specimen into a chaotic, three-dimensional network of poly sodium aluminosilicate. In addition, the solubility of the starting materials in the matrix can be explained by a geopolymer SEM analysis (Hoa et al., 2002).

TGA allows measuring the variation in weight while raising the temperature to determine thermal stability; the results are expressed on weight loss curves or the derivative of the weight loss versus temperature; the results provide information on the composition of the sample. In TGA, the powdered specimens were used to ensure that the thermal equilibrium was achieved during transient heating. The thermal behaviors of some selected geopolymer composites (different S/B ratios) and various starting materials (MK, RM, and GP) as a function of temperature under atmospheric conditions are presented using TGA.

The phase composition and crystalline content of the geopolymers were investigated using XRD. The existence of the amorphous structure of the geopolymer is shown by XRD patterns. The solubility of the starting materials can be explained using the geopolymer XRD patterns. The amorphous composition of the geopolymer reveals a high solubility of the starting materials of the matrix, and therefore, it indicates the precursors that are better in terms of solubility.

3.5 Effect of High-Temperatures on Geopolymers

TGA and other methods can be used to assess the thermal stability of the materials. Different forms of geopolymers have strong thermal stabilities at high temperatures. At 600 °C, the MK geopolymer loses about 13% of its weight. In contrast, when the OPC paste is heated to 600 °C, it loses more than 25% of its weight (Alarcon-Ruiz et al., 2005; Chen et al., 2012; Caicedo et al., 2015; Ranjbar et al., 2016; Zhao et al., 2015).

Water evaporation and dihydroxylation are critical factors that affect the weight loss of the GPC at high temperatures. Physical, chemical water, and hydroxyl are present in the cured geopolymer products; the physical and chemical water evaporate at 20–100 °C and 100–300 °C, respectively, whereas hydroxyl groups evaporate at temperatures above 300 °C. The nepheline phase is generated when the GPC are heated to 1000 °C, and this phase is one of the main causes of weight loss at high temperatures (Duxson et al., 2007; Rashad et al., 2016; Rahier et al., 2007; Baco et al., 2015; El-Maghraby et al., 2013; Colangelo et al., 2017).

Changes in the mechanical properties of the geopolymers are attributed to changes in their internal microstructure. Several researchers have used SEM to observe and understand the shape and evolution of the microstructure under thermal stress. Compared to OPC, the geopolymer microstructure remains stable when the heating temperature rises. The GPC structure becomes denser even after a 400 °C exposure. These findings indicate that geopolymers perform better than OPC in terms of heat resistance (Morsy et al., 2019; Duan et al., 2016). The addition of boiler slag (BS) to the geopolymer improves its thermal stability. When heated to 1250 °C, the

geopolymer composite of 30% BS and 70% MK loses 9.43% of its weight at 1250 °C (Caicedo et al., 2015).

3.6 Effects of (Solid /Liquid) Weight Ratio on Geopolymer Strength

Many studies have investigated the effects of activator solution to binder ratio by weight; for the MK geopolymer production, the ratio ranged between 0.6–0.8 to achieve the highest f_c (Brahim et al., 2017). If the amount of the activator solution content is greater than that of the raw material at low solid to liquid (S/L) ratios, the product becomes fluid and limits the interaction between the alkaline solution and starting materials (Leong et al., 2017). Further, an S/L ratio of 0.8 achieves the maximum compressive strength for MK geopolymer (Leong et al., 2017; Jaya et al., 2018).

Chapter 4

MATERIALS AND METHODS

4.1 Introduction

The materials and methods used in this study to investigate the mechanical properties of the produced geopolymer mortar are presented in this section; the details of each stage of the work are provided including the case of the GF addition and the issue of changing river sand to binder (S/B) ratio. Experimental tests to measure the strength properties of the produced mortar were conducted according to American standards, ASTM.

4.2 Experimental Investigation

4.2.1 Properties of Materials Used

The RM used in this study was provided by the Eti Seydişehir (Konya-Turkey) Aluminium Plant. The Kaolin Industrial Mine Company in Izmit supplied the MK used in this work; the MK had a specific gravity (SG) of 2.52 g/cm^3, and this class of MK is considered an effective primary material. The “Mey Kimya” company in Istanbul provided the GP used in this work; its particle size was 30 microns. The “Erdoganlar” company in Ankara provided the RHA used. The Bolu Cement Company provided the GBFS; it had a SG of 2.88 g/cm^3. In this study, the river sand is Izmit's river sand, which had a nominal grain size of 4.5 mm, a SG of 2.64 g/cm^3 and a fineness of 2.36 mm. Table 1 summarizes the chemical compositions of the used materials.

The activators solution involved a blend of Na_2SiO_3 (SiO_2 = 27%, Na_2O = 8.2%, and H_2O = 64.8%, specific gravity= 1.32 g/cm^3) solution and NaOH flakes. The activator solutions were sourced from the AS Kimya company in Istanbul; the chemical properties and compositions of the activator solutions are provided by the manufacturing company and listed in Tables 2 and 3. Also, images in Figures 1 and 2 show the used materials.

Table 1: Chemical compositions of the used materials*

Compound (% wt.)	RM	MK	GP	RHA	GBFS
SiO_2	12.6	51.52	69.42	92.33	40.55
Al_2O_3	14.8	44.53	1.09	0.18	12.83
Fe_2O_3	39.61	0.48	0.48	0.17	1.1
CaO	9.23	0.02	8.27	0.02	35.58
K_2O	0.85	0.51	0	0	0.68
Na_2O	8.8	0.24	12.31	0.29	0.79
MgO	1.75	0.16	4.25	0	5.87
TiO_2	8.13	0.55	0	0	0.75

*Chemical compositions are provided by the manufacturing companies

Table 2: Chemical properties of NaOH (%)

NaOH	Na_2CO_3	Cl	SO_4	Al	Fe
99.1	0.3	≤ 0.01	≤ 0.01	≤ 0.002	≤ 0.002

Table 3: Chemical properties of Na2SiO3

Na_2O (%)	SiO_2 (%)	Density (20 °C) (g/ml)	Fe (%)	Heavy metals (as PB) (%)
8.2	27	1.36	≤ 0.005	≤ 0.005

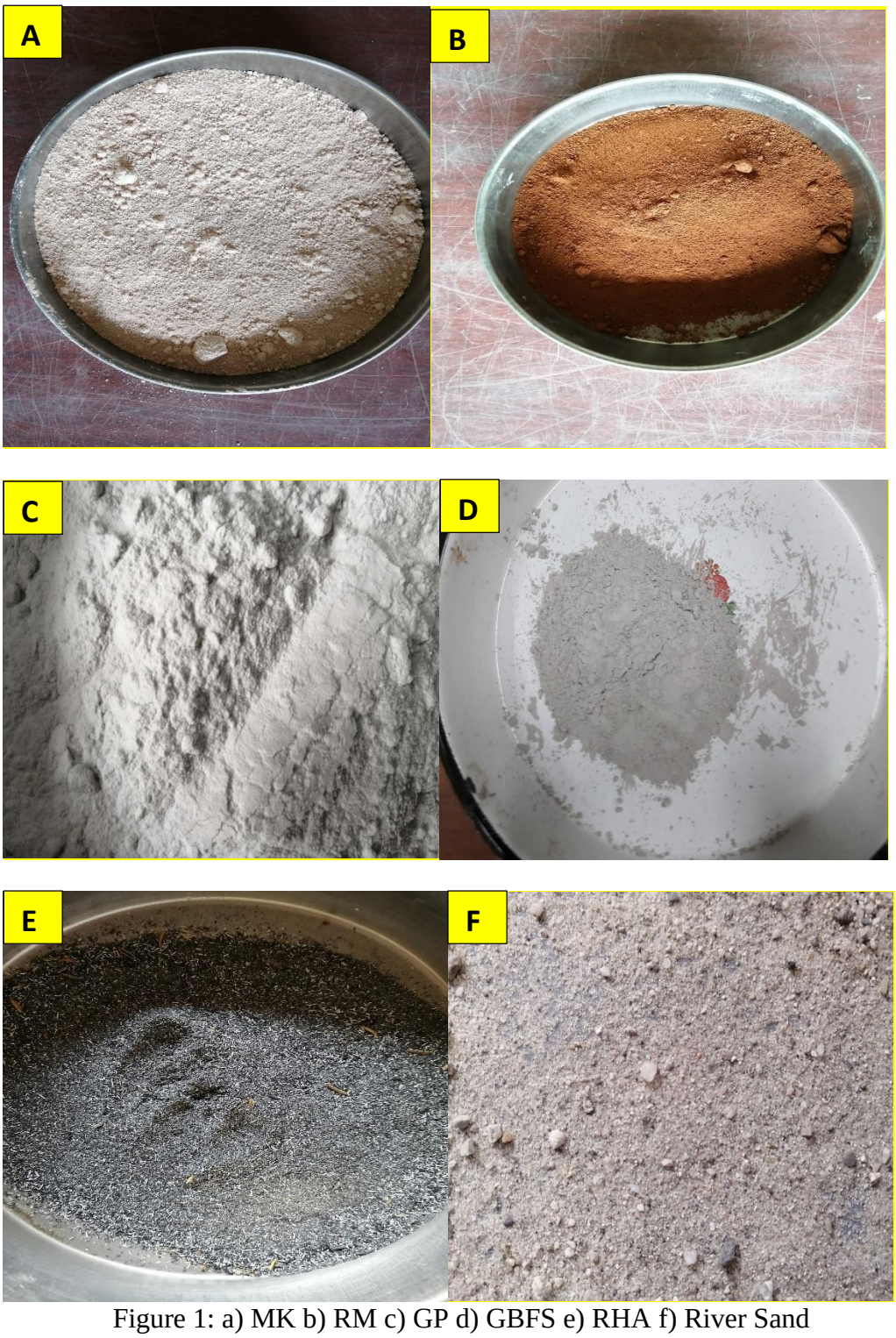

Figure 1: a) MK b) RM c) GP d) GBFS e) RHA f) River Sand

Figure 2: a) NaOH b) Na_2SiO_3 c) GF

4.2.2 Experimental Setup

4.2.2.1 Experimental Work Stages

The experimental methodology of this study comprises three stages:

Stage 1: The optimal content of the waste materials in various binary and ternary combinations is determined using the strength parameters. According to the results of stage 1, tests are conducted for 3, 7, and 28 d to study the strength, microstructural characterization, and durability properties.

Stage 2: The effects of adding glass fiber to two different proportions are studied: f_c, f_f and f_s; abrasion resistance; and high temperatures resistance are evaluated.

Stage 3: Combinations that achieve acceptable results at stage 1 are examined in different conditions (sea water, freezing–thawing cycles, sulphate environment, and high temperatures conditions) under two different S/B ratios. The details of each stage are documented below.

4.2.2.1.1 First Stage

In the first stage, 22 trials mixes are produced to decide the combinations that need to be explored. The selection parameters are f_c and f_f at 3, 7, and 28 d; the binder/solution ratio is fixed to 1 and the S/B ratio is set as 2.5, for all trial mixes.

The optimum percentage of each material was 50%, while the molarity of NaOH was kept constant at 12 M. Although 10 and 14 M were investigated for the trial mixes.

4.2.2.1.2 Second Stage

After the trial mixes stage, the effect of adding GF in two different proportions (6 mm and 12 mm) on f_c, f_f, and f_s; abrasion resistance; and high-temperature resistance will be investigated. In addition, the results of the SEM, XRD, and TG-DTA analysis conducted for the different ages and conditions are listed in Table 4.

Table 4: Experimental work plan outline for Stage 2

Test	Period
Compressive strength	3, 7, and 28 d
Flexural strength	3, 7, and 28 d
Split Tensile strength	28 d
Abrasion resistance	28 d
High temperatures	28 d at 400, 600, and 800 °C
SEM	Different ages and conditions
XRD	Different ages and conditions
DTA/ TGA	28 d

4.2.2.1.3 Third Stage

After investigating the effects of adding the glass fiber to the geopolymer mortar in stage 2, combinations that achieve acceptable results in stage 1 are investigated under different conditions: sea water, sulphate environment, high temperatures (400, 600, and 800 °C), and freeze–thaw cycles. Further, the effects of the S/B ratio are investigated as the combinations are tested for two different S/B ratios of 2.5 and 2.25. The SEM, XRD, and TG-DTA analyses also have been conducted as presented in Table 5.

Table 5: Experimental work plan outline of Stage 3

Test	Period
Compressive strength	3, 7, and 28 d
Flexural strength	3, 7 and 28 d
Sulphate resistance	7, 28, and 56 d
Sea water resistance	7, 28, and 56 d
High temperatures	28 d at 400, 600, and 800 °C
Freezing–Thawing	50 and 100 cycles
SEM	Different ages and conditions

4.2.2.2 Test Setup and Procedure

Previous studies (Uysal et al., 2018; Al-Majidi et al., 2016) were referred to determine the procedures to be followed for geopolymer mortar preparation when conducting the related experimental work because a standard or a specification for the preparation of

geopolymer composites is unavailable due to difference of sources of materials and preparation procedures.

Binder raw materials were first mixed for minutes, and then, the activator solution ($NaOH+Na_2SiO_3$) was poured into the mixture. Then, river sand was added to complete the mixing procedure. Mixing was completed after 8 min, and then, 50 mm cubes and 40 × 40 × 160 mm prisms were cast for f_c and f_f tests, respectively. After the casting process, samples were dried for 25 ± 2 °C for 24 h, heated in an oven at 80 °C for 48 h and finally cured at room temperature until the test dates. During curing, the samples were placed in thermal plastic pockets to avoid evaporation and reduce carbonation and calcite ($CaCO_3$) formation.

The flow table test has been conducted according to the standard ASTM C1437, two layers of each mix was poured in the mould and the tamping rod was used for compacting the placed layers for 20 time for each layer. The mould is then lifted and the table should be dropped 25 times to let the mix flow, the flow is measured as the average of mix spreading diameters minus the original diameter of the mould, the steps of the test are shown in Figure 3.

Figure 3: Steps of flow table test

Physical properties, namely unit weight, water absorption and voids ratio were investigated in this study, the major objective behind conducting the tests of these properties was to evaluate the effect of using various binding materials, in this scope of these tests, the sample were firstly put in an oven for two days, and then the tests were conducted in the Archimedes pool which is linked to the sensitive weigh, the values of the a forementioned properties were calculated depending on the equations shown below:

Unit weight (gm/cm^3) = X / (X-Z)

Voids ratio (%) = [(Y-X) / (Y-Z)] × 100

Water absorption = [(Y-X) / X] × 100

Here,

X: oven dry weight (g)

Y: saturated surface dry weight (g)

Z: weight of soaked sample in water (g)

The compressive strength (f_c) test was conducted to perform the test procedure following ASTM C 109 after 3, 7, and 28 d of curing using 50 mm side cubes as shown in Figure 4. According to the aforementioned standard, the compressive strength was calculated based on the formula P/A, where P represented the maximum compressive load obtained by the specimen and A as the surface area subjected to the load P.

Figure 4: Compressive strength test

Further, the flexural strength (f_f) test was also conducted after 3, 7, and 28 d of curing using the prismatic samples (40×40×160 mm) based on the f_f procedure mentioned in ASTM C 348, and according to the formula (F= 0.0028 P) as shown in Figure 5, where P is the maximum flexural load of the specimen in KN and F is the flexural strength in MPa. A testing machine maximum loading capacity of 35 ton and ± 1% mm

displacement and ± 0.2% mm accuracy in accordance with the standard specification ASTM E4 10002-2 was used to determine the designated compressive and flexural strength tests. After conducting the tests, each compressive and flexural strength value presented in the results and discussion chapter is the average value of three measurements.

Figure 5: Flexural strength test

The abrasion test was used to test wear resistance of produced geopolymer composites. The purpose of abrasion testing was to generate data that will rank geopolymer mortars in their resistance to abrasion under certain conditions. Abrasion testing was an important durability issue in mortar and concrete. In order for the produced geopolymer mortars to be used as repair mortars, their abrasion resistance must be determined. The ability of a substance to overcome surface wear induced by flat rubbing contact with another material is called abrasion resistance. The samples were cut into 7.06 cm cubes and heated for 24 h at 110 °C. Given that the initial weight and thickness were measured. Specimens were then placed on the test track of a 750 mm diameter rotating

disc on which a 20 g of standard abrasive (artificial corundum) is poured. Prior to testing, the density of the specimens was determined by measurements, to the nearest 0.1 mm, and by weighing, to the nearest 0.1 g. the weight loss and wear depth were investigated after a determined number of cycles (4 periods, where each period is 22 cycles) using the Bohme apparatus in compliance with TS 2824 EN 1338 as shown in Figure 6.

Figure 6: Abrasion resistance test

The test specimens were subjected to temperatures of 400, 600, and 800 °C by an increasing rate of 5 C°/min and kept for 1 h on the maximum temperature to determine the effects of high temperatures on the f_c, f_f, and weight loss of the specimens that contain different GF sizes. These temperatures were selected to investigate the evaporation effects until 400 °C, the effect of reaching the melting point of the GF at 800 °C, and the behaviour of mortar between these two stages at 600 °C. The same temperatures (400, 600, and 800 °C) were used to investigate the heat resistance of the

geopolymer mortar samples with the same increasing rate (5 C°/min) and then immediately allowed to cool down after reaching the maximum temperature to examine the thermal behaviour of the sample when the S/B ratio is different. The heat resistance test was applied on the cubic and prismatic specimens after curing for 28 d; the geopolymer mortar specimens were placed in an electric furnace. Figure 7 shows the samples at around 800°C and after heating test.

Figure 7: Elevated temperature test (800 °C)

The splitting tensile strength (f_s) test was conducted by recording the maximum applied load on the cylinder specimens (height = 200 mm, diameter = 100 mm) and tested using a machine according to ASTM C496 as shown in Figure 8. To avoid the sudden shock, a constant increasing rate of 1.5 KN/ min was applied, the split tensile strength is calculated after reaching the maximum load, according to the equation of: $F_s = 2P/\pi LD$

Where:

Fs= Split tensile strength in MPa

P= maximum load KN

L= sample length mm

D= sample diameter mm

Figure 8: Split tensile strength test

According to ASTM C666 / C666M-15, the influence of freezing–thawing (F–T) cycles on the strength characteristics and weight change was evaluated as shown Figure 9. The F–T resistance was tested using 50 mm cubes and 40×40×160 mm prisms after

28 d of room temperature curing. The mortar specimens were frozen in a deep freezer at −20 °C for 4 h and then thawed in water at ambient temperature for 4 h. The F–T test cycle was repeated for 50 and 100 times and then compressive and flexural strength tests were conducted in addition to the weight change.

Figure 9: Freezing-thawing resistance test

After complete curing, the samples were immersed in sea water as shown in Figure 10, the test was done in correspondence to ASTM D1141-98 standard with the composition summarized in Table 6 for 7, 28, and 56 d. The f_c and f_f of all geopolymer samples after immersion were investigated for S/B ratios of 2.5 and 2.25.

Table 6: Artificial Sea water composition (ASTM D1141-98)

Sodium chloride	NaCl	24.53 g/l
Magnesium chloride	$MgCl_2$	5.2 g/l
Sodium sulphate	Na_2SO_4	4.09 g/l
Calcium chloride	$CaCl_2$	1.16 g/l
Potassium chloride	KCL	0.695 g/l
Sodium bicarbonate	$NaHCO_3$	0.201 g/l
Potassium bromide	KBr	0.101 g/l
Boric acid	H_3BO_3	0.027 g/l
Strontium chloride	$SrCl_2$	0.0025 g/l
Sodium fluoride	NaF	0.003 g/l
Water	H_2O	988.969 g/l
Total		1025 g/l

Figure 10: Geopolymer Samples Immersed in Sea Water

The sulphate resistance test was investigated, and this test method accelerates the sulphate attack mechanism using a solution with a sulphate concentration of 5% wherein mortar specimens are immersed as shown in Figure 11. The geopolymer samples were immersed in a magnesium sulphate ($MgSO_4$) solution for 7, 28, and 56 d. The compressive and flexural strength of all geopolymer samples after immersion were investigated for S/B ratios of 2.5 and 2.25.

Figure 11: Geopolymer samples immersed in sulphate solution

Images related to the microstructural analyses of geopolymer specimens were obtained using the SEM machine at Marmara University, Turkey. According to ASTM C1723-16, all SEM images were captured up to a magnification of 5000 times. For the SEM analyses; 4-mm-thick geopolymer specimens, which were obtained from the centre of each specimen with a diamond saw, were prepared. The specimens were immersed into an alcoholic solvent for 24 h to obtain clearer images. Then, the specimens were placed into an oven to dry. The platinum plate was performed over gold plating for the specimens when high magnification imaging was required. Further, differential thermal analysis (DTA)/ TGA (DTA/TGA) was conducted on some of the produced geopolymer samples according to ASTM E794-06 (2018); XRD was conducted according to ASTM C1365-18.

4.3 Testing Methods and Specimens

Table 7 lists the tests that were conducted with a brief explanation of the experimental conditions and samples sizes and dimensions.

Table 7: List of tests and sizes of specimens

Number	Test name	Description	Sample dimensions (mm)	Standards
1	Compressive strength	At 3, 7, and 28 d	50 × 50 × 50	ASTM C 109
2	Flexural strength	At 7 and 28 d	40 × 40 × 160	ASTM C 348
3	Split tensile strength	At 28 d	200 (height), 100 (diameter) Cylinders	ASTM C496
4	Abrasion resistance	At 28 d	70.6 × 70.6 × 70.6	TS 2824 EN 1338
5	heat resistance	At 400, 600, and 800 °C	50 × 50 × 50 and 40 × 40 × 160	
6	Sea water resistance	At 7, 28, and 56 d	50 × 50 × 50 and 40 × 40 × 160	ASTM D1141-90
7	Sulphate resistance	At 7, 28, and 56 d	50 × 50 × 50 and 40 × 40 × 160	
8	XRD analysis	X-ray diffraction analysis	Small samples	ASTM C1365-18
9	DTA/ TGA	Differential thermal analysis / thermogravimetric analysis	Powder	ASTM E794-06 (2018)
10	SEM analysis	Scanning electron microscope	4-mm-thick specimens	ASTM C1723-16
11	Freezing and thawing resistance	50 and 100 cycles	50 × 50 × 50 and 40 × 40 × 160	ASTM C666 / C666M-15

4.4 Mix Proportions

The general mixing proportions of the composites are listed in Table 8. In this experimental work, the binder comprises MK, RM, RHA, and GP.

Table 8: Mixing proportions of manufactured geopolymer composites (grams)

Binder	River sand	Slag	Activator solution	
			NaOH (12M)	Na_2SiO_3
450	1125	60	150	300

Alkaline chemicals used as activators were created by combining the sodium silicate and sodium hydroxide solution. The activator from the Na_2SiO_3 solution (SiO_2 = 27%, Na_2O = 8.2%, and H_2O = 64.8% by weight), and NaOH flakes with 99% purity was dissolved in distilled water to prepare the NaOH solution. The concentration of the NaOH solution used was 12 M, which was achieved by dissolving 40 g of NaOH for each Mole (480 g to produce 1 l of 12 M NaOH solution); the proportion of NaOH to Na_2SiO_3 activators was 1:2. The Na_2SiO_3 solution is considerably cheaper than the NaOH solution. Therefore, to reduce the cost, this ratio is commonly fixed around 2. The molarity significantly affects the strength properties of the geopolymer mortar. The molarity of the NaOH solution was determined based on experimental trials and errors. 10, 12, and 14 M of NaOH were tested, and it was found that the best f_c development was observed at 12 M, as shown in Figure 12. Hence, the molarity was fixed to 12M for the rest of the experimental work.

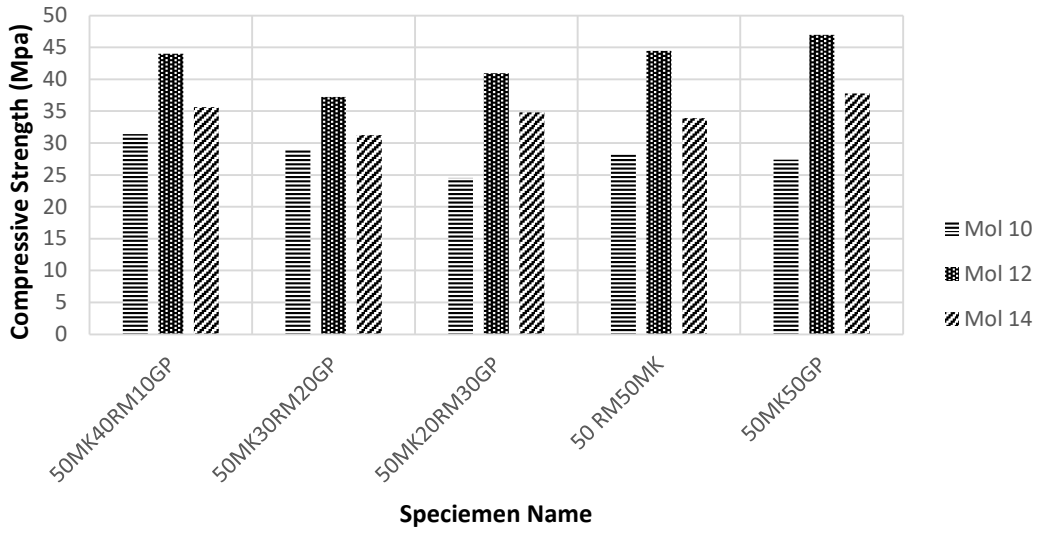

Figure 12: Effect of molarity on compressive strength

A fixed quantity (60 g) of GBFS, which is rich in SiO_2 and Al_2O_3 (53.38%), was added to all mixes, and the activator solution and river sand content were kept constant to investigate the effect of the binders. A total of 69% of the entire mixture by weight was river sand, and the proportion of the S/B ratio was 2.5, which was kept constant for all mix combinations (Stages 1 and 2).

In this study, the ratio of the activator solution to the binder was fixed as 1 by weight before the addition of GBFS; after adding GBFS, the ratio was 0.88. Note that GBFS was added as an additive to increase the Al_2O_3 and SiO_2 content in the mix and to prolong the geopolymerization reaction period.

4.4.1 Stage 1: Trial Mixes Stage (Binary and Ternary Composites)

In this stage, the activator solution to binder ratio was 1 by weight, the river S/B ratio was 2.5 for all mixes, and the sodium silicate to sodium hydroxide ratio was 2 for all mixes.

The strength properties of the geopolymer mortar specimens containing three by-products (RM, GP, and RHA) in addition to MK are investigated in binary (Mixes 1–6) and ternary (Mixes 7–22) combinations based on the following assumptions:

- RM must be included in all ternary binders (minimum 10%) because of the abundant availability of RM as a waste material in Turkey.
- The maximum content of each material is 50% of either binary or ternary binders to investigate the synthesis effects of the materials together.
- The maximum solution activator to binder ratio is 1 to be practical. If a higher ratio is included, it will be expensive and impractical; therefore, the combination would be neglected. For instance, mixes containing RHA need more solution to be workable otherwise they cannot be cast.
- The river S/B ratio is fixed at 2.5 for all mixes.
- NaOH used with sodium silicate to form the activator solution is prepared at a fixed molarity of 12M for all combinations; the effects of 10M and 14M on the best 5 combinations are investigated.
- The sodium silicate to sodium hydroxide ratio is 2 for all mixes.
- The heating temperature (for all specimens, heat curing is conducted for 2 d for all specimens before room temperature curing) in the oven during the first 48 h is 80 °C.
- The river sand used for all mixes was sieved using a number 4 sieve (size = 4.75 mm).

The first six mixes only included two combinations of materials used at a 50–50% ratio. Furthermore, the rest of the specimens (Mixes 7–22) included various combinations of materials at several proportions.

Table 9 presents the mix proportions of the binary blended specimens and Table 10 presents the mix proportions of specimens comprising three different materials.

Table 9: Mix proportions of binary blended specimens (grams)

Specimen	RM	GP	RHA	MK	GBFS	River sand	Activator solution
50RM50GP	225	225	0	0	60	1125	450
50RM50RHA	225	0	225	0	60	1125	450–900
50RM50MK	225	0	0	225	60	1125	450
50MK50GP	0	225	0	225	60	1125	450
50MK50RHA	0	0	225	225	60	1125	450–900
50GP50RHA	0	225	225	0	60	1125	450–900

Table 10: Mix proportions of ternary blended composites (grams)

Specimen	RM	GP	RHA	GBFS	River sand	Activator solution
50RM40GP10RHA	225	180	45	60	1125	450
50RM30GP20RHA	225	135	90	60	1125	450
50RM20GP30RHA	225	90	135	60	1125	450
50RM10GP40RHA	225	45	180	60	1125	450
50MK40RM10RHA	225	180	45	60	1125	450
50MK30RM20RHA	225	135	90	60	1125	450
50MK20RM30RHA	225	90	135	60	1125	450
50MK10RM40RHA	225	45	180	60	1125	450
50MK40RM10GP	225	180	45	60	1125	450
50MK30RM20GP	225	135	90	60	1125	450
50MK20RM30GP	225	90	135	60	1125	450
50MK10RM40GP	225	45	180	60	1125	450
50GP40MK10RM	225	180	45	60	1125	450
50GP30MK20RM	225	135	90	60	1125	450
50GP20MK30RM	225	90	135	60	1125	450
50GP10MK40RM	225	45	180	60	1125	450

4.4.2 Stage 2: Effect of Glass Fiber Addition

In this stage, the strength and durability properties of the geopolymer mortar specimens that contains MK partially replaced by two by-products (RM and GP) that obtained the highest strength properties in stage 1 are investigated (Specimens 1–5). The same

combinations contain 6-mm- (specimens 6–10) and 12-mm-long (specimens 11–15) GFs as listed in Table 11.

Table 11: Mix proportions of all samples

Mix #	Combination	MK	GP	RM	Slag	River sand	Activator solution	Glass fiber	Glass fiber length (mm)
1	100MK (0 mm GF)	450	0	0	60	1125	450	0	0
2	50MK50GP (0 mm GF)	225	225	0	60	1125	450	0	0
3	50MK20RM30GP (0 mm GF)	225	135	90	60	1125	450	0	0
4	50MK40RM10GP (0 mm GF)	225	45	180	60	1125	450	0	0
5	50MK50RM (0 mm GF)	225	0	225	60	1125	450	0	0
6	100MK (6 mm GF)	450	0	0	60	1125	450	0.3% Vol	6
7	50MK50GP (6 mm GF)	225	225	0	60	1125	450	0.3% Vol	6
8	50MK20RM30GP (6 mm GF)	225	135	90	60	1125	450	0.3% Vol	6
9	50MK40RM10GP (6 mm GF)	225	45	180	60	1125	450	0.3% Vol	6
10	50MK50RM (6 mm GF)	225	0	225	60	1125	450	0.3% Vol	6
11	100MK (12 mm GF)	450	0	0	60	1125	450	0.3% Vol	12
12	50MK50GP (12 mm GF)	225	225	0	60	1125	450	0.3% Vol	12
13	50MK20RM30GP (12 mm GF)	225	135	90	60	1125	450	0.3% Vol	12
14	50MK40RM10GP (12 mm GF)	225	45	180	60	1125	450	0.3% Vol	12
15	50MK50RM (12 mm GF)	225	0	225	60	1125	450	0.3% Vol	12

4.4.3 Stage 3: Effect of Changing the River Sand to Binder Ratio

In this stage, the same materials in previous two stages are used; the activator solution to binder ratio is 1 by weight; the river S/B ratios are 2.5 and 2.25 for the same 5 combinations (highest strength properties in stage 1) for all mixes; and the sodium

silicate to sodium hydroxide ratio is 2 for all mixes. The mixing proportions of composites are summarized in Table 12.

Table 12: Mixing proportions of manufactured geopolymer composites (grams)

Binder	River sand	GBFS	Activator solution	
			NaOH (12M)	Na_2SiO_3
450	1125/ 1012.5	60	150	300

The effect of the S/B ratio on the strength properties of geopolymer mortar are investigated in this part of the study; two different ratios are used for (2.5 and 2.25) for each combination, and the mix proportions of all samples are summarized in Table 13.

Table 13: Mix proportions of geopolymer with different S/B ratios

Mix Number	Combination (S/B ratio)	MK	GP	RM	Slag	River sand	Activator solution	S/B
1	100MK (2.5)	450	0	0	60	1125	450	2.5
2	50MK50GP (2.5)	225	225	0	60	1125	450	2.5
3	50MK20RM30GP (2.5)	225	135	90	60	1125	450	2.5
4	50MK40RM10GP (2.5)	225	45	180	60	1125	450	2.5
5	50MK50RM (2.5)	225	0	225	60	1125	450	2.5
6	100MK (2.25)	450	0	0	60	1012.5	450	2.25
7	50MK50GP (2.25)	225	225	0	60	1012.5	450	2.25
8	50MK20RM30GP (2.25)	225	135	90	60	1012.5	450	2.25
9	50MK40RM10GP (2.25)	225	45	180	60	1012.5	450	2.25
10	50MK50RM (2.25)	225	0	225	60	1012.5	450	2.25

Chapter 5

RESULTS AND DISCUSSIONS

5.1 Introduction

The experimental work was conducted in Stages 1, 2, and 3, as presented in Chapter 3. In this chapter, the results and discussions were presented according to the stages detailed in Chapter 3.

5.2 Stage 1: Trial Mixes Stage (Binary and Ternary Composites)

5.2.1 Physical Properties

In order to examine the physical properties of the geopolymer mortar samples, the unit weight, porosity and water absorption properties were investigated, while the flow table test was carried out for the consistency. The results obtained are shown in Table 14. When the effect of GP on the workability of the mixtures was examined, it was observed that there was a systematic decrease in the flowability as the glass powder content in the mixture increased compared to the metakaolin. While this situation was seen as a greater decrease in the series with RM, the maximum decrease was observed in the series with RHA. The high specific surface area of RHA was effective on this situation. The dense structure of the RM has enabled the unit weight value to be higher. This resulted in lower porosity and water absorption rates. While the unit weight value decreased with the addition of RHA, the water absorption and void ratio values increased more. This was due to the slowing of geopolymerization with the addition of RHA. The results obtained were compatible with other studies (Khatib et al., 2012; Aygörmez, 2021; Sharmin et al., 2017). It could be noticed a differences in the weights

of the samples in Table 14 compared to the expected weights obtained from the mix proportions and physical properties of the materials, these variations are due to the effects of mixing of large batches, also due to the variations of the materials density itself and the effects of geopolymerization reactions which produced new components.

Table 14: Physical properties of geopolymer samples

No	Specimen name	Flow (mm)	Unit weight (g/cm^3)	Porosity (%)	Water absorption (%)
1	100MK	189	2.38	23.2	8.56
2	50RM50GP	158	2.48	21.1	7.23
3	50RM50RHA	132	2.33	25.6	10.21
4	50RM50MK	165	2.45	21.7	7.52
5	50MK50GP	181	2.41	22.8	7.95
6	50MK50RHA	133	2.29	27.1	10.78
7	50GP50RHA	127	2.30	26.6	10.55
8	50RM40GP10RHA	152	2.45	21.4	7.42
9	50RM30GP20RHA	148	2.43	22.3	8.51
10	50RM20GP30RHA	143	2.42	23.6	9.38
11	50RM10GP40RHA	137	2.37	24.7	10.12
12	50MK40RM10RHA	160	2.42	22.9	7.98
13	50MK30RM20RHA	154	2.38	24.2	8.51
14	50MK20RM30RHA	147	2.34	25.5	9.06
15	50MK10RM40RHA	139	2.31	26.3	9.89
16	50MK40RM10GP	168	2.44	21.9	7.63
17	50MK30RM20GP	171	2.44	22.1	7.69
18	50MK20RM30GP	174	2.42	22.5	7.78
19	50MK10RM40GP	178	2.41	22.7	7.87
20	50GP40MK10RM	178	2.43	22.6	7.79
21	50GP30MK20RM	172	2.44	22.2	7.62
22	50GP20MK30RM	167	2.46	21.8	7.44
23	50GP10MK40RM	163	2.47	21.4	7.31

5.2.2 Compressive Strength Tests Results

In Figure 13, the compressive strength results of trial mixes are showed according to the binary and ternary combinations of these three materials (RM, MK, and GP). The compressive strengths were investigated and Figure 2 showed that amongst the first six specimens, specimens 50RM50MK and 50MK50GP had the maximum compressive strength at 3, 7, and 28 days (62.39, 46.6, and 44.45 MPa) and (42.57, 54.55, and 46.98

MPa), respectively. These results indicated that further investigation should be conducted on the binary and ternary combinations of these three materials (RM, MK, and GP). According to the results, the RHA content up to an optimum percentage of 30% enhanced the compressive strength of the mixes. After this percentage, the results began to decrease. Nevertheless, when RHA was used as binder material, it needed a higher amount of the activator solution to be workable compared to the optimum value, which was 1 for the activator solution: binder ratio. Therefore, RHA was neglected in the later stages, because the trial mix stage was conducted to investigate the compositions which achieved reasonable strength properties and could be produced by a ratio of activator solution to binder equal or less than 1. Because the amount of chemical solutions increased the cost of production.

Along with this situation, the situation of RHA with other binders was also investigated. For the specimens of the MK+RM+RHA composites, Figure 13 indicated that increasing the RHA content affected the strength properties negatively. Further, the maximum compressive strength for specimen 50MK40RM10RHA was achieved at 7 days; it decreased at 28 days, which was attributed to the slow chemical reactions between these different materials. For the specimens of the MK+RM+GP composites, the results shown in Figure 13 presented reasonable strength properties for all specimens comprising ternary binders

(MK, RM, and GP) compared to those of other specimens. The maximum compressive strength (44.01 MPa) was obtained at 28 days for specimen 50MK40RM10GP that contained only 10% of GP. For specimens of GP+MK+RM composites, Figures 13 showed that the maximum compressive strength of the ternary binder combinations comprised the GP, MK, and RM obtained by specimen 50GP40MK10RM; it was

decreased with increasing RM content and decreasing MK content. In addition, the results showed that the compressive strength decreased with time for all four combinations.

5.2.3 Flexural Strength Tests Results

The flexural strength test results of the 22 trial mixes were examined in this section. Figure 14 shows that, in the first six specimens (binary composites), the specimens 50RM50MK and 50MK50GP achieved the maximum flexural strength with 6.63, 6.82 and 9.21 MPa and 10.87, 10.62, and 9.19 MPa at 3, 7, and 28 days, respectively. These results indicated that further investigations should be undertaken on the binary and ternary combinations of these three materials (RM, MK, and GP).

For the specimens of the RM+GP+RHA composites, the maximum flexural strength was obtained with an optimum percentage of 20% RHA, and it decreased for higher percentages (30% and 40%). These results indicated that, in addition to the high cost of chemical solutions, the ternary combinations of these materials didn't attain acceptable strength properties. For the specimens of the MK+RM+RHA composites, increasing RHA content affected the strength properties negatively in addition to the previously mentioned drawback regarding the use of a higher amount of activator solution to be workable. Further, it has been shown that the flexural strength for specimen 50MK40RM10RHA reached the maximum value at 28 days. For the specimens of the MK+RM+GP composites, all flexural strength results for the four combinations were found acceptable, as shown in Figure 14. The maximum flexural strength of 11.98 MPa was obtained at 28 days for specimen 50MK30RM20GP, which contained only 20% GP.

For the specimens of the GP+MK+RM composites, the results in Figure 14 indicated that the maximum flexural strength of the ternary binders' combinations comprising GP, MK, and RM was obtained from specimen 50GP40MK10RM, and it decreased with increasing RM content and decreasing MK content.

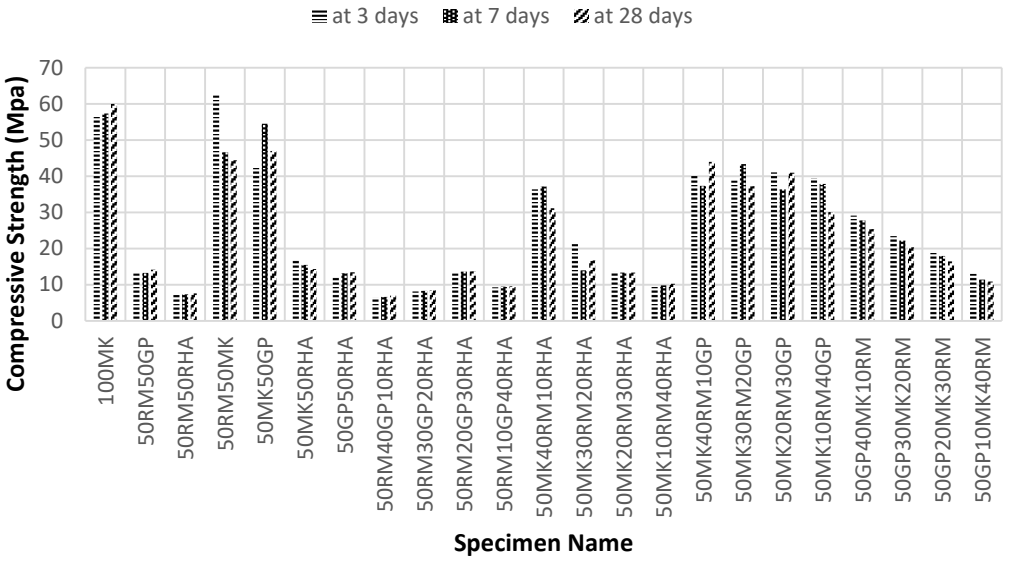

Figure 13: Compressive strengths of blended composites

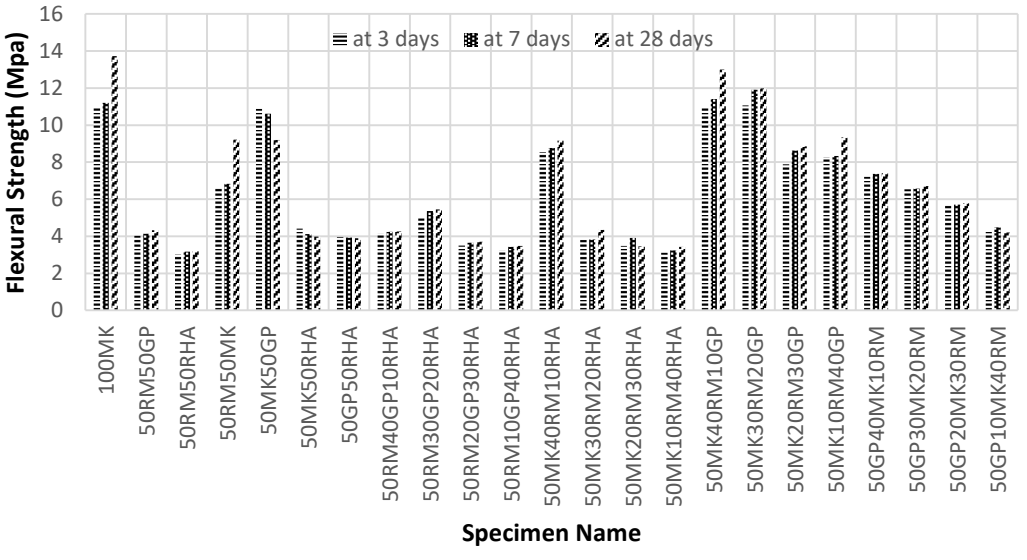

Figure 14: Flexural strengths of blended composites

5.2.4 Discussions

The compressive strength results of specimens incorporated with RM, MK, RHA, and GP in different percentages were plotted in Figure 13. All results were compared with the specimen 100MK, which was the control specimen. It can be stated that the incorporation of MK at different percentages in the mix combinations considerably influenced the compressive strength development. MK behaved in a considerably promising manner compared to other materials in strength development. This was attributed to the high reactivity of MK. Metakaolin was a traditional material formed because of dehydroxylation of kaolin mineral in the temperature range of 700 – 1000 ^{o}C (Kaya and Soyer-Uzun, 2016). The thermal process that kaolin was exposed to from 700^{o}C results in loss and dehydroxylation of internal water and conversion of crystalline kaolin into amorphous metakaolin (Özer and Soyer-Uzun, 2015). When kaolinite underwent thermal dehydroxylation, it dissolved in alkaline environment and this dissolution made metakaolin an ideal raw material for geopolymerization (Kaya and Soyer-Uzun, 2016). For this reason, among the reasons for using metakaolin material in the production of geopolymer materials, it can be counted that this material had a homogeneous structure and was an industrial mineral that can be obtained in large quantities (Rovnanik, 2010). However, due to the cost of calcining, its substitution with different binders should also be investigated (Uysal et al., 2018).

When binaries (two-parts combinations) were examined, the RM created an effective chemical combination with MK but not with GP and RHA. The percentage reduction in the compressive strength values of specimens 50RM50MK, 50RM50GP, and 50RM50RHA relative to 100MK were 26%, 76%, and 87%, respectively. MK was good both with GP and RM but not with RHA. Here, the percentage reduction in the compressive strength values of specimens 50MK50GP, 50MK50RM, and

50MK50RHA relative to control were 22%, 26%, and 76%, respectively. The compatibility of MK with GP was slightly better than that of RM. When RHA combined with MK (specimen 50MK50RHA) was compared with RHA combined with RM (specimen 50RM50RHA), MK performed better because the compressive strength for specimen 50RM50RHA was 87% less than that of 100MK; for specimen 50MK50RHA, it was only 76%. The GP created an effective combination with MK; however, it was not good with RM and RHA. The compressive strength for specimen 50GP50MK was only 22% less than that of 100MK, whereas those of specimens 50GP50RM and 50GP50RHA were 76% and 78% less than that of the control (specimen 100MK), respectively.

For ternary combinations, it was more complicated to make a comment on the compressive strength (f_c) results. The RM, GP, and RHA (50%RM and 50% (GP+RHA)) combinations were examined. The RM created an effective chemical combination only with MK (26% decrease in f_c), but not with GP (76% decrease in f_c), and RHA (87% decrease in f_c). Here, f_c was controlled by GP and increased by decreasing the amount of GP (from 40 to 10) until it reached the maximum value at 20% GP (50RM20GP30RHA). Then, it was further decreased for 10% GP.

When RM was kept constant at 50% and the ratios of GP and RHA were varied, the results indicated that an increment was observed in the compressive strength development when GP reduced to 20% and RHA increased to 30%; however, at 40% RHA addition with GP decreased to 10%, a significant reduction of strength development was observed. The MK, RM, and RHA (50%MK and 50% (RM+RHA)) combinations were examined next. MK was compatible with RM but not with RHA; therefore, with increased RHA (from 10–40) and decreased RM (from 40–10), the

value of f_c was reduced. Here, it was important to note that there was a sharp decrease (nearly half) in f_c when the RHA content increased from 10% to 20%. Then, the decrement in f_c continued linearly for 20, 30, and 40% RHA contents.

Several ternary mix designs were proposed when RM and RHA materials were incorporated into the 50% MK. When the MK was kept constant at 50% and the RM reduced from 40% to 10% in parallel to the increment in the RHA ratio from 10% to 40%, a linear change was observed by means of strength development. There was a linear reduction in the compressive strength parallel to the increase in the curing age from 3 d to 28 d. This showed that any ratios lower than 40% for RM would detrimentally influence the strength development even though there was an increase in the RHA content from 10% to 40%. Therefore, as proved in the first stage of the trials with the binary mix designs, MK and RM performed well in terms of compressive strength not only individually, but also when they got together at reasonable ratios (50:50) was the optimum level where they reached the maximum values). Additional 10% RHA incorporation can cause an approximately 50% reduction in the strength development. The MK, RM, and GP (50%MK and 50%(RM+GP)) combinations were examined. MK was compatible both with RM and GP. Therefore, the fc results of all combinations (RM from 40% to 10% and GP from 10% to 40%) were similar and close to those of specimens 50MK50RM and 50MK50GP. GP, MK, and RM (50%GP and 50%(MK+RM)) combinations were examined. GP was compatible with MK, but not with RM. Therefore, the fc results of GP, MK, and RM combinations decreased linearly; with the decreased MK (from 40% to 10%) and increased RM (from 10% to 40%), the fc result of specimen 50GP40MK10RM (the best one in this group) was found to be 58% less than that of control (100MK). The worst percentage decrement for the 50GP10MK40RM

specimen was 82%. The highest fc for 28 d of curing was for specimens 50MK50GP (22% less than 100MK), 50MK50RM (26% less than 100MK), and 50MK40RM10GP (27% less than 100MK). Therefore, using MK and GP and RM in geopolymer concrete production was appropriate.In conclusion, when the obtained substitution results were examined in general, it was seen that the positive effect of GP on the strength results was greater. Then came the effect of RM, while at the lowest rate came the effect of RHA. However, since the difference between the substitution results was very small, there were differences in the rankings in the other tests. It was thought to have the potential to be used as a binding material in geopolymer production due to the high amorphous SiO2 in the GP. Having a high SiO2 content and having a mostly amorphous structure, it played an important role in geopolymerization and also contributed to the formation of hydration due to its CaO content. Thus, a higher proportion of C-A-S-H, C-S-H, and N-A-S-H gel formation was observed, while the products formed the driving force in geopolymerization. With this situation, a denser and more homogeneous product was formed (Siddika et al., 2021). But similar results were obtained with studies in which it was found that an increased percentage of the GP ratio relative to the metakaolin reduced the compressive strength due to a decrease in the adhesive force on the surface of the glass particle (Rajabipour et al., 2010; Topcu and Canbaz, 2004). Except for the 3-day result of the 50RM50MK sample, there was a decrease in all samples compared to the control sample. This was mostly attributed to the early strength development potential of RM. In RM series where metakaolin was used as a constant by 50%, it has been observed that the strength values had generally decreased compared to GP. Nevertheless, red mud had a significant binding potential. Further, RM had a very fine-particle structure, which was promising for geopolymer mortar.

Although the contribution of red mud to amorphous silica was low, it has shown the potential to increase the alkalinity of the geopolymer mixture. With this situation, while the dissolution of silica accelerated, polymerization also became faster. An important contribution of alkalinity to the geopolymerization process has also been identified (Khale and Chaudhary, 2007; Zhang et al., 2010; He and Zhang, 2011). It allowed the encapsulation of red mud, radioactive waste, heavy metals and toxic chemicals in the geopolymer network.

Due to this encapsulation, they became part of the polymer chain and hematite. This fast rate of geopolymerization is resulted in a homogeneous and well distributed gel. The elemental mapping of 50MK50RM sample shown in Figure 15 reveals the fact that the elements that form the produced matrix have been distributed evenly. Such an even distribution results in a fact that the resulting gel possesses a reasonable degree of compactness. The compact matrix in turn explains the good strength results obtained, these findings comply to the findings of the previous studies and theories (Davidovits, 2008; Almashhadani et al., 2018).

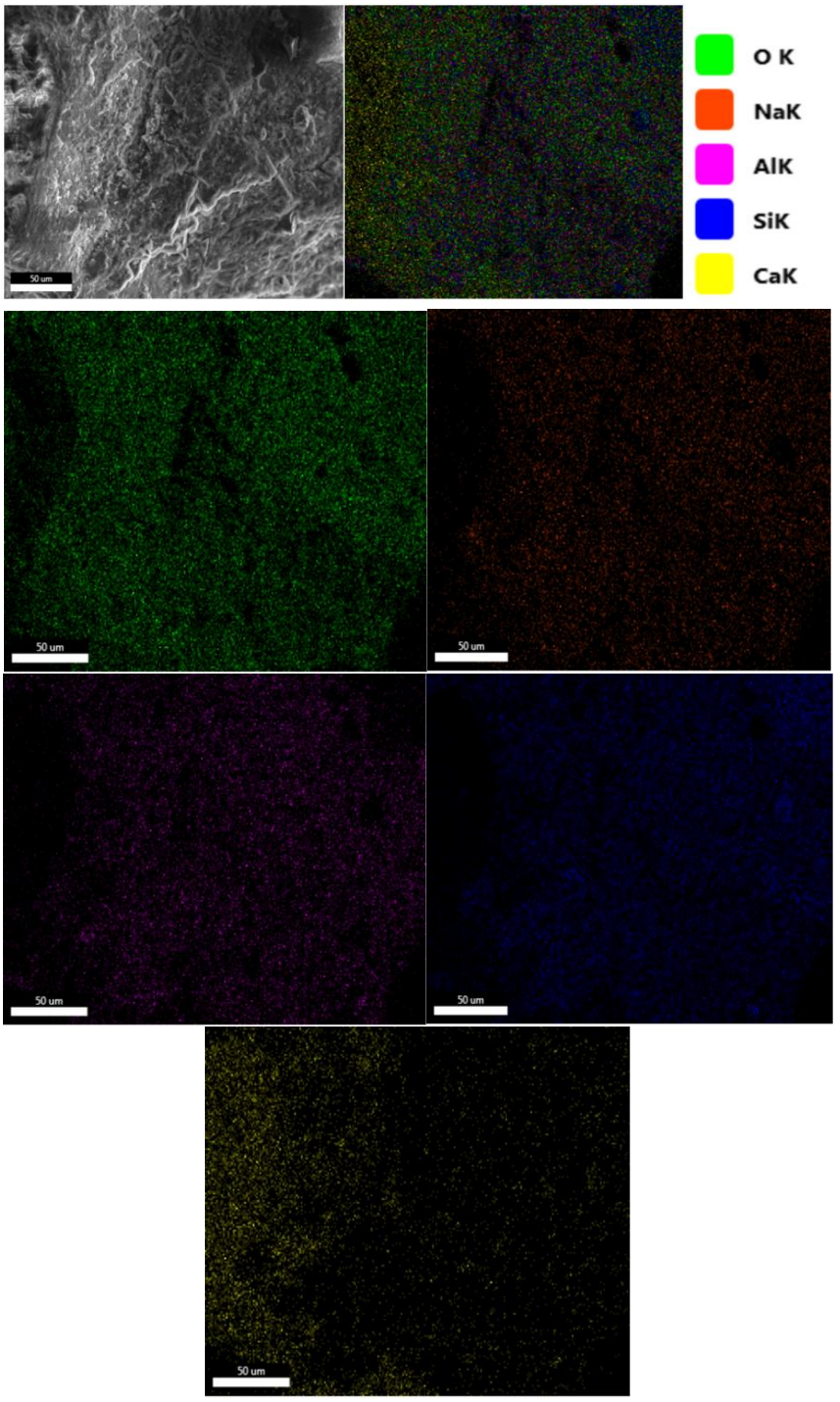

Figure 15: Elemental mapping of the geopolymer sample (50MK50RM)

Thus, RM can be used in geopolymer applications by acting as a binding material. It had the potential to serve as a colouring additive in some engineering applications, especially due to the fact that it had a red colour. Despite these situations, there was a limit to its use. An increase in the utilization rate compared to metakaolin increased

shrinkage cracks, resulting in a more fragile structure. In addition, the fact that red mud had a high specific surface area due to its fine particle size increased ductility at low rates and played the opposite role in the case of high rates of use (Aygörmez, 2021). The fact that RHA had a high SiO_2 content has played an important role in geopolymerization and has had an effect on converting large cavities into thinner ones. It has made a positive contribution to the strength results in the case of substitution up to 20%. However, its high rate of substitution had a negative impact on the characteristics of the mortars produced. This can be explained by the fact that the workability of mortars due to the high specific surface area possessed by RHA particles was reduced (Sharmin et al., 2017). Out of all mix designs studied, it was observed that RHA worked with MK better than all other materials. Further, the results proved that RHA worked better with GP than with RM. Thus, these results indicated that better performances via strength development with combination of GP and MK can be achieved for a 50:50 mix ratio. Therefore, the use of MK as the main ingredient of a geopolymer mortar and concrete would be considerably advantageous for reaching better mechanical properties in addition to better durability; most importantly, it would help produce a very environmentally friendly concrete that had little impact on the environment compared to cement concrete. The MK-based geopolymers can reach better performances in the case of strength parameters such as compressive, flexural, and split tensile strengths. Another result of the study was that there was no parallelism between the results on different days. This created a different situation from traditional Portland Cement. While the strength results increased with increasing day in traditional Portland Cement, variable results were seen in the production of geopolymer mortar where high temperature was applied for curing. The application of high temperature dissolved the solid binder materials, accelerating the

reaction. This adversely affected the homogeneity of the microstructure. Due to the formation of a denser and more heterogeneous microstructure, variability was observed in the strength results (Şahin et al., 2021).

SEM-EDS analysis was performed to support the obtained results in terms of analysis. The results obtained by scanning the area on the mortar samples with SEM-EDS analysis are shown in Figures 15-19 for 5 different series (100MK, 50MK50GP, 50MK20RM30GP, 50MK40RM10GP, 50MK50RM). The distribution ratios of the elements were also shown. According to these tables, the five most common elements in the mortar were silicon, sodium, magnesium, aluminium and calcium. Concerning SEM analysis, the continuousness of geopolymer gel can be observed by the rich distribution of elements in the relevant SEM micrographs. On the other hand, the EDS mapping revealed the fact that the major atomic ratio for geopolymer, namely Si/Al, ranged from 1.4 to 2.53, these values indicated that the fabricated matrices lie in the categories of fire and heat resistant composites, due to the fact that the resulting binding network is a three dimensional very rigid one that explains the reasonable strength results in this stage (Davidovits, 2008). The potential to form a higher amount of SiO_2 positively affected the strength results. In addition, the formation of the rich silica zone indicated the presence of quartz. As far as SiO_2/Al_2O_3 was higher, a higher amount of SiO_2 positively affected the fc value. However, CaO was also important; an excessive amount of CaO can cause the material to become unsound and result in expansion, and therefore, disintegration. These results were consistent with compressive strengths (Uysal et al., 2018).

Also, it is noticed that hydrogen element is not detected although it is existed in the geopolymer matrix, since it is not possible to detect hydrogen with EDS analysis

because of it is low atom weight and therefore the chemical compositions excluding the content of hydrogen. The high distribution of Na, Al, Si and supposed H elements in all the samples as shown in the EDS images in Figures 16-20 prove the presence of Sodium aluminosilicate hydrate (N-A-S-H gel), which is the primary binding phase in geopolymers. The N-A-S-H gel structure leads to mechanical properties which are like C-S-H gels in cement paste, and this could explain the reasonable strength properties for all geopolymer samples, in the mechanical properties' related sections in this chapter.

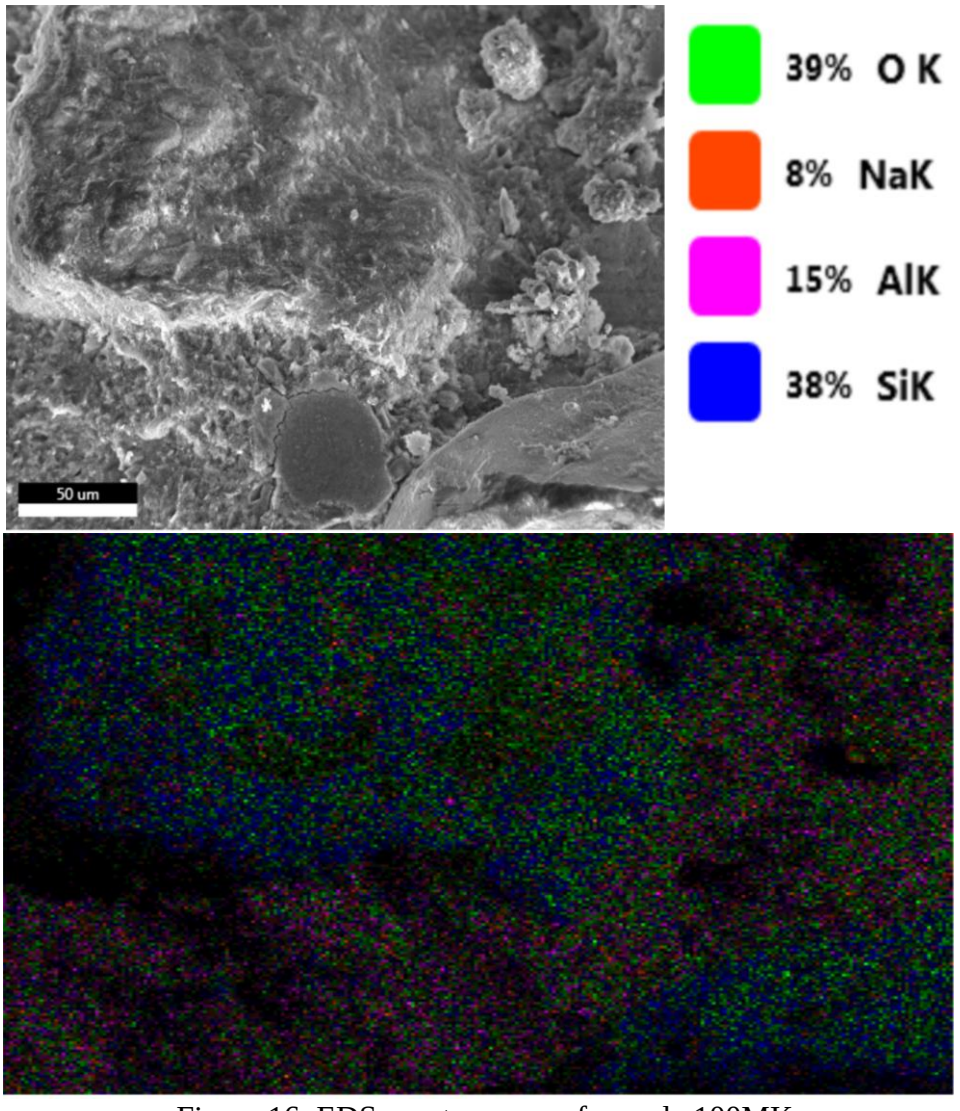

Figure 16: EDS spectroscopy of sample 100MK

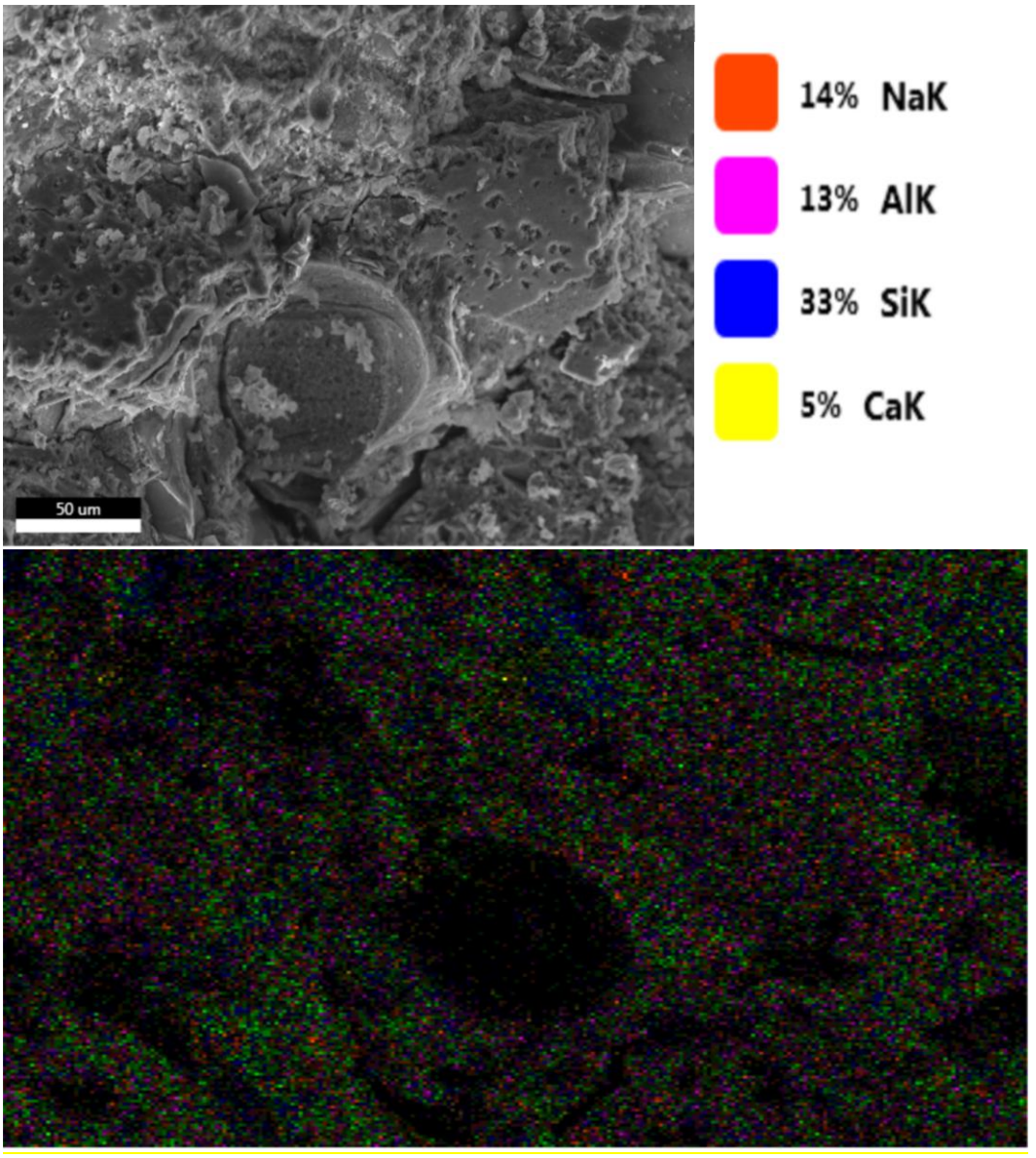

Figure 17: EDS spectroscopy of sample 50MK50GP

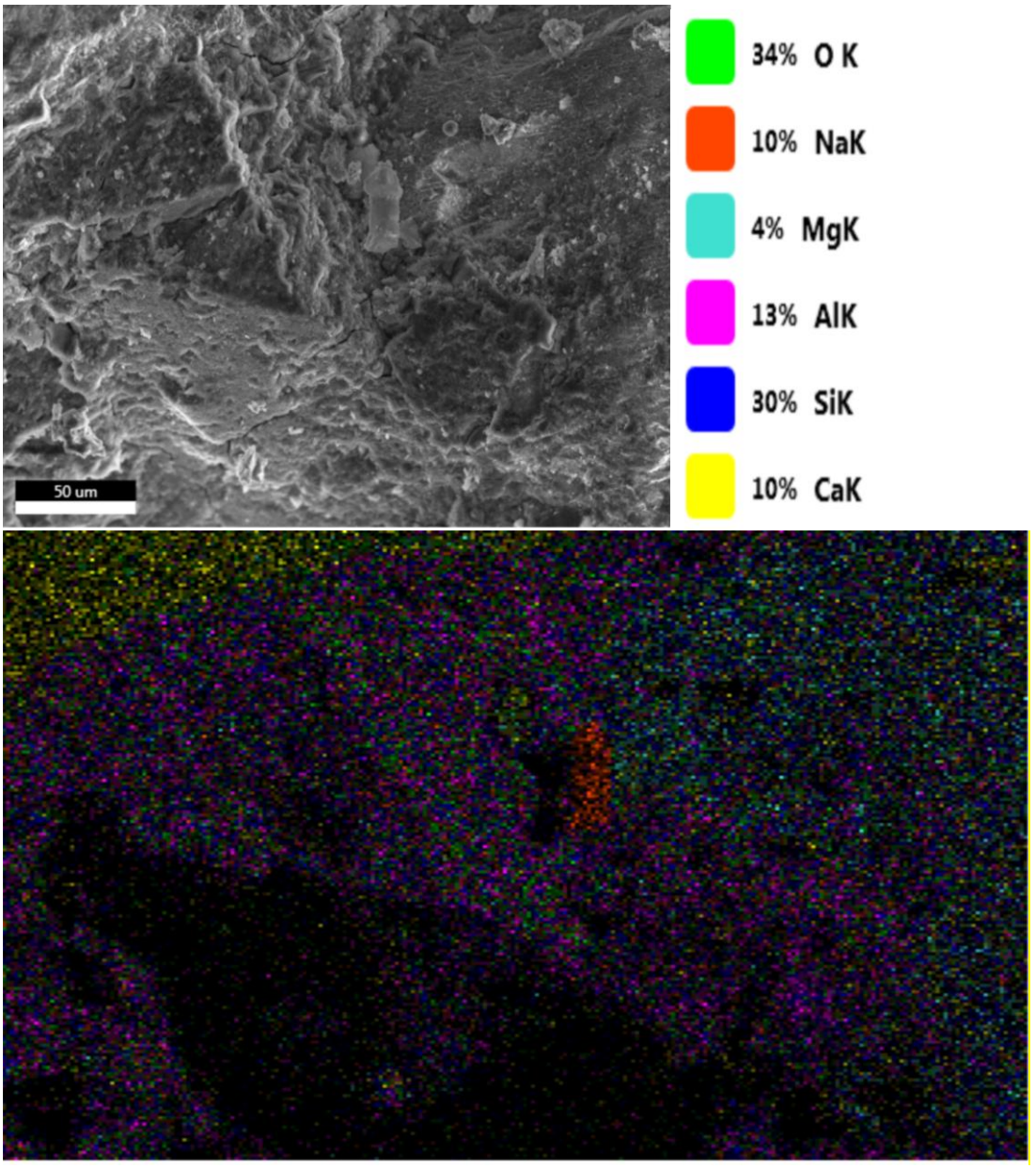

Figure 18: EDS spectroscopy of sample 50MK20RM30GP

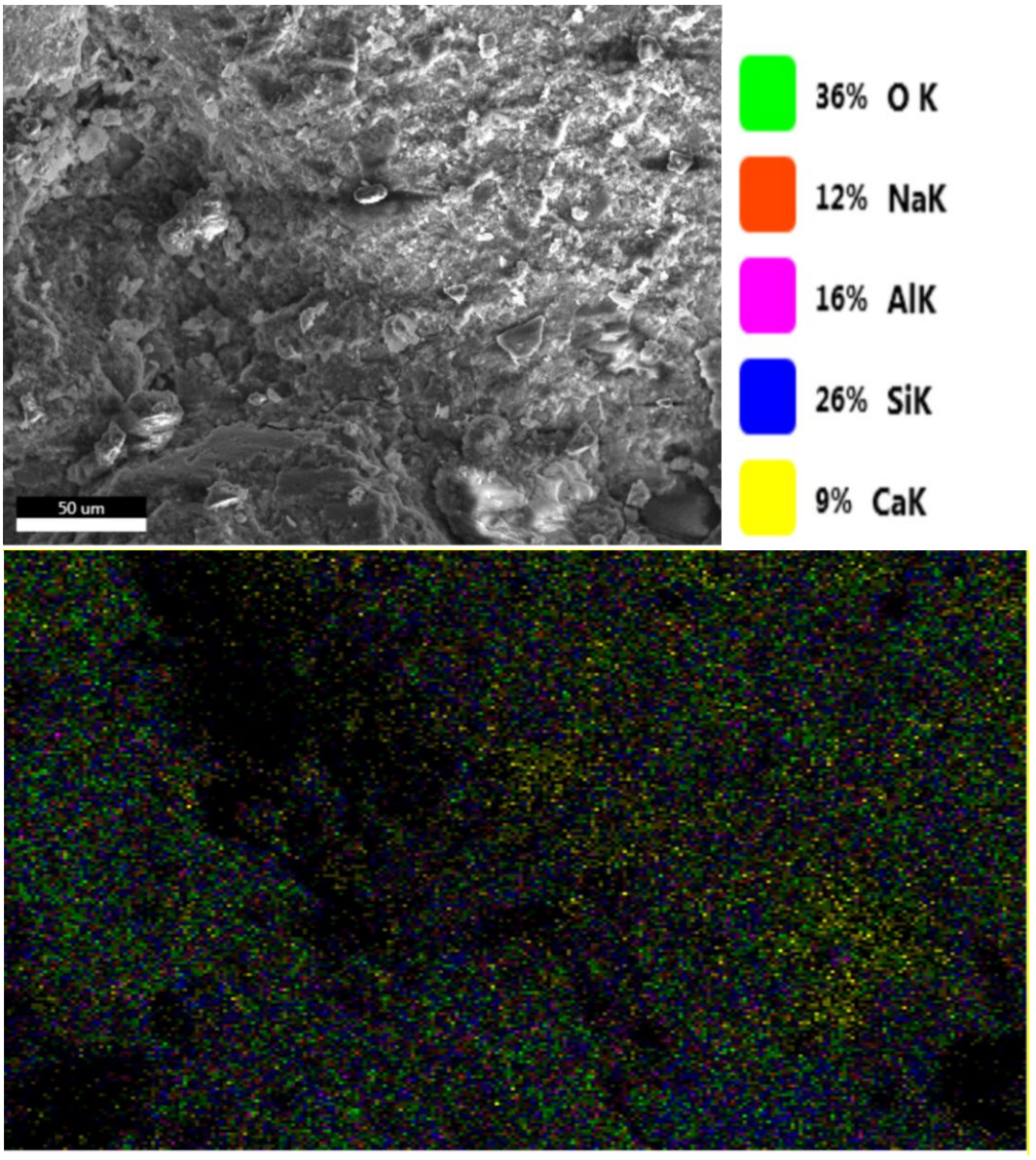

Figure 19: EDS spectroscopy of sample 50MK40RM10GP

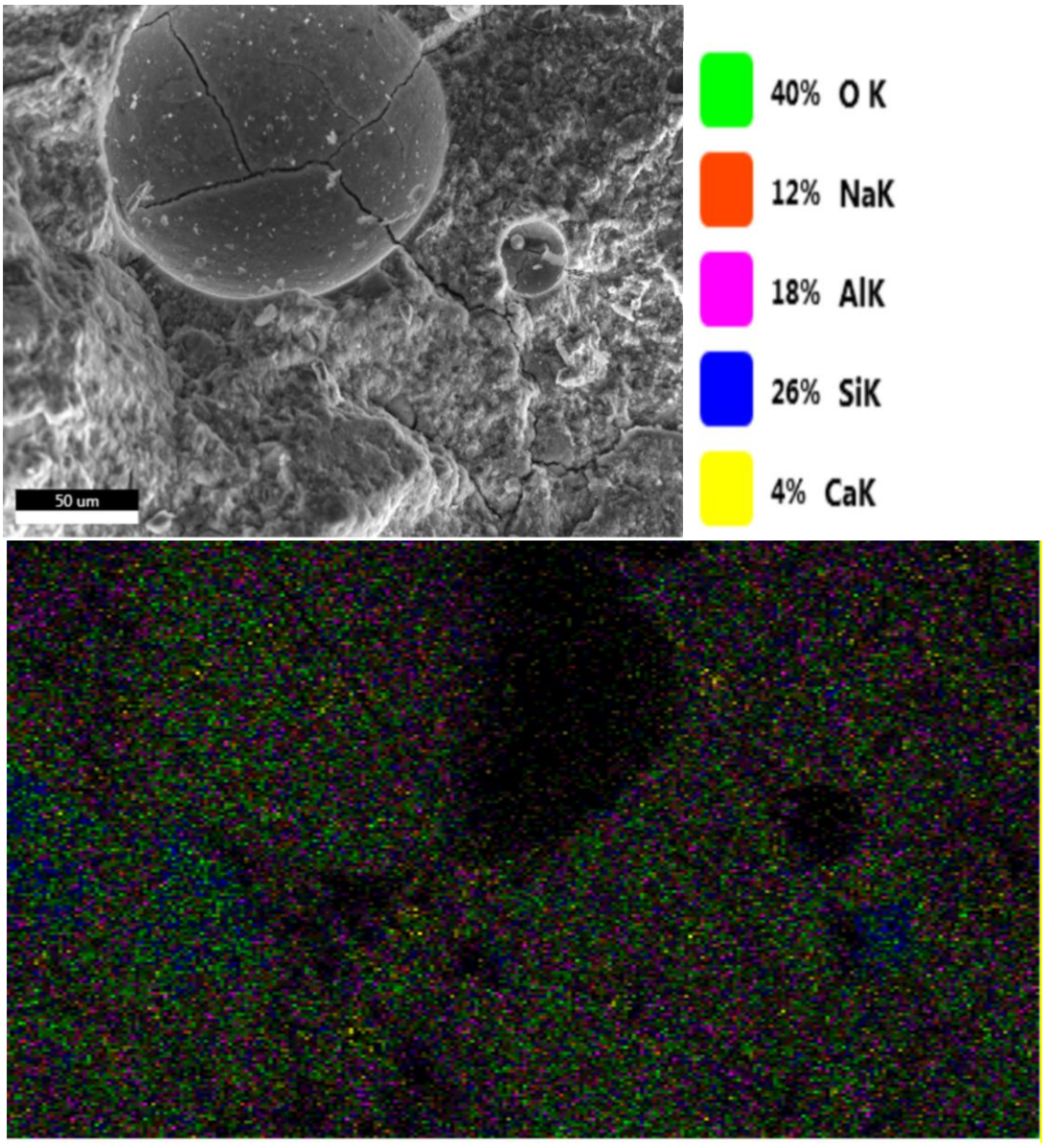

Figure 20: EDS spectroscopy of sample 50MK50RM

5.3 Stage 2: Effects of Adding Glass Fiber on the Strength

5.3.1 Effects of Adding Glass Fiber on Compressive and Flexural Strength

Figure 21 shows the compressive strength values at 3, 7, and 28 d of curing for the 15 different mixes summarized in Table 11. The reasonable strength properties of the main pure geopolymer samples have been explained in the previous section, and the SEM-EDS images and the elemental mapping of the geopolymer samples shows the presence of Sodium aluminosilicate hydrate (N-A-S-H gel), which is the primary binding phase in geopolymers. Also, the elemental mapping shows a presence of Ca+ in a significant quantity in some samples which concentrated in specific zones indicates the possibility to have calcium silicate hydrate (CSH) and geopolymeric gel forming simultaneously within a single binder. The coexistence of the two phases leads to a strong geopolymer matrix structure and finally high strength properties.

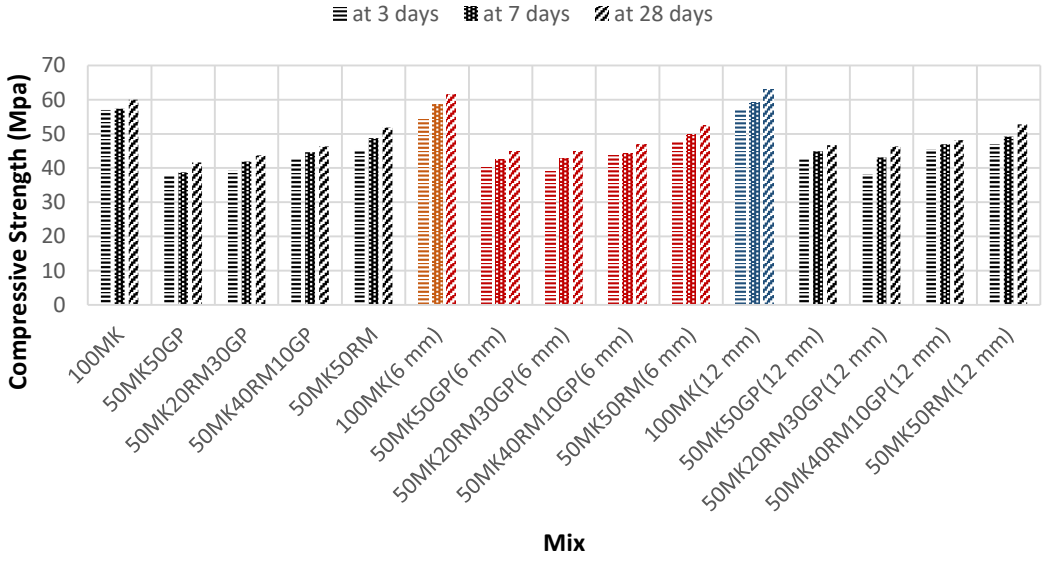

Figure 21: Effects of glass powder (GP), red mud (RM), and glass fiber (GF) on compressive strength

The results showed that RM was more compatible with MK than GP. This was because while the f_c of specimen 50MK50GP was 31% less than that of specimen 100MK, that of specimen 50MK50RM was only 13.61% less than that of specimen 100MK. Therefore, the higher the RM content relative to the GP content both in the binary and ternary combinations, the higher was the f_c value. This was because of the relative high content of Na^+ in GP (Na_2O =12.31%), which instead of being incorporated into the reaction products, remained free to weaken the microstructure after the formation of carbonates (Burciaga-Díaz et al., 2010). The improvement in the microstructure features of mortars containing RM can be attributed to the stabilization of some alkali ions in the NASH gel formed because of the introduction of aluminum oxide (Al_2O_3) and hematite (Fe_2O_3) from MK and RM, which reacted with alkalis from the activator and GP content (Duxson et al., 2007; Xie and Xi, 2001). This was in addition to the fine granulometry of RM, which played an important role by ensuring the cohesion of the geopolymeric paste as obtained in the previous studies (Hajjaji et al., 2013).

The addition of the 6-mm and 12-mm-long GFs slightly increased the f_c. Because of GF's effectiveness in crack reduction by postponing the first crack load. Another explanation could be the GF's high elastic modulus and tensile strength, which enhances the geopolymer matrix flexural load bearing capacity (Tassew and Lubel, 2014). It can be shown that as fiber length increased, the cracking load of the specimens increased, indicating that longer fibers supplied a greater cracking resistance role. The idea behind this conclusion is that longer short fibers create a larger contact area between fibers and the matrix, which intensifies the cohesive force and requires more energy to pull out the fiber, delaying crack formation (Dezfouli et al., 2018; Ranjbar and Zhang, 2020). Furthermore, the 6 mm-glass fibers also help to

increase final bearing capacity, because the distributed fibers contributed to enhance the stress transfer capacity inside the matrix, as well as achieving an even and progressive stress distribution in the layers to improve the ultimate bearing capacity. This amount of increment in strength was a bit higher in the specimens incorporated with the 12 mm fibers. The greater the length of the fiber, the greater was its positive effect on f_c (Awad et al., 2021). When the glass fiber length is increased to 12-mm, it can bridge microcracks and prevent them from developing and propagating in the geopolymer matrix, the fiber-bridging mechanism would be initiated, and the post-cracking toughness of the brittle geopolymer matrix would be increased due to the energy absorption of the brittle geopolymer matrix by the fiber reinforcement (Dezfouli et al., 2018). The glass fiber represent a barrier against the cracks, and the debonding needs more energy to pass through it due to the glass fibers ability to be pulled out, ruptured or acting as bridge. As a result, the glass fiber reinforcement increases the required energy for fracture and leads to a higher bending strength (Wan et al., 2020. Thus, it had a positive effect on flexural and compressive strength by making the fiber longer. The reason for this situation was that the longer fibers passing through the crack region, the cracks were significantly reduced and the stress can be redistributed by transferring the load again with higher efficiency. As the fibers transmitted the stress in a longer time, crack development slowed down and the strength values increased. In studies with similar results, the strength results increased with increasing fiber length (Ma et al., 2010; Ali et al., 2020).

The SEM images in Figure 22 shows the integral adhesion and mechanical interactions between fiber and matrix, when the cracks reach the glass fiber an additional energy is needed to pass through it and to debond the fiber by the deformation of the fibers itself during crack bridging, the compressive and flexural

strength results indicate that the fiber-matrix interaction is strong (Novais et al., 2018). Anyway, the accumulated stress may affect the glass fiber and causing cracks, deformation, and rapture. However, the cracks observed around the fiber indicate the stage of microcracks reaching to the fiber and prove the glass fiber ability to be pulled out, ruptured or acting as bridge.

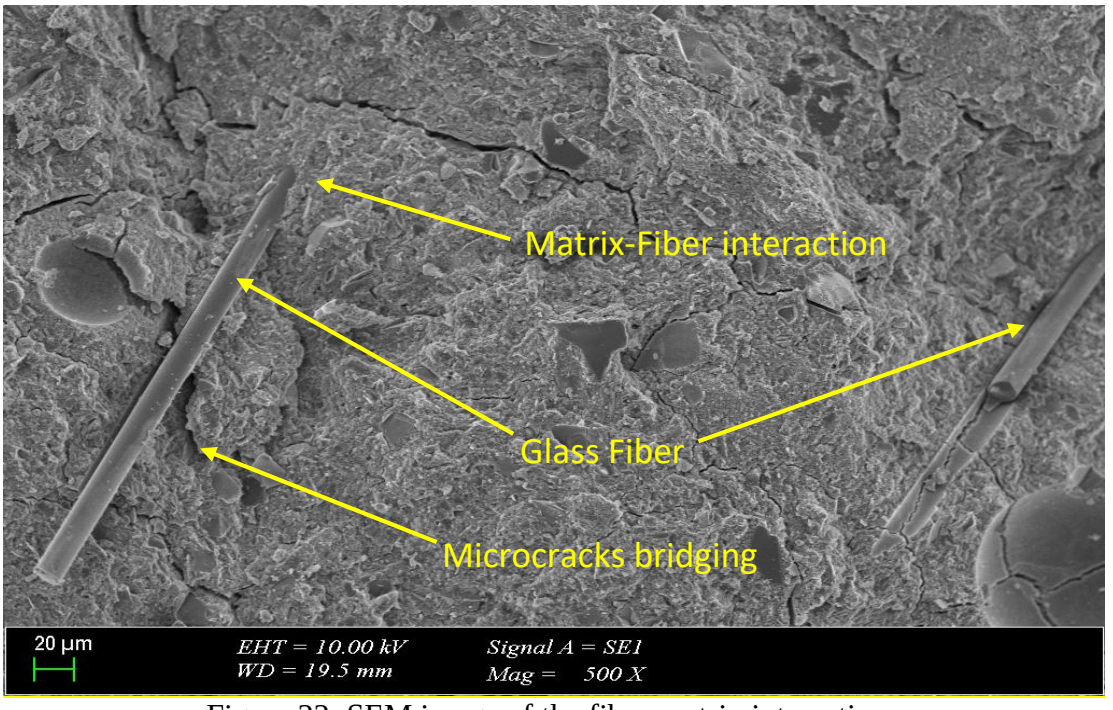

Figure 22: SEM image of the fiber-matrix interaction

Specimen 100MK with a 12-mm-long fiber achieved the highest f_c at 3, 7, and 28 d amongst all samples investigated. The addition of GFs of different sizes always had a positive impact on strength development regardless of the curing age. The f_c enhancement caused by GF addition was not significantly noticeable in the early age but it can be observed after 7 d very clearly. The f_c of the 100MK specimen at 28 d increased by 2.27% and 4.98% by adding 6 and 12-mm-long GFs (61.34 and 62.97 MPa, respectively); the f_c of the 50MK50GP specimen at 28 d increased by 7.45% and 12.2% by adding 6- and 12-mm-long GFs (44.73 and 46.71 MPa, respectively);

the f_c of the 50MK20RM30GP specimen at 28 d increased by 2.77% and 5.98% by adding 6 and 12-mm-long GFs (44.88 and 46.28 MPa, respectively); the f_c of the 50MK40RM10GP specimen at 28 d increased 1.36% and 4.06% by adding 6 and 12-mm-long GFs (46.92 and 48.17MPa, respectively); and the f_c of the 50MK50RM specimen at 28 d increased by 1.08% and 1.87% by adding the 6 and 12-mm-long GFs (52.38 and 52.79 MPa, respectively), respectively. Therefore, it can be concluded that the addition of the GF increased the f_c of the geopolymer mortar; further, the GF length affected f_c, and the 12-mm-long GF improved the f_c slightly more than that when using the 6-mm-long GF (up to 12.2% for 12-mm and 7.45% for 6-mm). In general, the f_c of samples was increased as the Si/Al ratio increased from 1.84 to 1.97 (50MK50RM and 100MK, respectively). A small decrease was observed in f_c in all combinations beyond Si/Al=1.97, for specimens 50MK40RM10GP, 50MK20RM30GP, and 50MK50GP (2.27, 3.27, and 4.51 respectively), which agreed with a previous study (Duxon, 2006). This was attributed to the decrease in f_c of the highest Si/Al ratio specimens being linked to the increase in the unreacted material presented in these specimens (Lee et al. 2002).

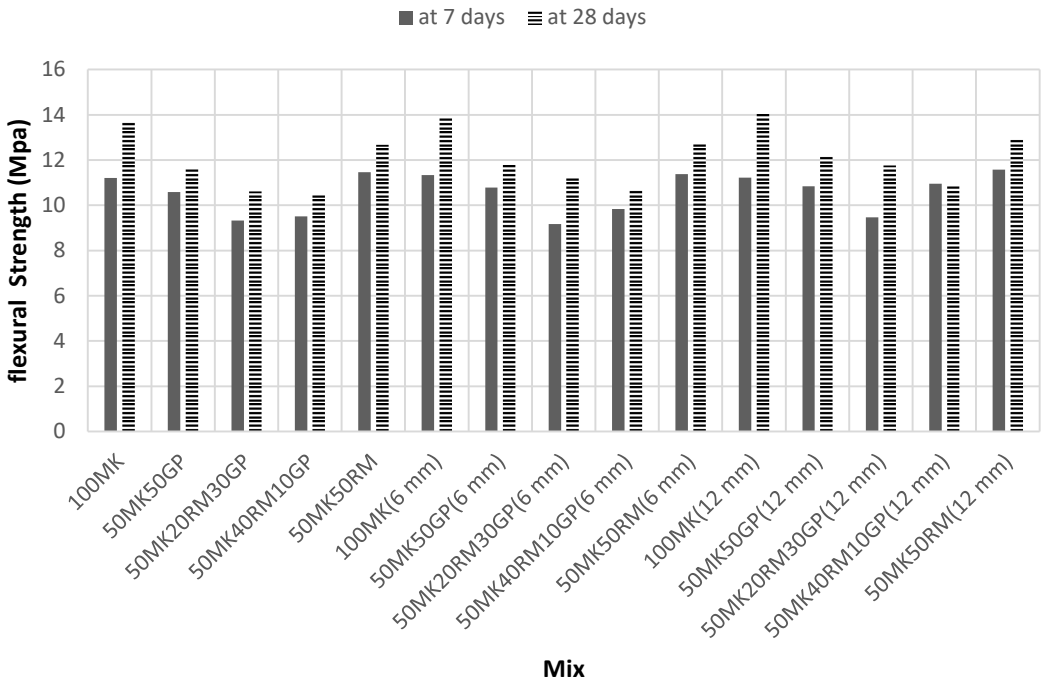

Figure 23: Effects of GP, RM, and GF on flexural strength

Figure 23 shows the f_f results at 7 and 28 d of curing. The f_f development was similar to f_c development. Specimen 100MK with the 12-mm-long GF achieved the highest f_f at 7 and 28 d (13.88 and 14.06 MPa, respectively) amongst all investigated samples. The strength development was different for all mixes; however, f_f increased with time for all mixes, and f_f increased slightly because of the addition of the GF. Further, adding the 12-mm-long GF improved f_f more than that using the 6-mm-long GF (up to 10.84% for 12-mm and 5.94% for 6-mm). The f_f enhancement caused by GF addition was not noticeable in the early age (sometimes it was a bit lower than the mixes without the glass fiber); however, it can be observed after 28 d clearly.

5.3.2 Effects of GP, RM, and GF on Split Tensile Strength (Fs)

The obtained results are comparable to those of concrete suggested by Winter (1964), when he suggested that high-strength concretes can yield up to approximately 3 MPa. This means that the performance of non-fibrous and fibre reinforced geopolymer

mortar specimens is comparable to that of Portland cement concrete. The split tensile strength results at 28 d of curing are shown in Figure 24.

The 15 mixes listed in Table 11 were tested. The crack initiation and propagation were different for specimens with various fiber sizes; crack propagation allowed the cylinders to split into two halves, which led to a longitudinal splitting failure. When different fibers were added in the geopolymer mixes, less cracks were developed compared to specimens without the glass fiber, and all cracks observed vertically can be seen in Figures 25 and 26. The positive effect of the fibers was due to the fact that they carried the stresses and increased the toughness of the material with the bridging effect, the results prove that adding GF to the geopolymer mixes increases the split tensile strength. Stress is transferred to the fiber through shear stresses at the interface in glass fiber composites until the fiber attains its tensile strength and fractures, the segmented fiber continues to carry load and fracture into shorter segments until shear load transfer is no longer sufficient (Lin et al., 2009). Furthermore, the GF also help to increase final bearing capacity, because the distributed fibers contributed to enhance the stress transfer capacity inside the matrix, as well as achieving an even and progressive stress distribution in the layers to improve the ultimate bearing capacity. In compliance with previous study findings (Bagherzadeh et al., 2012), the bridging of the diametric splitting crack causes an increase in split tensile strength. The addition of fibers reduced fracture propagation due to the splitting tensile load utilizing the maximal tensile strength capability and the GF bridging effect. Due to the bridging effect of the fibers, the crack formation is slowed, and stress concentration around cracks is reduced. Finally, the geopolymer matrix split tensile strength has been improved (Abousnina et al., 2021). These results were a positive

expression of the contribution of fibers to the split-tensile strength of samples. This was in accordance with the literature (Ali et al, 2020; Tammam et al., 2021).

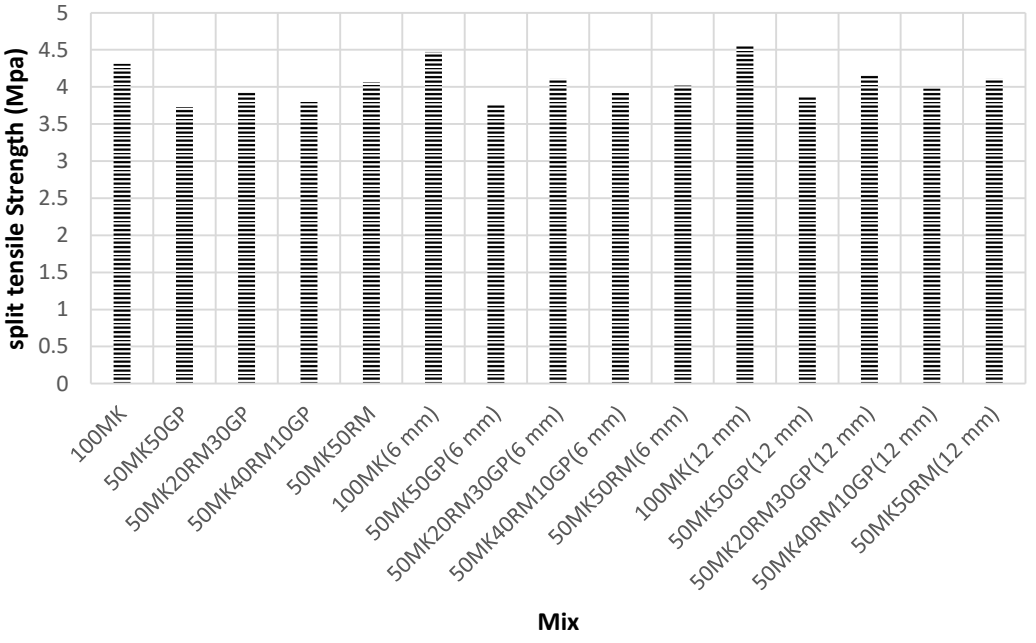

Figure 24: Split tensile strength results after curing for 28 d.

There was an up to 5.8% increase in fs when 12-mm-long GF was added into the 100MK specimen (4.56 and 4.47 MPa, respectively). An up to 5.58% increase was observed when 12-mm-long GF was added into the 50MK20RM30GP specimen. An increase in the range of a 0.8–5.8% was observed in the mixtures when a 6- or 12-mm-long GF was incorporated into the mixtures. The highest split tensile value was observed for 100MK amongst the samples with no addition of GF (4.31 MPa). However, with the addition of GF, the highest split tensile value was achieved for 100MK (12 mm).

Even with the addition of the GF, none of the samples obtained a value higher than that of the 100MK mixture. Further, no significant decrement was observed; the

reduction was in between 0–0.99% due to the weak interfacial bonding between the fibers and the geopolymer matrix based on MK, RM and GP.

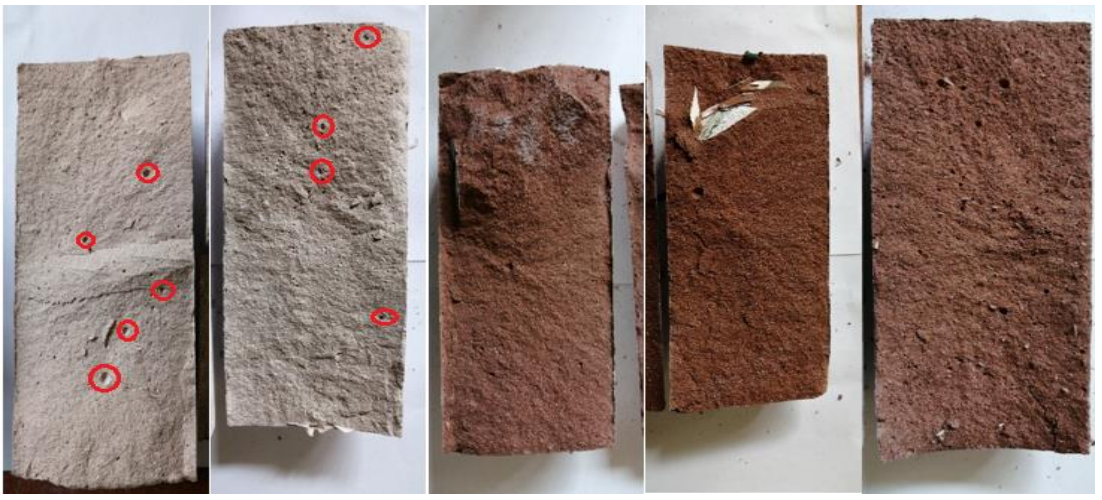

Figure 25: Samples without GF after split tensile strength test

Figure 26: Samples contains GF after split tensile strength test

5.3.3 Effects of GP, RM, and GF on Abrasion Resistance

The weight loss and wear depth caused by abrasion is shown in Figure 27. The investigated wearing depths were within the 2.5 mm range, and hence, it was concluded that the geopolymer mortar samples had very good abrasion resistance due to the reasonable strength properties of the pure main geopolymer samples which have been explained in the SEM-EDS images and the elemental mapping of the

geopolymer samples shows the presence of Sodium aluminosilicate hydrate (N-A-S-H gel), which is the primary binding phase in geopolymers (Lyngdoh et al., 2020). Also, the elemental mapping shows a presence of Ca+ in a significant quantity in some samples which concentrated in specific zones indicates the possibility to have calcium silicate hydrate (CSH) and geopolymeric gel forming simultaneously within a single binder. The coexistence of the two phases leads to a strong geopolymer matrix structure and finally reach high strength properties (Yip et al., 2004).

The findings revealed that increasing the fiber content improved both the length change and weight reduction by a small percentage. This can be attributed to the fact that the presence of the fibers created a layer more resistant to abrasion, which resulted in less length change and weight loss (Almashhadani et al., 2018).

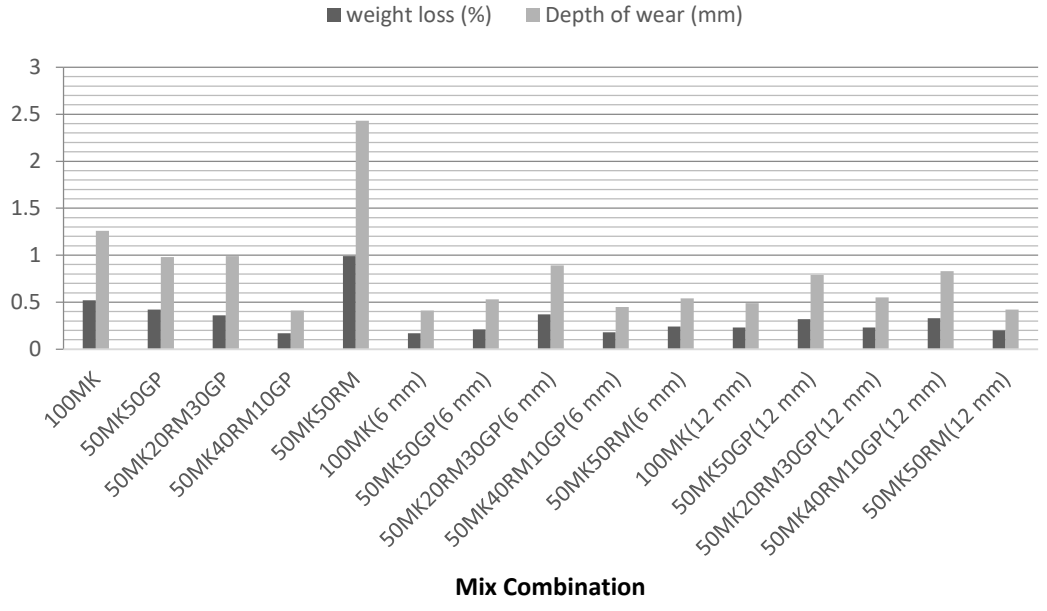

Figure 27: Weight change and depth of wear after abrasion test

The GFs addition achieved reductions of between 1% and 35% in the abrasive wear of specimens, as indicated in Figure 27. Therefore, there was a bit difference in the

abrasion resistance between the 6-mm- and 12 mm-long GF reinforced specimens. The least weight loss was observed for specimens 50MK40RM10GP and 100MK with the GF addition (only 0.17% reduction). The highest weight loss was observed for specimen 50MK50RM, which was an almost 1% reduction in weight.

After the abrasion tests, weight loss was observed for all samples. Therefore, it was reported that the inclusion of GF provided significant contributions to the geopolymer mortar in terms of abrasion resistance, the addition of glass fibers into the mixes reduces the porousness, the size of the pores and strengthens the connections between parts of geopolymer matrix, making them more resistant to abrasive erosion (Grdic et al., 2012). The crack arresting and crack-thinning effects of glass fibers, as well as the bridge effect of glass fibers on cracks and diversion effect of glass fibers on geopolymer matrix components, improve the abrasion resistance of geopolymers containing glass fibers. When glass fibers are pulled out of the geopolymer matrix, friction exertion is also consumed (Liao et al., 1999). The rigid character of the fiber, as well as strong bonding between the fiber and the geopolymer matrix are critical factors for the considerable reduction in wear rate of these composites. These results were consistent with previous findings, which stated that adding glass fiber to gepolymer composites improves their wear properties (Shalwan and Yousif, 2014; Vina et al., 2008). Finally, fibers act as crack arresters in geopolymer matrix, improving the tensile strength and toughness of the pastes, and mitigating the abrasion damage.

5.3.4 Effects of GP, RM, and GF on Elevated Temperature Resistance

The produced geopolymer composites were subjected to elevated temperatures of 400, 600 and 800^{o}C. In general, the results after conducting this test show that there is a reduction in the performance of the specimens. The main reason for the decrease

in strength results was the evaporation of free water and dehydration of the geopolymer matrix with the thermal reaction mechanism that occurred after 500 °C temperature (Aygörmez et al., 2020; Şahin et al., 2021). After 600 ºC, these decreases started to increase. To better explain the loss of strength after 500 ºC temperature, the concept of steam effect should be used. The water in the matrix structure turned into steam with temperature. Temperature increases above 100 °C continuously increased the internal pressure. After the vapor pressure was at its maximum, the matrix condensed with less permeability. In this way, the resistance against thermal effects decreased. This created thermal cracks on the surfaces. Evaporation of the water in the matrix structure also caused weight loss. Cracks formed by the effect of thermal shrinkage led to loss of strength along with loss of weight. In addition, high temperatures created thermal incompatibility by creating microcracks in the interface transition zone between paste and aggregate (Jiang et al., 2020). Also, the aluminosilicate gel structure underwent more crystallization with higher temperatures. This situation led to the thermochemical decomposition of the crystal lattices at the end of the crystallization stress that occurred with increasing temperature. Ductility and strength were adversely affected by the recrystallization process. This inhomogeneous situation created a thermal incompatibility. This was another event that triggered the formation of microcracks. Against these effects, the stronger the structure of the geopolymer sample, the faster it is emitting heat and is exposed to less thermal gradients. This limited thermal cracks and fragmentation. In addition, flexural strength results were significantly affected by microstructural defects caused by crack propagation and growth of porous structures after high temperature (Zhang et al., 2016; Aygörmez et al., 2020; Ali et al., 2020; Şahin et al., 2021).

The addition of GF served to limit the thermal damage of the mortar. The results presented in Figures 28-30 show that at 400 °C, the mortar with GFs degraded less rapidly than the mortar without the GFs.

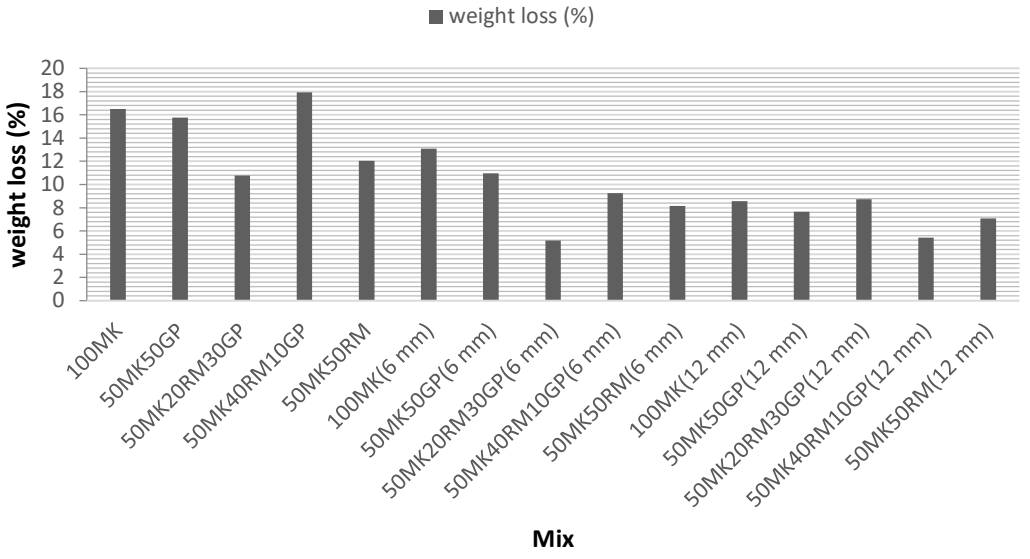

Figure 28: Weight loss at 800 °C temperature

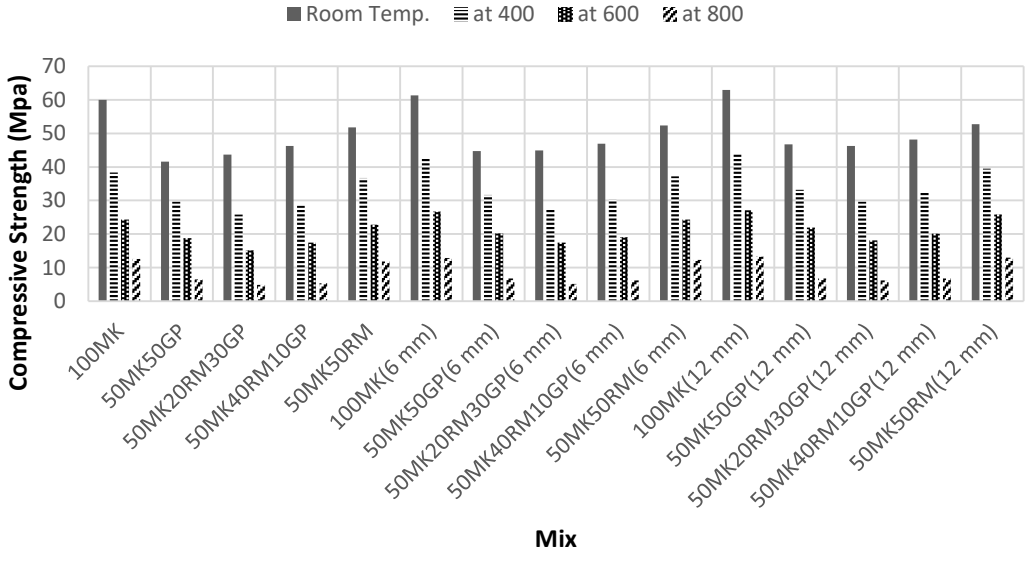

Figure 29: Compressive strength results under different temperatures

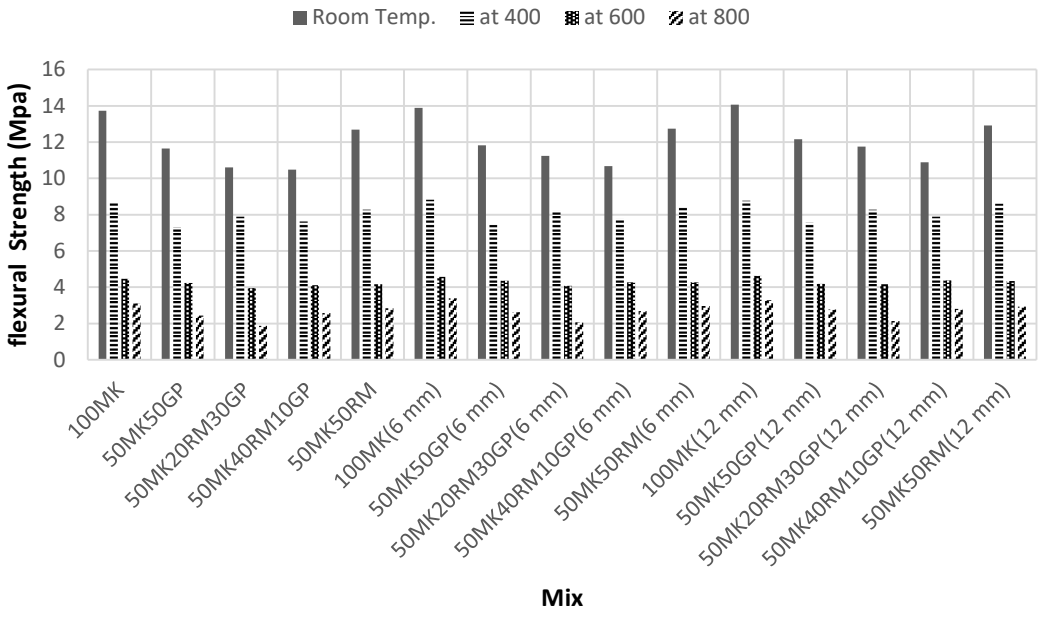

Figure 30: Flexural strength results under different temperatures

The results of this study stated that GF addition decreased the weight loss of mortar if it was exposed to elevated temperatures; further, it improved the f_c and f_f under elevated high temperatures as shown in Figures 29 and 30. Figure 28 shows the weight loss under an exposure of 800 °C. The GF addition decreased the weight loss relative to the specimens without the GF, and there was no significant relationship between weight loss and the length of the fiber. Significant weight loss was observed for samples under high temperatures (400 °C and 800 °C). The f_c of the samples decreased sharply under high temperatures (400, 600 and 800 °C) as shown in Figure 29. The highest reduction of f_c (dropped from 43.67 to 4.87 MPa) after exposure to 800 °C was 88.85% for the specimen 50MK20RM30GP without the GF; when the GF was added, the reduction rate of f_c decreased to 88.52% and 86.58% for the 6-mm and 12-mm-long GFs, respectively. Figure 30 shows that the highest reduction of f_f (dropped from 10.61 to 1.87 MPa) after exposure to 800 °C was 82.38% for specimen 50MK20RM30GP without the GF. When the GF was added, the reduction rate decreased to 81.67% and 81.89% for the 6 and 12-mm-long GFs, respectively.

The reduction rate of f_c for specimen 50MK20RM30GP without the GF was the highest among all combinations under 400, 600 and 800 °C (40.87%, 65.26%, and 88.85%, respectively) when compared to f_c at 28 d (43.67 MPa) without high temperatures exposure. f_f still had the highest reduction rate at 800 °C (82.38%); however, for temperatures before 800 °C it was not the combination that had the highest rate because of the exothermic reactions (600–800 °C) explained in more details in the TGA section.

The f_c loss (%) at 800 °C of the samples decreased as the Si/Al ratio increased from 1.84 to 1.97 (50MK50RM and 100MK, respectively). A small increase was observed in the f_c loss in all combinations beyond Si/Al = 1.97 for specimens 50MK40RM10GP, 50MK20RM30GP, and 50MK50GP (2.27, 3.27, and 4.51, respectively); specimen 50MK50GP had a better strength loss resistance than other two even it had the highest Si/Al ratio (4.51) because of the activation of the unreacted quartz in the geopolymer matrix during high temperatures exposure. This result indicated a relationship between the Si/Al ratio increasing and the mechanical properties weakening under high temperatures. However, the f_c loss was related to the loss of weight promoted by evaporation, and it depended on the microstructural rearrangement of the geopolymeric N-A-S-H gel (Burciaga Díaz et al., 2016).

At 800 °C, the glass fiber as shown in Figure 31 were found beneficial in terms of strength behaviour after exposure to high temperatures such as 800 °C. having a high melting point which is close to or higher than the highest applied temperature, the fibres used helped in improving the compressive and flexural behaviour of the produced samples. These findings are in line with the previous studies in this field (Aygörmez et al., 2020; Şahin et al., 2021).

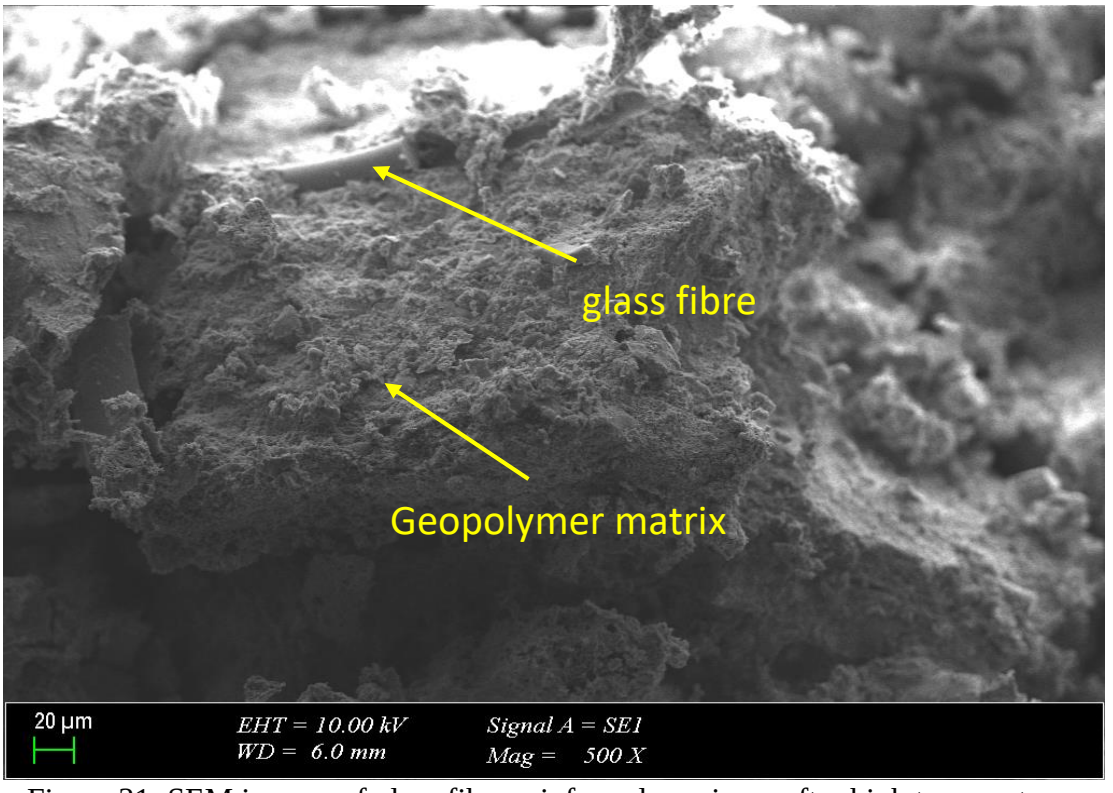

Figure 31: SEM images of glass fiber reinforced specimen after high temperature exposure (800 °C)

However, thermal damage occurred at 600 °C, and the ternary blended mortars deteriorated more than specimens 100MK and 50MK50GP. Beyond 800 °C, all specimens deteriorated as rapidly as the 100MK mortar specimens.

With respect to f_c, there were no positive or negative effects of the length of GF. Further, specimens 100MK and 50MK50RM achieved the highest f_c at 800 °C, which were 13.26 MPa and 12.98 MPa, respectively. The 100MK sample had a better temperature stability than other combinations because of the presence of a highly cross-linked N-A-S-H gel (as shown in Figure 32) that incorporated a low content of chemically bonded water and due to the absence of calcium bearing phases as reaction products in its structure that were in agreement with the previous studies (Davidovits, 2013; Provis, 2009).

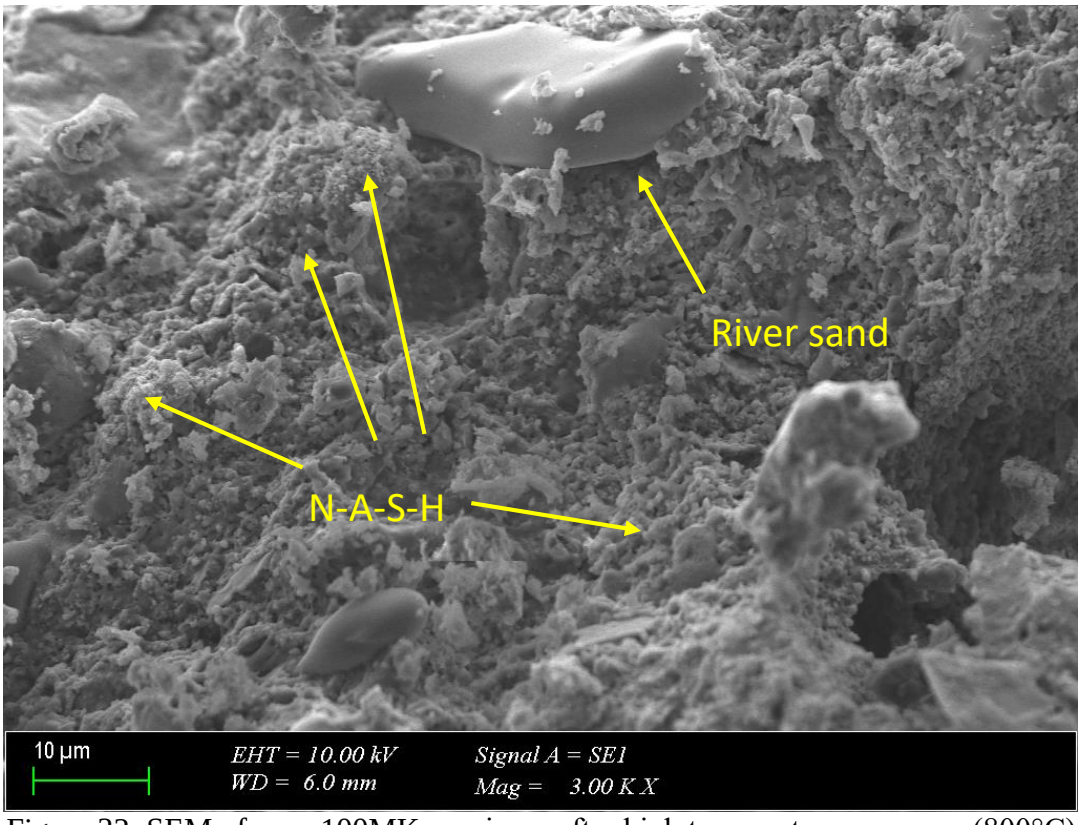

Figure 32: SEM of pure 100MK specimen after high temperature exposure (800°C)

5.3.5 Effects of GP, RM, and GF on XRD Measurements

Geopolymer materials were predominantly of an X-ray amorphous nature, with the diffraction crystals being those of the parent minerals (calcite, dolomite, and quartz) according to the XRD patterns of the geopolymer mortar samples. Between two values of around 20° to 40°, there was an amorphous hump in the diffraction pattern, which can be attributed to the existence of amorphous glassy materials. The crystal phase percentages of samples according to XRD analysis results of the five samples are summarized in Table 15.

Table 15: XRD analysis of the geopolymer samples (crystal phases)

Component / Sample	Calcite (%) $CaCO_3$	Dolomite (%) $CaMg(CO_3)_2$	Quartz (%) SiO_2
100MK	43	33.7	23.3
50MK50GP	15	-	85
50MK20RM30GP	57.4	-	42.6
50MK40RM10GP	60.3	4.1	35.6
50MK50RM	66.7	6.4	26.9

The XRD patterns of sample 100MK are shown in Figure 33 (a). Following the geopolymerization chemical reaction between the MK and the activation solution, the main phase specific to the raw material, quartz (SiO_2), whose peak was located at 26.65 (2θ) decreased in intensity as the glass phase decreased; however, the calcite ($CaCo_3$) intensity increased significantly at 29.45 (2θ). New peaks specific to the phases generated as a result of the reaction between Ca and the other components appeared as a significant rise in the intensity of dolomite ($CaMg(CO_3)_2$) at 30.98 (2θ). However, dolomite was slightly harder (3.5–4) than calcite (3) on the Mohs scale, which were considerably lower than the hardness of quartz (7).

The XRD patterns of the sample 50MK50GP in Figure 33 (b) shows the formation of the most important phase specific to geopolymerization. In this phase, quartz showed four peaks between 20.86° and 39.47°, with the highest intensity at 26.64° (2θ), which confirmed that some part of the aluminosilicate source did not react after geopolymerization. However, prior to and after activation, other phases such as calcite with the highest intensity peak at 29.43° (2θ) was confirmed, and it was possible to visualize that the amorphous structure of the glass powder did not change the geopolymer crystalline behavior, as illustrated in Figure 33 (b). Quartz (SiO_2) was the major crystalline phase contaminant present in sample 50MK50GP. However, quartz was considerably harder than calcite; Quartz reached 7 on the Mohs scale of mineral

hardness, whereas calcite reached third sample 50MK50GP, which had the highest quartz phase (85%), had the lowest strength properties due to a weak geopolymer matrix and the unreacted quartz particles.

The XRD patterns of sample 50MK20RM30GP in Figure 33 (c) shows the formation of quartz, which was the most important phase of geopolymerization. In this phase, quartz showed four peaks between 20.85° and 39.45°, with the highest intensity at 26.63° (2θ). However, prior to and after activation, other phases such as calcite with the highest intensity peak at 29.42° (2θ) was confirmed. The XRD patterns of this sample were similar to the patterns of 50MK50GP and had the same peaks points; further, it was observed that the highest peaks of these two combinations were achieved by calcite around 29.42° (2θ). Owing to the poor activity in alkaline solutions, a portion of quartz crystals did not participate in the geopolymerization reaction and stayed as fine particles inside the structure of the material.

The XRD patterns of sample 50MK40RM10GP in Figure 33 (d) shows five peaks between 20.84° and 40.03°, with the highest intensity at 26.65° (2θ). Further, prior to and after activation, phases such as calcite with the highest intensity peak at 29.41° (2θ) was confirmed. This geopolymer matrix with a quartz content was a composite material made up of geopolymeric gel with the matrix and quartz particles as reinforcement. Quartz particles improved the mechanical responsiveness of the material by acting as barriers to crack formation, and formed during geopolymerization, was embedded and dispersed in the geopolymer matrix and contributed to reinforcing the structure of geopolymer mortar (Kouamo et al., 2017). This was a good agreement with the value of the compressive strength of this

combination, which was higher than the one of the 50MK50GP that had a similar high content of quartz.

The XRD patterns of sample 50MK50RM in Figure 33 (e) show four quartz peaks between 21.11° and 39.72°, with the highest intensity at 26.88° (2θ). Further, a sharp peak of calcite ($CaCo_3$) intensity was noticed at 29.69° (2θ). However, prior to and after activation, secondary phases such as dolomite with the highest intensity peak at 31.2° (2θ) was confirmed. The presence of quartz, calcite, and dolomite phases in the geopolymer structure produced a high strength geopolymer matrix similar to the 100MK geopolymer matrix with the crystalline phases; this explained the improved strength properties of the two combinations (100MK and 50MK50RM) which were in agreement with the previous studies (Wan et al.2019 and Wang et al.2019).

The major component identified in the XRD patterns of samples 100MK and 50MK50RM were quartz, calcite, and dolomite, which explained the significant mechanical properties of sample 50MK50RM. All XRD patterns of the geopolymer samples showed an amorphous structure with a few recognizable peaks; peaks associated with quartz (low intensity), which was the main crystalline phase, and calcite, were observed in all samples.

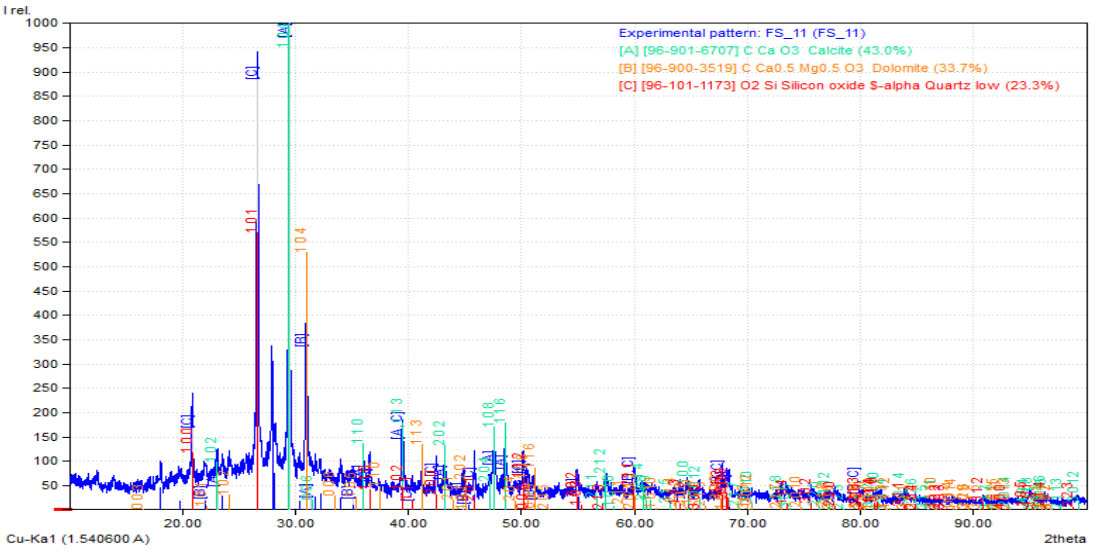

Figure 33 (a): XRD Patterns of Sample 100MK

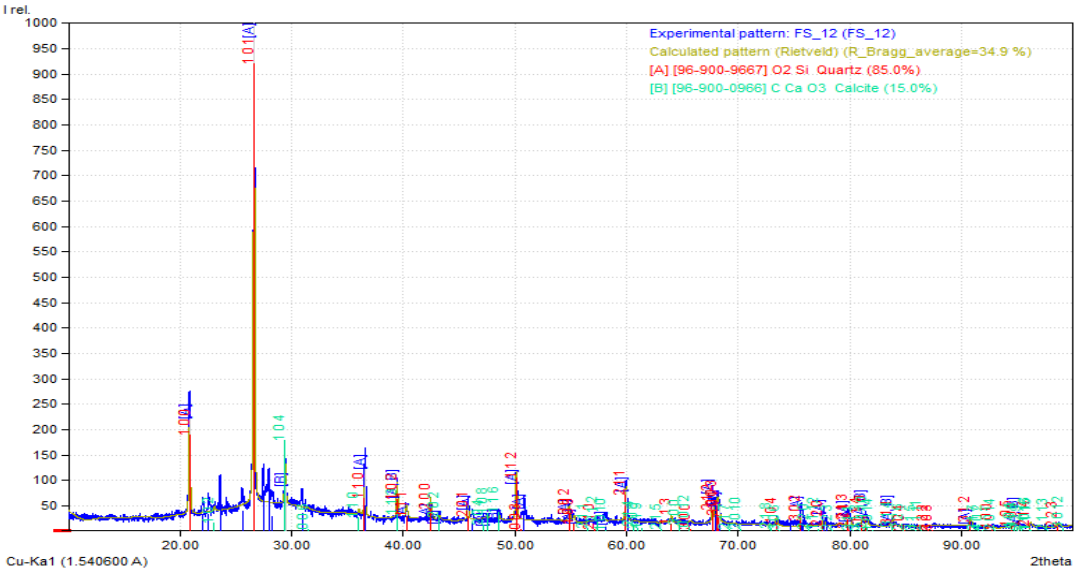

Figure 33 (b): XRD Patterns of Sample 50MK50GP

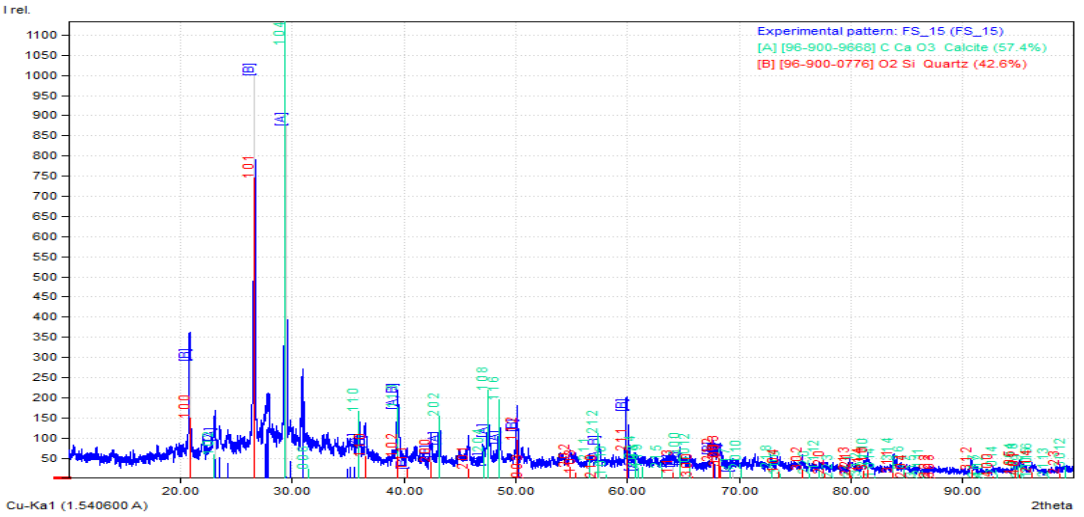

Figure 33 (c): XRD Patterns of Sample 50MK20RM30GP

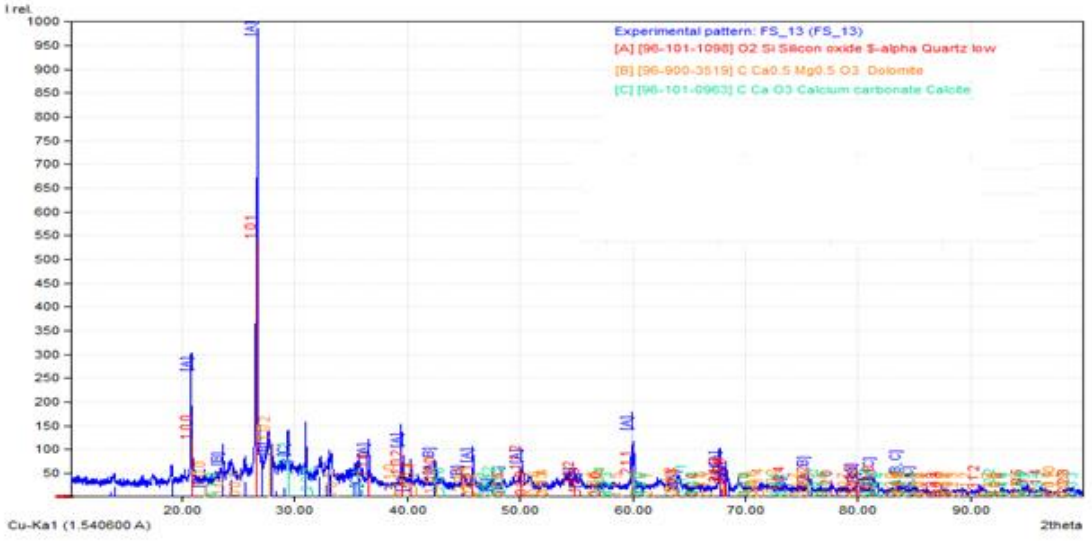

Figure 33 (d): XRD Patterns of Sample 50MK40RM10GP

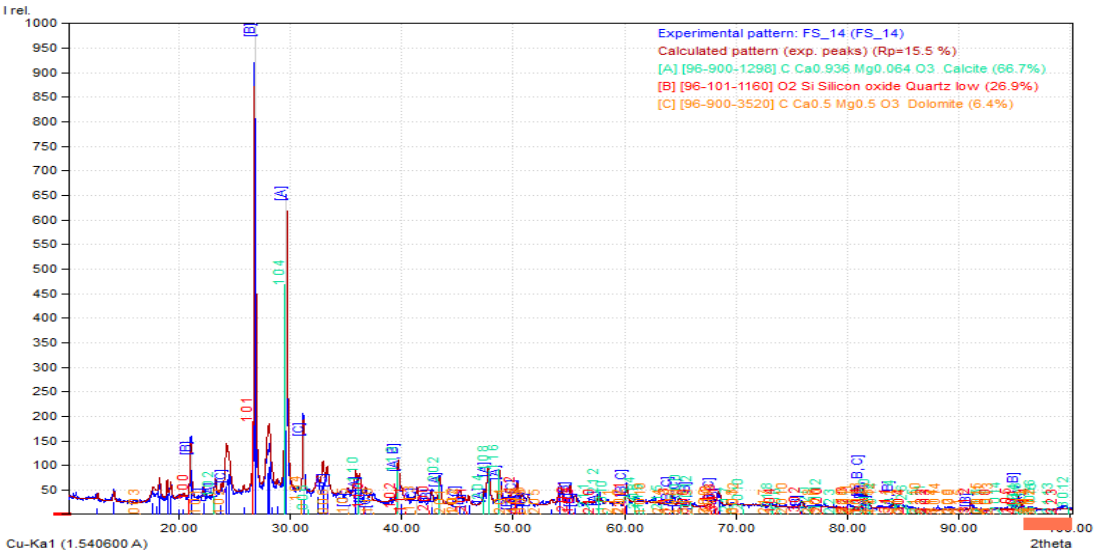

Figure 33 (e): XRD Patterns of Sample 50MK50RM

5.3.6 Differential Thermal Analysis (DTA)/ Thermogravimetric Analysis (TGA)

The thermal stability of geopolymer mortars was assessed using a DTA/TGA simultaneous thermal analysis. The fraction of volatile compounds can be calculated by monitoring the weight loss during sample heating; if the DTA curve was shown at the same time, the weight loss at specific temperatures can confirm the quantity of an inert ingredient (Nergis et al., 2020).

Figures (33–37) show the DTA curves of geopolymer samples after 28 d of curing, the endothermic peaks of the DTA curves were observed at approximately (100–500) °C for all geopolymer mortar samples (470, 324.5, 333.4, 332, and 326.3 °C) respectively, which caused weight loss; these peaks were a results of pore water evaporation. Geopolymers were stable at temperatures ranging from 500–1000 °C, with only minor reductions caused by sample shrinkage due to crystallization. These nanostructures were dehydrated entirely after being exposed to 500 °C; however, they did not collapse completely, which allowed us to conclude that all geopolymer samples are thermally stable. Further, samples without RM were more stable as they

retained more residual weight because of the decomposition of calcite ($CaCO_3$), quartz (SiO_2), and dolomite $CaMg(CO_3)_2$ to MgO and $CaCO_3$ at temperatures below 750 °C; the $CaCO_3$ decomposition to CaO occurred between 750 °C and 900 °C. Water was a fundamental structural component of a geopolymer; the loss of weight was caused by the evaporation of the absorbed and bonded water. Daniel et al. (2008) explained that the absorbed water evaporation was responsible to the weight loss until the 100 °C temperature; the increase in the temperature after 100 °C caused shrinkage and structure damages for the geopolymer samples. Perraki et al. (2005) explained that the evaporation of hygroscopic water caused continuous weight loss until around 500 °C.

There was a relationship between the obtained weight losses and the stability and compactness of geopolymer mortars. While the loss rate for sample 100MK was 14.13%, the weight losses were higher (14.68% and 14.81% for samples 50MK20RM30GP and 50MK50GP, respectively) with the use of GP, although close to the loss rate of MK. When the use of RM increased compared to the use of GP, weight losses increased. The weight losses for samples 50MK40RM10GP and 50MK50RM were 18.97% and 17.67%, respectively. This situation showed parallelism with the strength results. Since the use of GP and RM was known to reduce geopolymerization according to MK, weight losses were expected to be higher. The results obtained were also compatible with the literature (Arslan et al., 2019). The weight loss shown in the TGA figures corresponds to that of specimens exposed to elevated temperatures, in both cases the percentages of weight loss at 800 °C temperature was in the range between 10 and 17%.

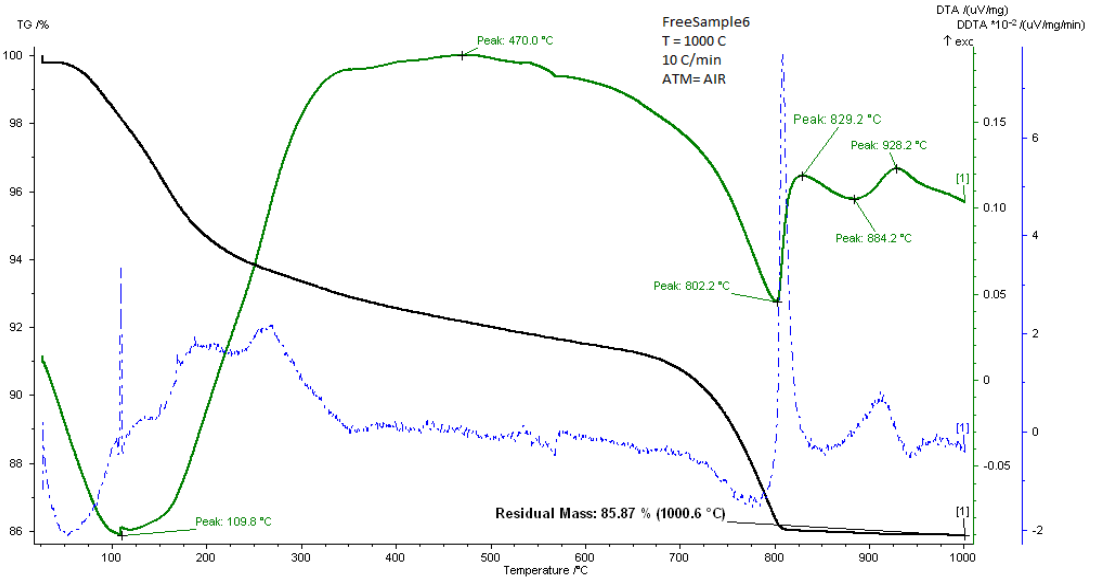

Figure 33: DTA/TGA of 100MK

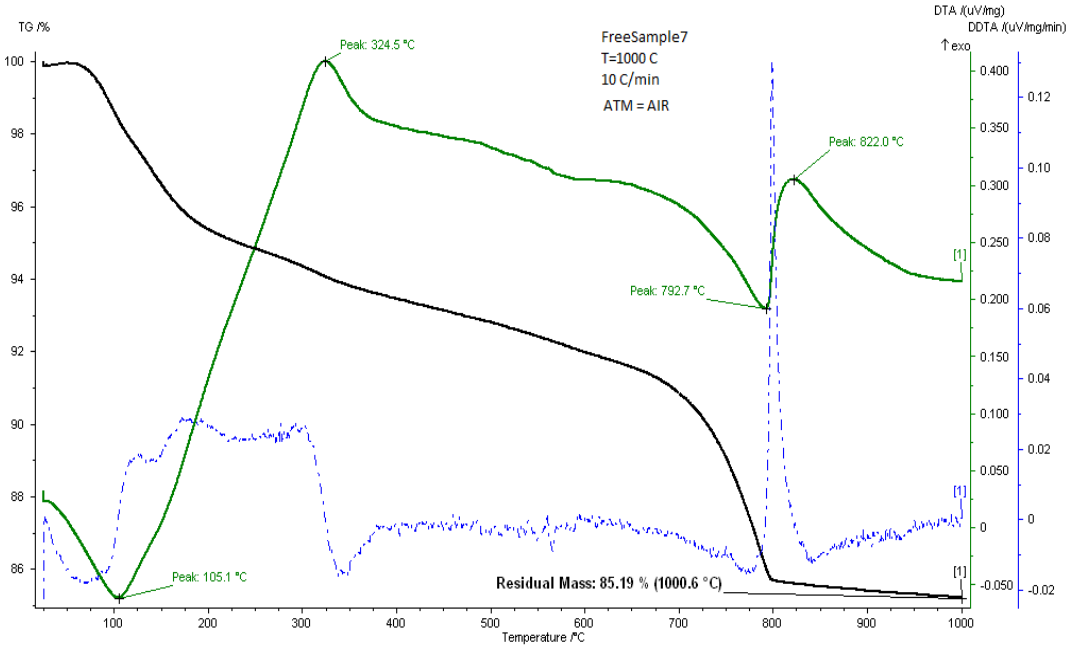

Figure 34: DTA/TGA of 50MK50GP

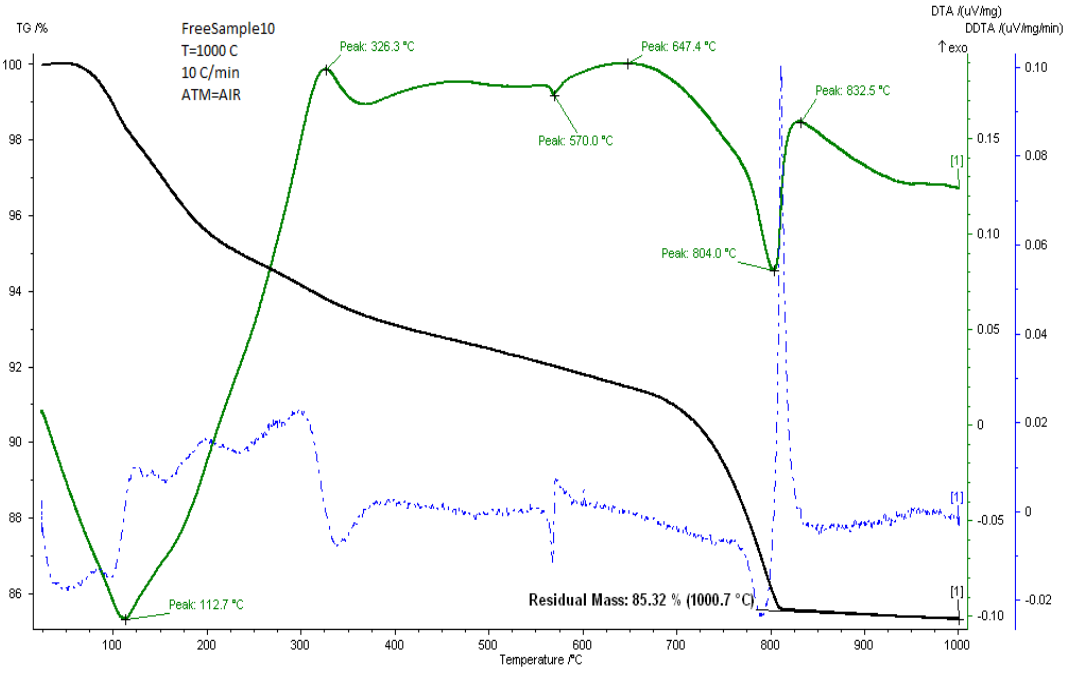

Figure 35: DTA/TGA of 50MK20RM30GP

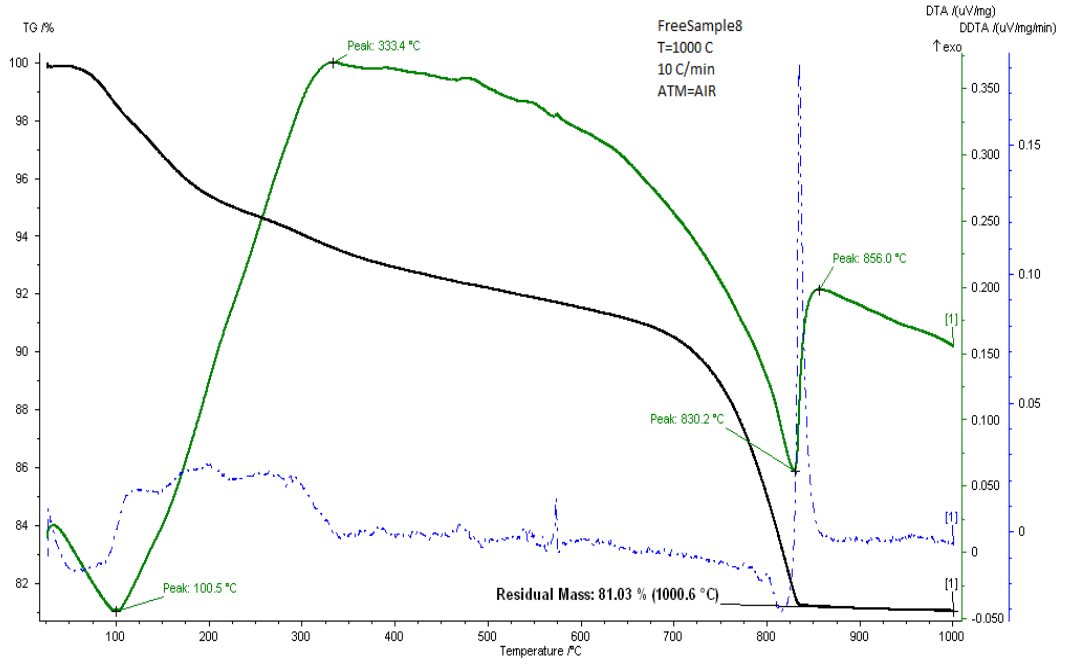

Figure 36: DTA/TGA of 50MK40RM10GP

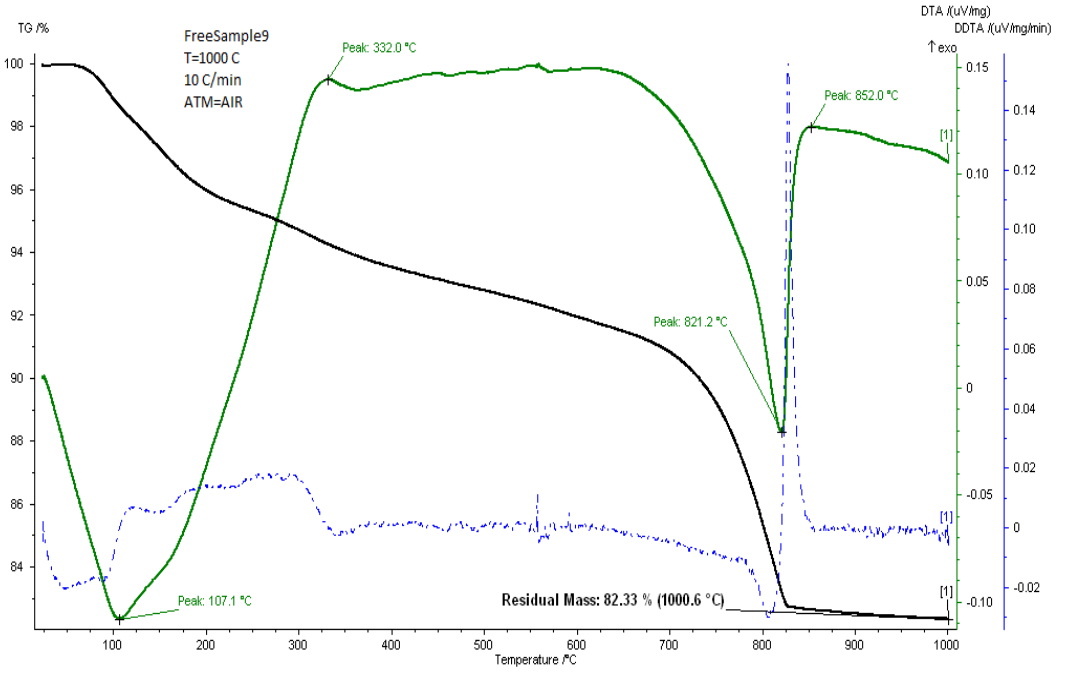

Figure 37: DTA/TGA of 50MK50RM

Figure 33 showed that the endothermic curve for sample 100MK increased smoothly from 109 °C until 470 °C (endothermic peak), and then, it decreased smoothly until 802.2 °C due to the combination of pore water evaporation and the elimination of water by the condensation of silanol or aluminol groups on the surface of the geopolymeric gel. Two peaks appeared at 829.2 °C and 920.2 °C because of the unreacted metakaolinite and the decomposition of calcite ($CaCO_3$) into CaO and dolomite $CaMg(CO_3)_2$ into CaO.MgO. Quartz (SiO_2) particles can combine with other metallic elements and oxides to form silicates that caused structural transformation.

The equation below showed the exothermic reaction, where T was either Al or Si (Duxson et al., 2007).

$$\equiv T\text{-}OH + HO\text{-}T\equiv \rightarrow \equiv T\text{-}O\text{-}T\equiv + H2O$$

Figure 34 showed the rapid increase in the endothermic curve for sample 50MK50GP was increasing at a rapid rate from 105.1 °C until 324.5 °C, this decreased smoothly until 792.7 °C because of the elimination of water by the condensation of silanol or

aluminol groups on the surface of the geopolymeric gel. Then a sharp exothermic effect was observed at around 822 °C and it decreased smoothly until 1000 °C. This endothermic peak appeared at 822 °C, and it was the nucleation temperature of waste glass (Tulyaganov et al., 2002). The GP comprised gel and unreacted GP can be associated to quartz (SiO_2) decomposition and silica combination with other metallic elements and oxides to form silicates that caused a structural transformation.

Figure 35 showed the endothermic curve for sample 50MK20RM30GP increasing rapidly from 112.7 °C to 326.3 °C (first endothermic peak) and then to 647.4 °C (second endothermic peak). Then, the curve decreased smoothly until 804 °C due to the elimination of water by the condensation of silanol or aluminol groups on the surface of the geopolymeric gel, followed by a sharp exothermic effect at around 832.5 °C that decreased smoothly until 1000 °C. This endothermic peak appeared at 832.5 °C and the reactions between 804 °C and 832.5 °C were mostly exothermic; the loss in weight was predominantly attributed to the decomposition of calcite ($CaCO_3$) into CaO, and Quartz (SiO_2) decomposition and silica combination with other metallic elements and oxides to form silicates that caused a structural transformation.

Figure 36 showed the endothermic curve for sample 50MK40RM10GP that increased rapidly from 100.5 °C until 333.4 °C (endothermic peak), which then decreased smoothly until 830.2 °C due to the elimination of water by condensation of silanol or aluminol groups on the surface of the geopolymeric gel. Then a sharp exothermic effect was observed at around 856 °C that decreased smoothly until 1000 °C, this endothermic peak appeared at 856 °C and the reactions between 830.3 °C and 856 °C were mostly exothermic and the loss in weight was predominantly caused by the decomposition of calcite ($CaCO_3$) into CaO and quartz (SiO_2) and silica combine with

other metallic elements and oxides to form silicates which caused a structural transformation.

Figure 37 showed the endothermic curve for sample 50MK50RM which increased at a rapid rate from 107.1 °C until 332 °C (endothermic peak); then, it decreased smoothly until 821.2 °C because of the elimination of water by condensation of silanol or aluminol groups on the surface of the geopolymeric gel, followed by a sharp exothermic effect at around 852 °C that decreased smoothly until 1000 °C. This endothermic peak appeared at 852 °C and the reactions between 821.2 °C and 852 °C were mostly exothermic and the loss in weight was predominantly attributed to the decomposition of calcite ($CaCO_3$) into CaO, quartz (SiO_2) decomposition, and the combination of silica with other metallic elements and oxides to form silicates which causes a structural transformation. The decomposition of dolomite $CaMg(CO_3)_2$ to MgO and $CaCO_3$ was at temperatures below 750 °C and the $CaCO_3$ decomposition to CaO was between 750 °C and 900 °C.

5.4 Stage 3: Effects of River Sand to Binder Ratio on Strength Properties

This section discussed the effects of S/B ratio on the performance of geopolymer mortar produced by MK binder partially replaced by RM and GP in different environments (sulphate environments, seawater, high temperatures, freezing and thawing conditions). Since decreasing the river sand content was consistent with the study's primary objective, which was producing more sustainable material and reducing the consumption of the natural resources, investigating the ability to achieve the same strength properties by less river sand has been presented in this section.

5.4.1 Compressive and Flexural Strength

The compressive strength of the geopolymer mortar samples is shown in Figure 38 for 3, 7, and 28 d; the results indicated that the S/B ratios affected the compressive strength slightly; the compressive strength for the S/B ratio of 2.5 was a little higher (up to 7.1%) than that for 2.25 and a little bit lower (up to 5.7%) for other samples after 28 d; At 3 and 7 d, there was no significant difference.

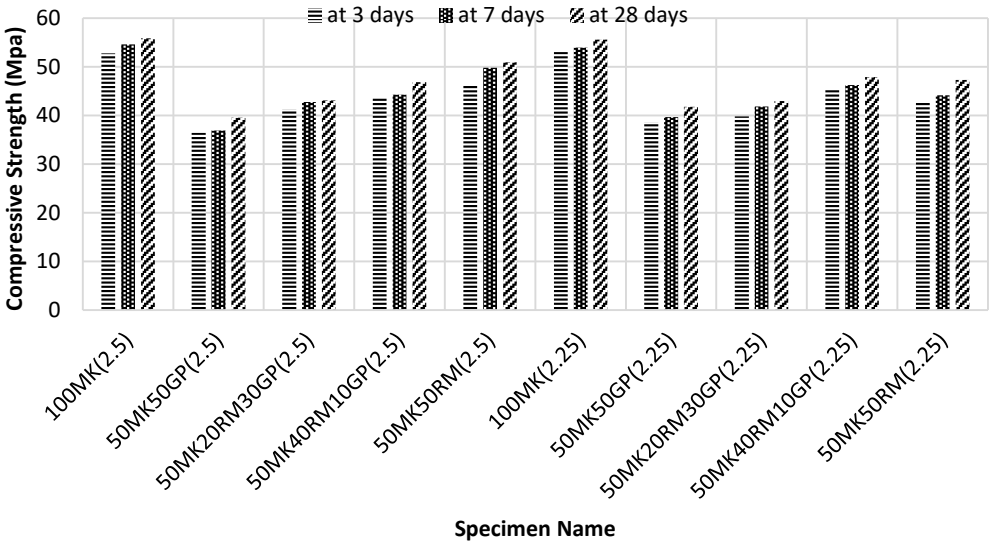

Figure 38: Compressive strength results

The flexural strength of the geopolymer mortar samples was shown in Figure 39 for 7 and 28 days; the results showed that S/B ratios affected the flexural strength slightly. The flexural strength for a S/B ratio of 2.5 was a little higher (up to 3.2%) than that for 2.25 for some samples and a little lower (up to 9.1%) for the other samples after 28 d; at 7 d, there was no significant difference.

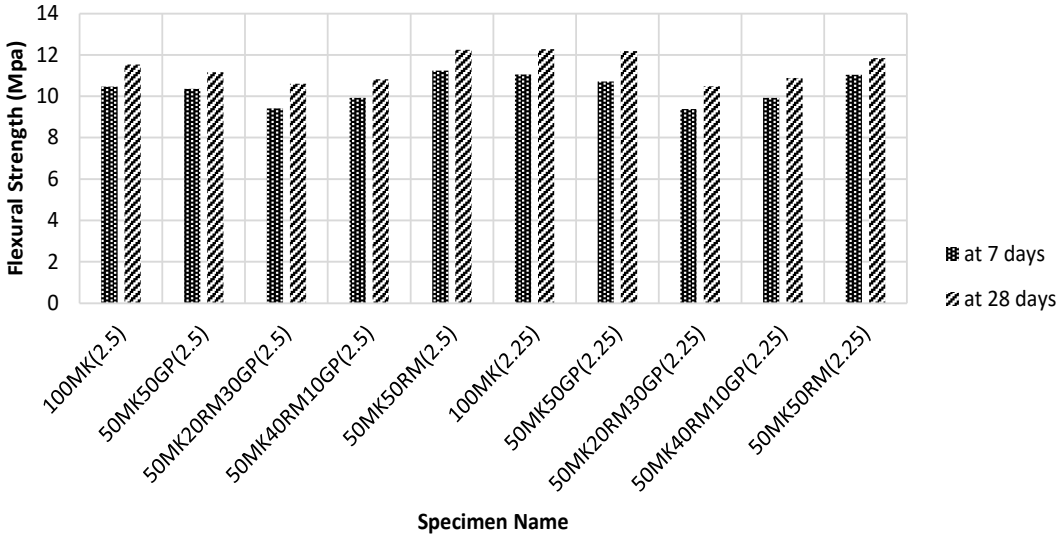

Figure 39: Flexural strength results

River sand could be considered a good filler in geopolymer matrix, showing a low concentration of impurities and grains with an irregular shape as shown in Figure 40, the sand grains have a critical role in geopolymer matrix adherence easily on the river sand grains surfaces. The SEM-EDS images presented previously show the high distribution of the N-A-S-H gel which is the main resulted product by geopolymerization among the geopolymer samples structure, which confirm the consistency between the geopolymer paste and the river sand grains, and the effective interactions which also have been observed by the mechanical properties of the samples.

The interaction on the surface of the river sand particles and increased the polysiloxo (-Si-O-), which combined with other elements in the geopolymer matrix, the alkaline solution dissolves the starting materials (MK, RM and GP) to form aluminosilicate gel. The reaction of these with the chemical elements present on the surface of the river sand grains leads to the formation of chemical bridges, the formed geopolymer

gel enables the river sand grains to be sticked together. The formed geopolymer gel and the river sand then perform as a binding matrix together.

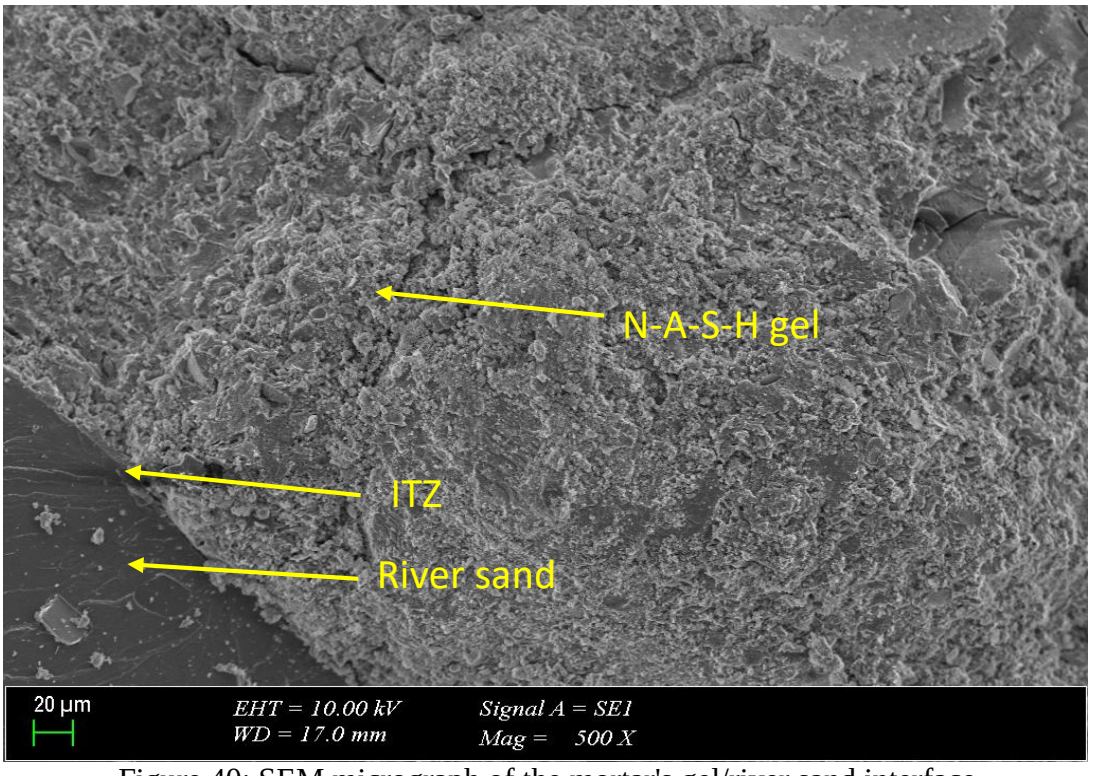

Figure 40: SEM micrograph of the mortar's gel/river sand interface

The river sand addition increases the matrix-filler interfaces and improve the cohesion, compactness, stability against cracks inside the samples. The matrix-filler bonds are effective in the compressive stress absorption and transfer it into the river sand particles. River sand addition enhance the structure of the geopolymer matrix because the river sand acted as a buffer which minimized the cracks, and due to the interaction between river sand and the matrix which formed a strong interface, in addition to the pores between the grains which allowed the geopolymer gel to fill it and resulted in minimizing the large voids (Steinerova, 2011). Also, increasing river sand content increased the Si species in the matrix, which led to an increase in the (SiO_2/Al_2O_3) ratio and the Si-O-Si bonds, which were stronger than the Si-O-Al and Al-O-Al bonds (Duxson et al., 2005).

The non-linear effects of the river sand (filler) to binder ratio as shown in the results is related to the pore size distribution change, also the high amount of silica in the river sand might decrease the full reaction between the starting materials and the activator solution. Additionally, the significant quantities of CaO in the river sand has a significant effect due to its richly presence in CaO composition as shown in the EDS analysis of the samples which weak the geopolymer matrix. On the other hand, the alkali content (K_2O, Na_2O, MgO) was higher for the geopolymer samples which contained lower river sand content in comparison to binder content, increasing the alkali content in the geopolymer had an adverse effect on the strength, as it delayed the geopolymerization process (Lingyu et al., 2021). By contrast, the decrease of (S/B) ratio increased the specific surface area, which meant a higher alkali-activated solution absorption, which had a critical role in silicate and aluminium dissolution during geopolymerization process, this factor explaining the higher strength of some samples of lower (S/B) ratio (Huseien et al., 2018).

5.4.2 Effects of Sea Water Environment on Strength Properties

The effect of seawater on the geopolymer samples could be noticed by the weight change and the strength properties terms. Due to the action of chloride, the formation of $CaCl_2$, NaCl and $MgCl_2$ products was increased, which created an accelerating effect mainly on tricalcium silicates (C_3S). In addition, seawater has reduced the voids in the geopolymer, which has led to an increase in weight values (Sikora et al., 2020; Astutiningsih et al., 2010). Over time, NaCl, Na_2SO_4, $MgCl_2$ and $MgSO_4$ salts and water showed negative effects. Alkalis passed from the sample to the seawater, while salt ions diffused from the seawater to the sample in the opposite direction. If the effect of magnesium was taken into account here, the Mg^{2+} ion led to decomposition in the main binding phases. In this case, the sodium aluminate silicate hydrate (N-A-

S-H) type was replaced by the magnesium aluminate silicate hydrate (M-A-S-H) type. In this case, it has led to a decrease in strength results by increasing the formation of microcracks (Rashad et al., 2018). Despite these effects, changes in the external appearance of the samples remained limited. Except for minor changes, no significant changes were observed in the external appearance of the samples. From here, it was observed that the damages remained at the level of micro-cracks. Thus, it was observed that the geopolymer sample preserved its stability (Zaidi et al., 2019).

Figure 41 shows the weight change after immersion of the samples in seawater for 7, 28, and 56 d at different S/B ratios (2.5 and 2.25). The results showed that the weight change in the samples prepared under an S/B ratio of 2.5 were a little higher (differences are less than 1%) than those of samples prepared under the S/B ratio of 2.25. The weight change increased with time for all samples (from 0.48% up to 1.08% at 56 d).

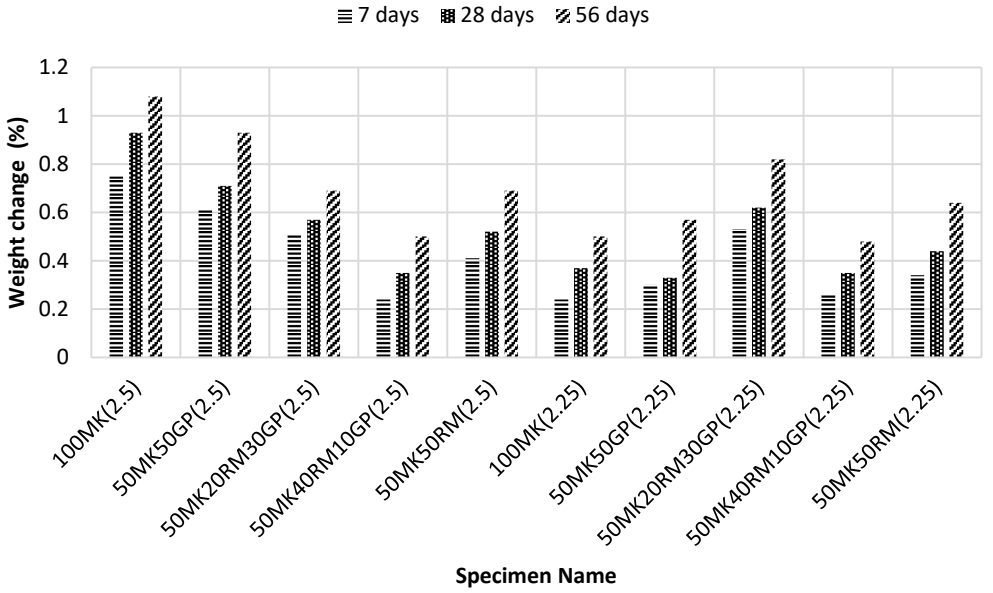

Figure 41: Weight change by sea water effects

Figure 42 shows the compressive strength of the geopolymer mortar samples after 7, 28, and 56 d in the seawater environment. The compressive strength of the samples prepared with the 2.5 S/B ratio at 56 days was a little higher (between 1.8% and 8.1%) than that of samples prepared with the 2.25 ratio; the compressive strength decreased for all sample with time (between 21.5% and 28.4% at 56 d).

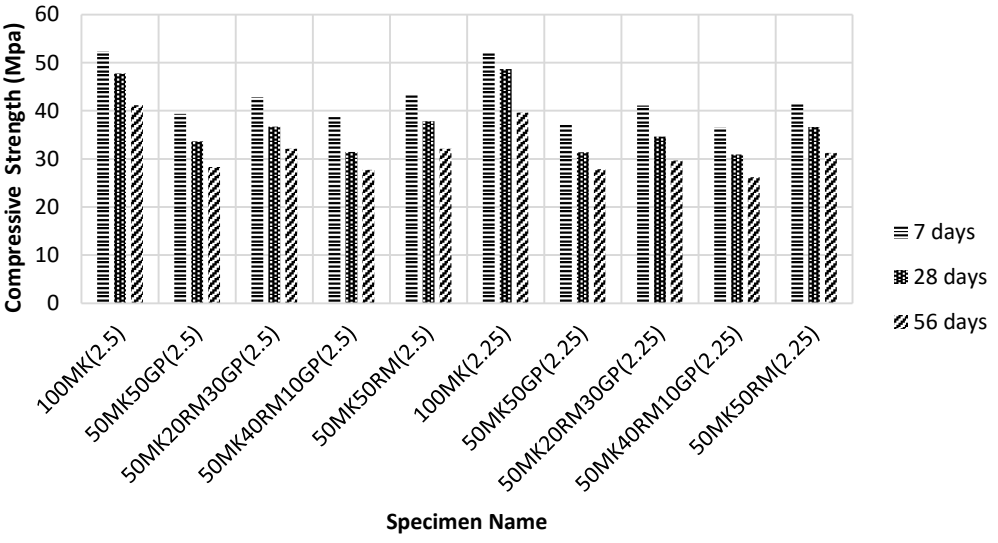

Figure 42: Compressive strength in the sea water environment

Figure 43 shows the flexural strength of the geopolymer mortar samples after 7, 28, and 56 days in the sea water environment. The flexural strength of the samples prepared with the 2.5 S/B ratio at 56 days were a little higher (between 0.6% and 1.8%) than those of samples prepared at a 2.25 S/B ratio; the flexural strength decreased for all sample with time (between 36.4% and 44.7% at 56 d).

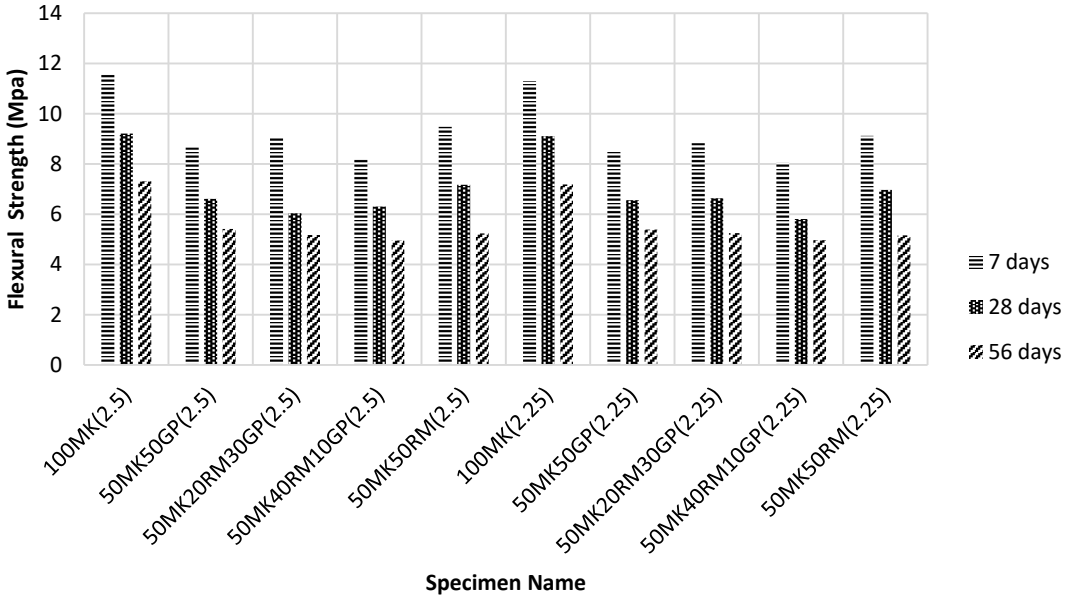

Figure 43: Flexural strength in sea water environment

The samples weight increased over time due to the voids in the geopolymer structure, which have been filled by the sodium sulphate salts and other reaction products (Tayeh et al., 2013), there was no significant difference in weight change (less than 1%) between samples of 2.5 and 2.25 (S/B) ratios for most combinations, the 100MK sample was exception due to the considerable porous structure of 2.5 (S/B) ratio sample resulted from the voids between the sand grains. The sea water decreased the strength properties of geopolymer for many reasons relates to the chemical reactions and the microstructural changes; it was known that sea water contained a significant amount of sodium sulphate, which caused the decomposition of -Si-O-Si- bonds in

the geopolymer gel structure and increasing the Si leaching from the geopolymer matrix (Bascarevic et al., 2014).

Also, it was mentioned before that increasing (S/B) ratio increased the -Si-O-Si- bonds, which were stronger than the Si-O-Al and Al-O-Al bonds (Duxson et al., 2005). So, the sulphate attack decreased the -Si-O-Si- bonds in samples of different (S/B) ratios. Therefore, the samples that contained higher (S/B) ratios have been affected lower. On the other hand, increasing river sand content in the samples causing a decrease in the total content of Ca because Ca content in the binder was much higher than the river sand, Ca content was so harmful to geopolymer samples in the seawater due to the reaction between the sodium sulphate and Ca which caused decomposition of C-A-S-H gel (Chakkor et al., 2021).

The outer surfaces of the samples are shown in Figure 44. The white layer shown on the samples indicated the formation of sodium carbonate (Na_2CO_3) which resulted by the reaction between the leached sodium hydroxide and the atmospheric carbon dioxide (CO_2), which also explain the mass increasing of the samples in addition to the previous mentioned factors (Bakharev, 2005).

Figure 44: Specimens after seawater effect

5.4.3 Effects of Magnesium Sulphate on Strength Properties

Different sulphate resistance results were obtained when geopolymer samples were immersed in a magnesium sulphate ($MgSO_4$) solution depending on the raw material and S/B ratios. Geopolymer mortars when immersed in an $MgSO_4$ solution showed a tendency to increase in weight (between 0.94% and 1.72% at 56 d) as shown in Figure 45 and decrease in compressive (between 32.5% and 49.2% at 56 d) and flexural strength (between 31.6% and 42% at 56 d) as shown in Figures 46 and 47.

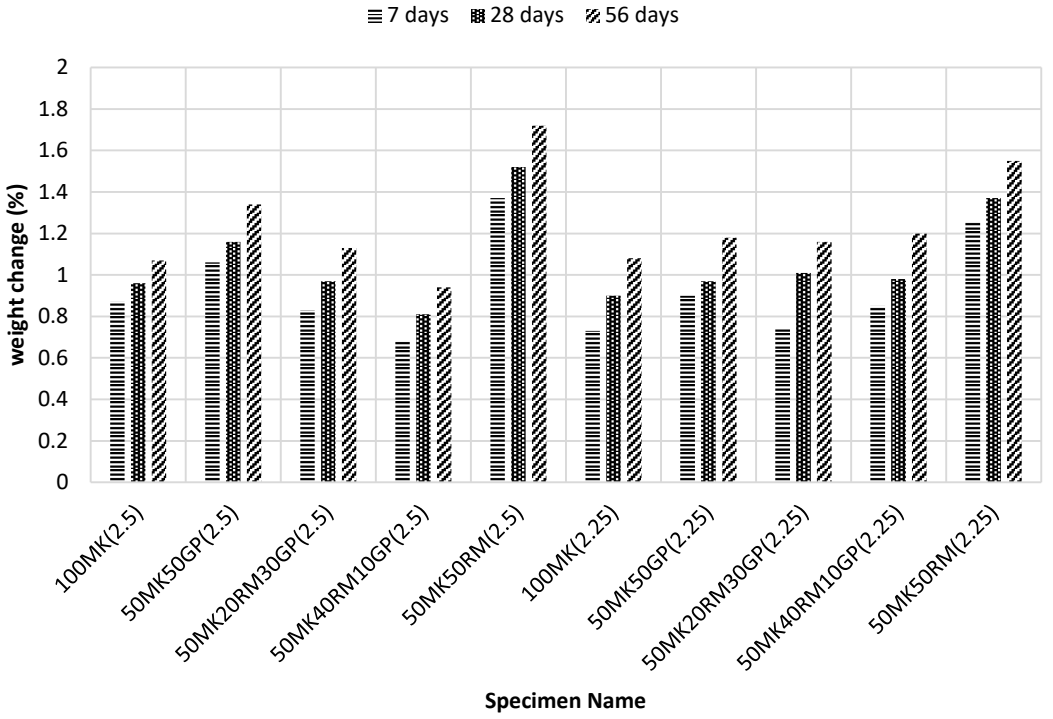

Figure 45: Weight change in a sulphate environment

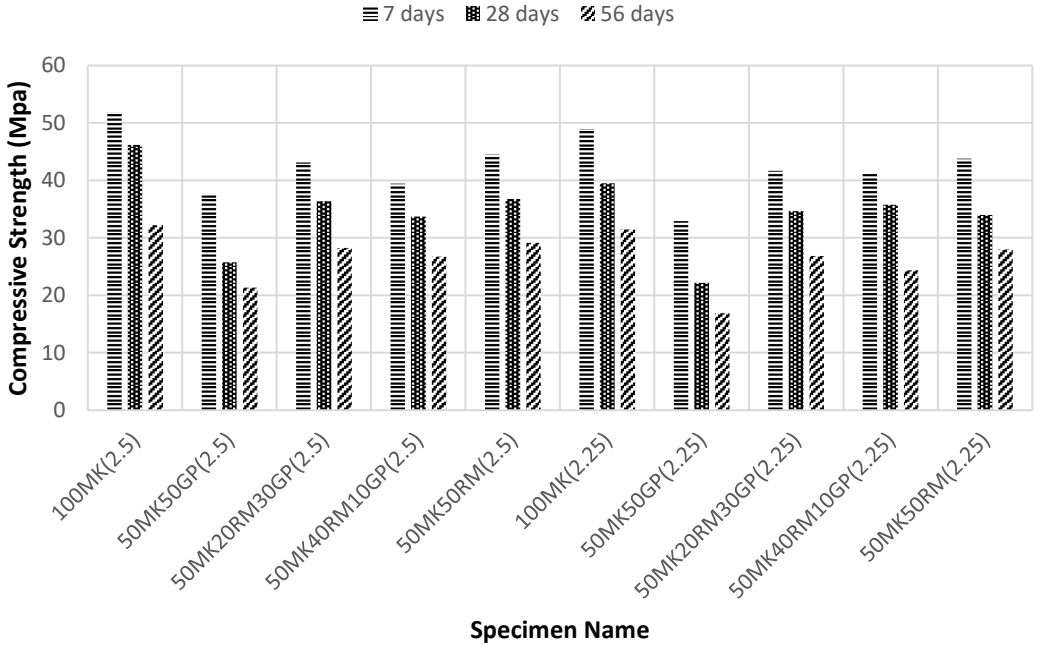

Figure 46: Compressive strength in a sulphate environment

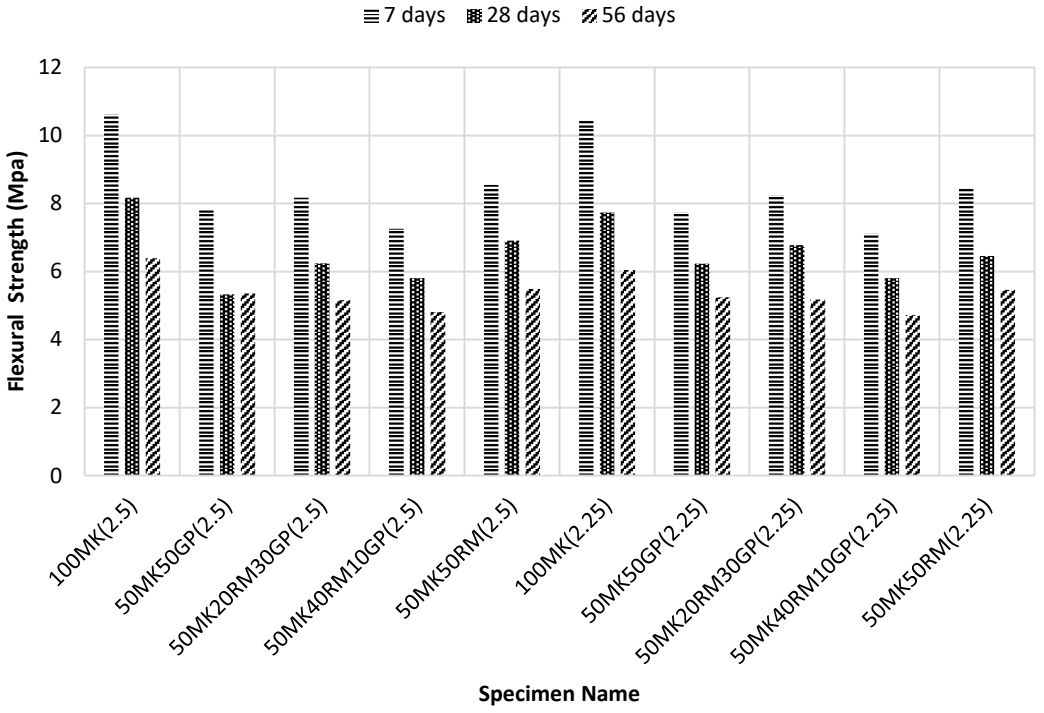

Figure 47: Flexural strength in a sulphate environment

Magnesium sulphate effect was similar to the sea water by the means of weight change and the strength properties change; the weight increased over time in the magnesium sulphate solution due to the voids in the geopolymer structure, which have been filled by the sulphate salts and other new reaction compounds (Tayeh et al., 2013). In addition, the weight increase in the lower (S/B) ratio was higher in some samples due to the higher specific surface area, enabling the sample to absorb more solution. Also, the SO_4^{-2} ions attacks to the geopolymer matrix which leads to the formation of new phases like gypsum ($CaSO_4 \cdot 2H_2O$), brucite ($Mg(OH)_2$) and ettringite, these formed phases have large volumes inside the geopolymer matrix, which increase the internal stress, the microcracks and alkalis migration from geopolymer samples into the solution through the pores are resulted by the increased internal stress (Elyamany et al., 2018). Another factor attributes to the mass increase in the geopolymer samples is the penetration of the magnesium ions into the Si-Al skeleton vacancy, which

remains on the N-A-S-H surface for a long time due to the stable Mg-O bonds, the Mg species which have been absorbed are rooted into the hydroxyl layer. The rearrangement of the geopolymer matrix by inhibiting Na ion immigration into the solution, Mg ions in the outer later forming also large Mg-SO_4 clusters (Zhang et al., 2018). On the other hand, the sulphate solution decreased the strength properties of geopolymer for many reasons related to the chemical reactions and the microstructural changes; one of the main reasons was the ion-exchange reaction occurred between the sulphate solution and the network-like structure, and the decomposition of C–S–H, which was the reaction product from magnesium ions. During the sulphate attack, the pores of the N-A-S-H gel's network structure altered, and microcracks occurred progressively, causing the geopolymer structure to deteriorate (Wang et al., 2020).

The magnesium sulphate caused the decomposition of -Si-O-Si- bonds in the geopolymer gel structure and increasing the Si leaching from the geopolymer matrix, resulting in diffusion to the geopolymer matrix formed (Bascarevic et al., 2014; Sata et al., 2012; Salami et al., 2017). In addition, it was mentioned before that increasing river sand to binder ratio increases the -Si-O-Si- bonds, which were stronger than the Si-O-Al and Al-O-Al bonds, so the higher (S/B) ratio samples were more resistant (Duxson et al., 2005).

Furthermore, the sulphate attack decreased the -Si-O-Si- bonds in different (S/B) ratios samples. Therefore, the samples that contained higher (S/B) ratios have been affected lower. On the other hand, increasing river sand content in the samples causing a decrease in the total content of Ca because Ca content in the binder was much higher than the river sand, Ca content was so harmful to geopolymer samples in the sulphate solution due to the reaction between the magnesium sulphate and Ca which caused

decomposition of C-A-S-H gel (Chakkor et al., 2021). When the changes of geopolymer samples under the influence of magnesium sulfate were examined, no significant damage was observed on the sample surfaces. It was observed that the resulting damages remained at the level of micro-cracks similar to sea water. Thus, it was observed that the geopolymer samples preserved their stability (Arslan et al., 2019). The outer surfaces of the samples are shown in Figure 48. The characteristics of N-A-S-H gel prevent the deterioration of the samples even in the sulphate solutions. However, the changes of strength properties depend on the type of the used activator solution, and the cations concentration and type into the solution (Bakharev, 2005).

The white layer shown on the samples in Figure 48 indicated the formation of sodium carbonate (Na_2CO_3) which resulted by the reaction between the leached sodium hydroxide and the atmospheric carbon dioxide (CO_2), which also explain the mass increasing of the samples in addition to the previous mentioned factors (Bakharev, 2005).

Figure 48: Specimens after magnesium sulphate effect

5.4.4 Freezing and Thawing Resistance

Table 16 and Figures 49 and 50 shows that all sample weights decreased at 50 and 100 F–T cycles; the weight loss increased with time; and it was between the range of 0.74% and 2.24%. Further, the S/B ratios had no significant effects under the F–T conditions. Further, the f_c decreased (6.4- 34.6% reduction at 100 cycles) and f_f also decreased (27.3% - 45.2% reduction at 100 cycles) after 100 cycles.

Table 16: Weight loss after freeze–thaw cycles

Mix	Combination	Initial Weight (gram)	W (50 cycle)	W (100 cycle)	W loss (50 cycle)	W loss (100 cycle)	loss % (50 cycle)	loss % (100 cycle)
1	100MK (2.5)	458.6	455.7	454.8	2.9	3.8	0.63	0.83
2	50MK50GP (2.5)	443.4	439.3	437.7	4.1	5.7	0.92	1.29
3	50MK20RM30GP (2.5)	489.4	486	484	3.4	5.4	0.69	1.1
4	50MK40RM10GP (2.5)	457.9	455.6	454.1	2.3	3.8	0.5	0.83
5	50MK50RM (2.5)	455.8	448	445.57	7.8	10.23	1.71	2.24
6	100MK (2.25)	464.7	462.4	460.9	2.3	3.8	0.49	0.82
7	50MK50GP (2.25)	457.8	455.2	454.1	2.6	3.7	0.57	0.81
8	50MK20RM30GP (2.25)	456.7	453	451.5	3.7	5.2	0.81	1.14
9	50MK40RM10GP (2.25)	462.3	460.1	458.9	2.2	3.4	0.48	0.74
10	50MK50RM (2.25)	437.6	434.8	433.5	2.8	4.1	0.64	0.94

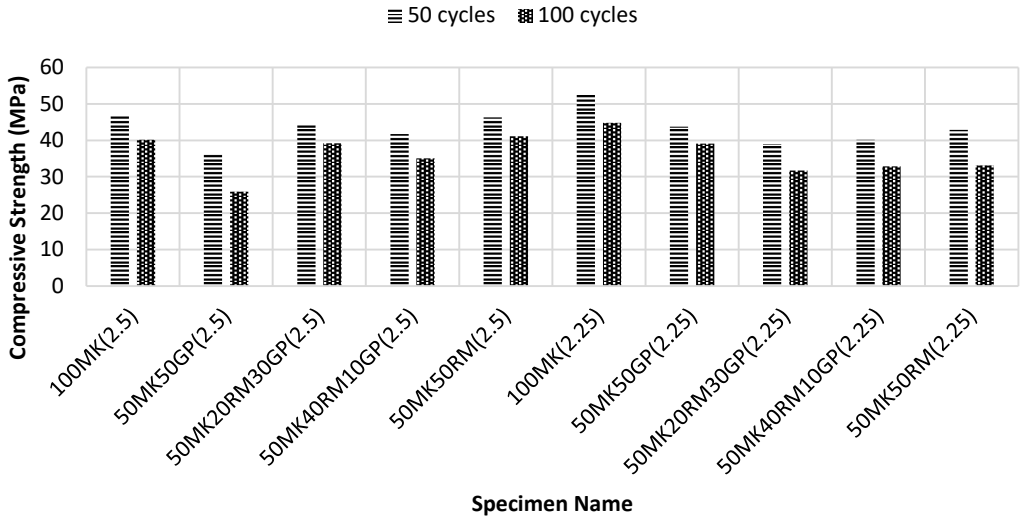

Figure 49: Compressive strength after 50 and 100 freeze–thaw cycles

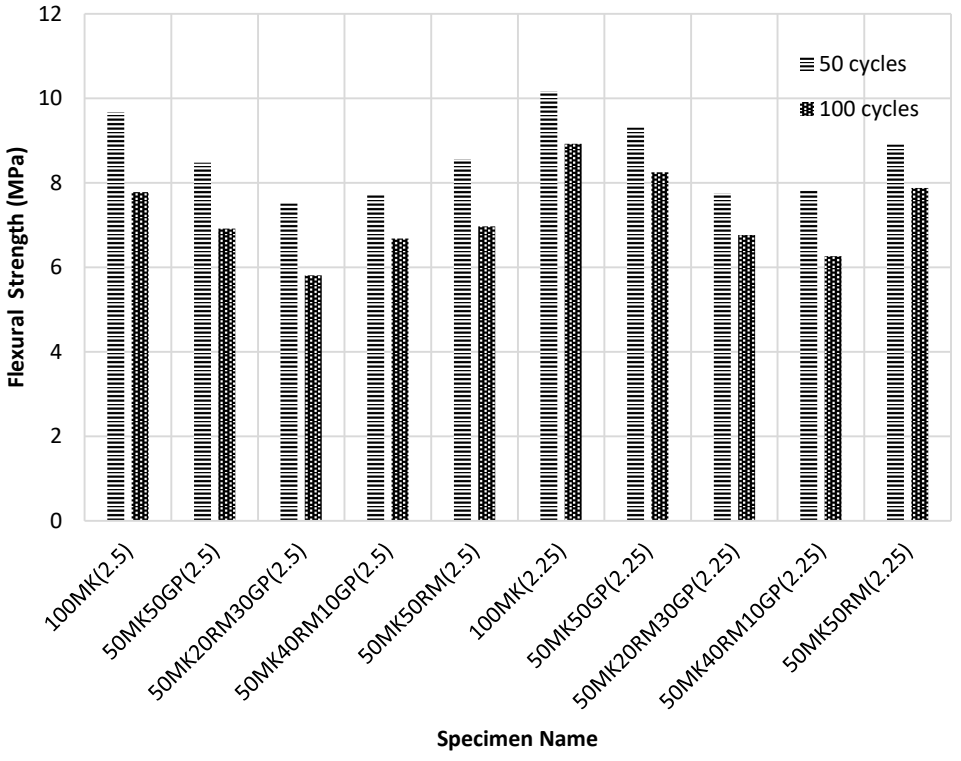

Figure 50: Flexural strength after 50 and 100 freeze–thaw cycles

During freezing and thawing, the production of crystals and the pace of degradation were the two most important factors that affected the samples. Furthermore, the Si/Al ratio influenced the geopolymer's freezing-thawing resistance, as geopolymers with

greater Si/Al ratios had higher porosity in correspondence to the results of physical properties. The porosity role explained the slight variance (maximum of 5.4% difference in f_c) in strength properties of 2.5 and 2.25 (S/B) samples after freeze-thaw cycles, despite the fact that strength properties of 2.5 ratio samples were higher than samples of 2.25 ratios before freeze-thaw cycles (Lingyu et al., 2021).

In addition to ice expansion in the pores and fissures, moisture dilation in combination with matrix internal stress was the cause of disintegration. At the end of the test, a decrease in strength values was observed. The expansion of the water in the mortar due to freezing caused a decrease in strength. The hydraulic pressure built up in the matrix around the ice increased as the empty spaces filled. When the acting force exceeded the tensile strength in the mortar structure, microcracks and subsequent deterioration occurred. Due to this effect, the strength values decreased (Pilehvar et al., 2019; Allahverdi et al., 2014; Basheer et al., 2001). The strength values before the freeze-thaw test affected the amount of microcrack formation. The air void ratio effect was also important. An increase in air voids increased the strength loss (Topcu et al., 2017). However, the geopolymer samples showed significant resistance. This was related to the compact structure and good adhesion of geopolymer matrices. When the surfaces of the samples were carefully examined after 100 cycles of freeze-thaw test, it was observed that there was no serious damage on the sample surfaces, but the damage remained at the micro-crack level (Aygörmez, 2021). The appearance of the samples at the end of the freeze-thaw test is shown in Figure 51.

Figure 51: Specimens after freezing-thawing effect

The limited effect of freezing and thawing on the external structure and the strength properties of the samples either 2.5 or 2.25 S/B ratio is due to the critical role of the sand presence in significant quantities, sand grains functioned as a buffer, blocking the fractures. Besides river sand's role in increasing the porosity, material cohesiveness was also critical in providing frost resistance, as evidenced by strength tests performed on samples before freezing and thawing. The presence of river sand in the samples improved the strength considerably due to their interaction with the matrix, which rearranged the matrix's structure on the grain surface and generated a strong interface, preventing cracks and providing frost resistance (Steinerova et al., 2011).

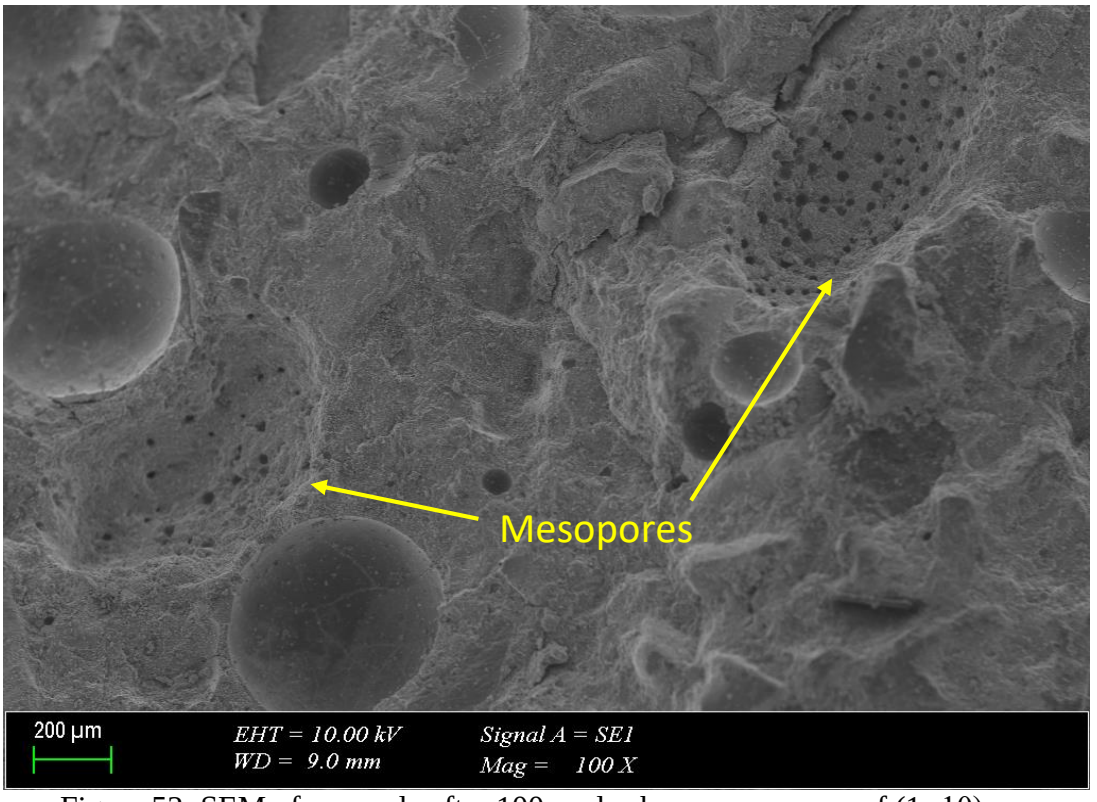

Figure 52: SEM of a sample after 100 cycle shows mesopores of (1- 10) µm

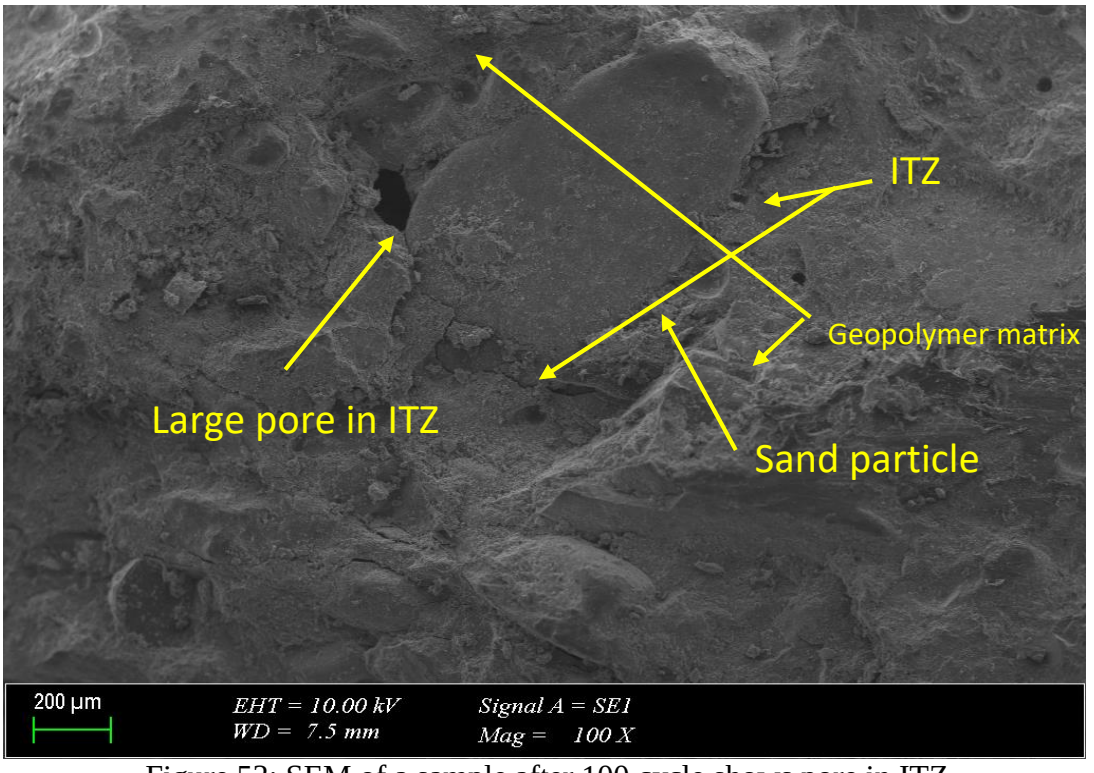

Figure 53: SEM of a sample after 100 cycle shows pore in ITZ

In SEM images shown in figure 52 a questionable 1- 10 μm mesopores have been observed, it indicates a rearrangement of the geopolymer matrix structure. Because condensed water plays such an important part in pore formation, water transport may play a function in mesopore enlargement. The key difference between the structure of interfacial transition zone (ITZ) and the primary matrix, such as the matrix near or far from the grains, could be the conditions in which condensate water is collected in mesopores. While water far from the sand grains has ample space to fill the numerous small nanoscale fissures, water close to the sand grains may have less space to condense, resulting in the formation of large micrometre-sized mesopores in the ITZ as shown in Figure 53 and agree to a previous study (Steinerova et al., 2011). The large pores formed around the sand grains in ITZ and the concentrated mesopores around the sand grains could explain the higher strength results of some samples which have lower S/B ratio (2.25), due to the high specific surface area of the binder materials, which led to more absorbed water inside the structure, and to avoid pores enlargement during water condensation.

5.4.5 High Temperatures Resistance of Geopolymer Mortar Samples

Figures 54, 55, and 56 show that the maximum weight loss at 800 °C was 18.55% for the 100MK combination with a S/B ratio of 2.25; however, for a S/B ratio of 2.5, the same combination was 15.28%, the significant weight loss of the 100MK sample is due to the water absorption of 100MK which is 8.56% which is the highest rate among the samples. This meant that it was meaningful to use some binary and ternary binder composites like 50MK20RM30GP, which had an 8.87% weight loss for the 2.25 S/B ratio to avoid the huge weight loss.

The effects of hight temperature started by the free and poorly bounded water removal at approximately 200 ◦C, the water vapour started to form in this stage, the

process of removing water from the materials starts significantly. Microcracks and pore structural changes occur as a result of rising intrapore pressure. Several factors influence the magnitude of the geopolymer microstructural alterations under high temperatures. One of these factors is the amount of water in the geopolymer matrix, the water content is determined due to the material absorption capacity and the desired workability of the mix, and as mentioned previously the activator solution (which contains the water) to binder ratio is fixed to 1 for all mixes, and the water absorption of the samples is in the range 7.44 to 8.56%, the high weight loss (15.28%) at 800◦C was for 100MK (2.5 S/B) due to the high-water absorption (8.56%) and the weak binding of water molecules in the geopolymer matrix structure (Kong et al., 2007), this is in agreement to the results of Thermogravimetric Analysis (TGA) in section 5.3.6 ,which shows that 100MK loss around 8% (92% residual mass) around 550 °C. Changes in the microstructure of the geopolymer are caused by sintering and thickening processes in the matrix starting at around 550°C (Duxson et al., 2006; Bakharev, 2005). The difference in thermal expansion coefficients between the binder and aggregate will also have an impact on the material's microstructure. After being exposed to high temperatures, samples show cracks in the binder matrix, the contact zone between the matrix and the aggregate, and cracks through the aggregate grains. The extent of aggregate damage is determined by the chemical structure of the material (Hager, 2012). According to Khoury (1992), at 350°C some silica aggregates (river sand) can decompose.

For compressive and flexural strength, even sample 100MK (specimens 1 and 6) showed significant weight loss (18.55%); it achieved the highest compressive strength at 800 °C for S/B ratios of either 2.5 or 2.25; then, sample 50MK50RM (specimens 4 and 9) showed the second-highest compressive strength at 800 °C for either S/B ratio of 2.5 (21.06 MPa) or 2.25 (19.94 MPa), as shown in Figures 55 and 56.

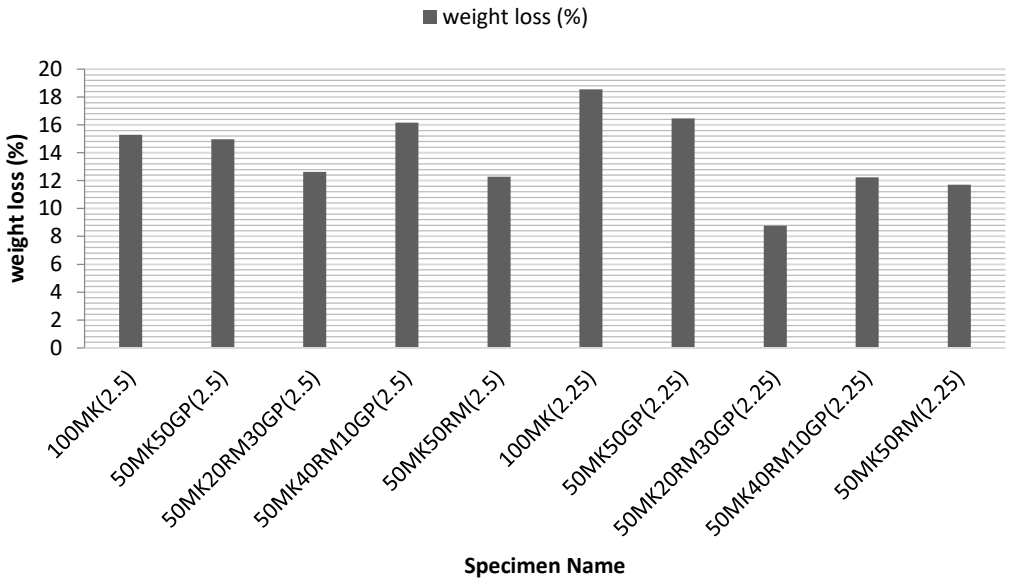

Figure 54: Weight loss after 800 °C exposure

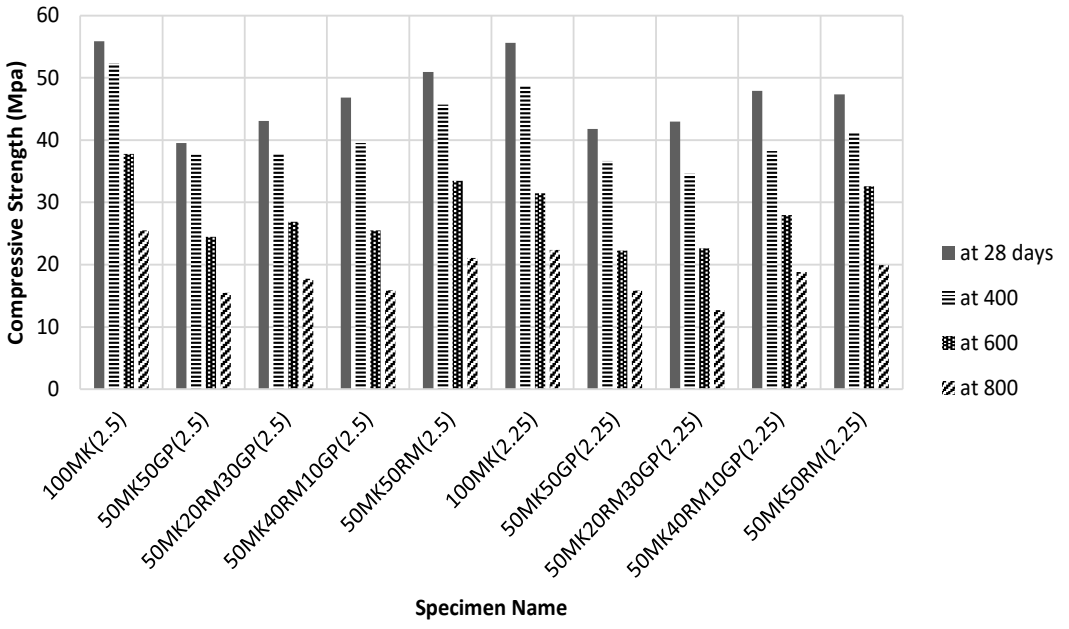

Figure 55: Compressive strength (MPa) after high temperatures test

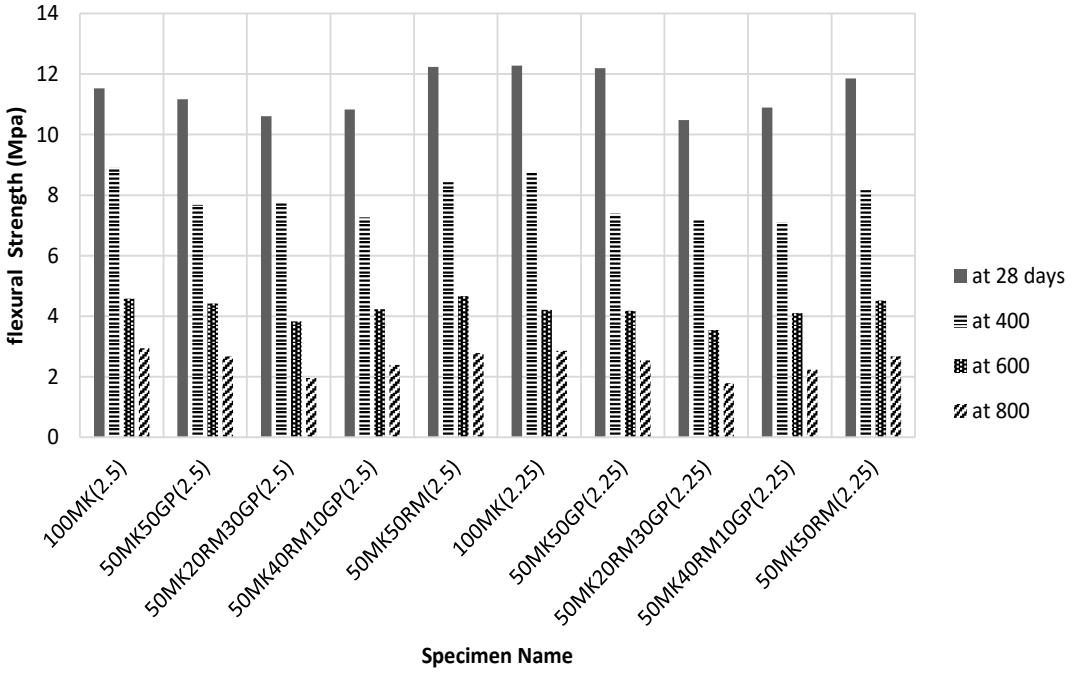

Figure 56: Flexural strength (MPa) after high temperatures test

The Si/Al ratio, alkali content, and activator solution quantity all played a role in the stability of geopolymer structures when exposed to high temperatures (Ye et al., 2014); High alkali content was detrimental to the strength properties of geopolymer specimens at high temperatures; alkalis inhibited crystallization, particularly at temperatures below 400° C; this stage was critical because formed crystals can reduce the effects of water evaporation and structural instability; and, as previously stated, higher (S/B) ratio samples had lower alkali content.

Furthermore, raising the Si/Al ratio caused the formation of additional zeolites, which were thermally stable and increased the material's strength properties stability by increasing the internal strain. Furthermore, higher (S/B) ratio samples absorbed less liquid into the structure due to the lower specific surface area, resulting in lower strength and weight loss than lower (S/B) ratio samples.

Higher (S/B) ratio samples, on the other hand, had a lower activator solution to binder (A/B) ratio, resulting in lower strength loss, as the activator solution evaporation during high-temperature exposure caused thermal structural disintegration (Abdulkareem et al., 2014). The visual change of the samples after 800ºC temperature is shown in Figure 57. The photographs of the samples were taken after the test when the temperatures of the samples returned to room conditions. When the surfaces were examined, the colour change was seen in the photographs. It has been observed that the sample surfaces tended to be more brittle and rougher due to the damage effect on the geopolymeric chains. Despite these conditions, surface cracks in the sample were limited. This showed that the geopolymer samples maintained their stability at high temperatures (Aygörmez, 2021).

Figure 57: Specimens after 800^{o}C effect

5.4.6 Microstructure and Pore Structure Changes

Figures 63 and 68 show the SEM analysis of the samples after 800 °C exposure, which revealed that MK-based geopolymers had more extensive microstructure degradation. This was attributed to the MK-based geopolymers' lower interconnectivity of the pore structure (Kong et al., 2008). At temperatures around 800 °C and above, sintering and densification as shown in figure 58 of the geopolymer matrix would cause changes in the microstructure and minor microcracks, the same image clearly shows the continuity of the geopolymeric matrix, which is correspondent to the reasonable behaviour of the specimens in the relevant strength tests.

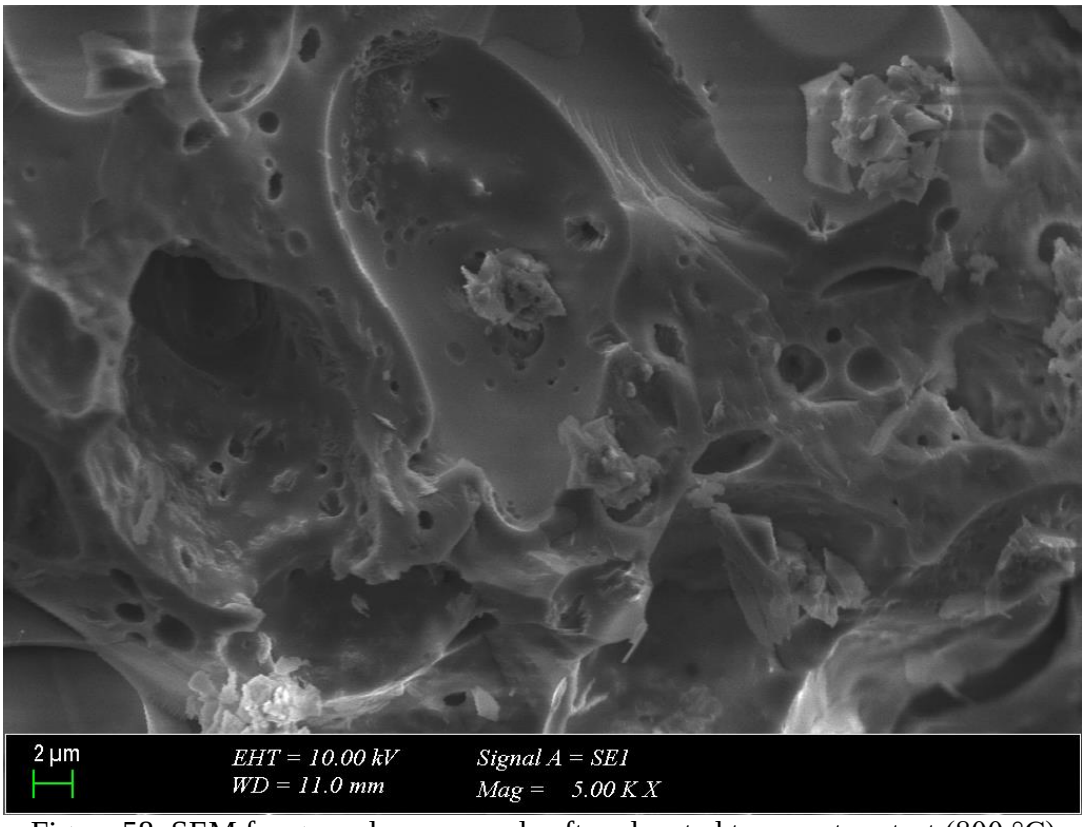

Figure 58: SEM for geopolymer sample after elevated temperature test (800 °C)

At 800 ℃, the number of cracks and the width of the ensuing microcracks, which can reach 10 µm, could be observed clearly. Samples show cracks in the binder matrix as shown in Figure 59, the contact zone between the matrix and the aggregate, and cracks through the aggregate grains. microcracks are mostly observed in the contact zone (ITZ) between the grain and the matrix as shown in Figure 60 and 61, as well as within the matrix. Cracks with a width of 1–2 µm are the most common, although microcracks can reach a width of 5 µm. At 800°C, cracks on river sand grains begin to appear as shown in SEM image in Figure 62.

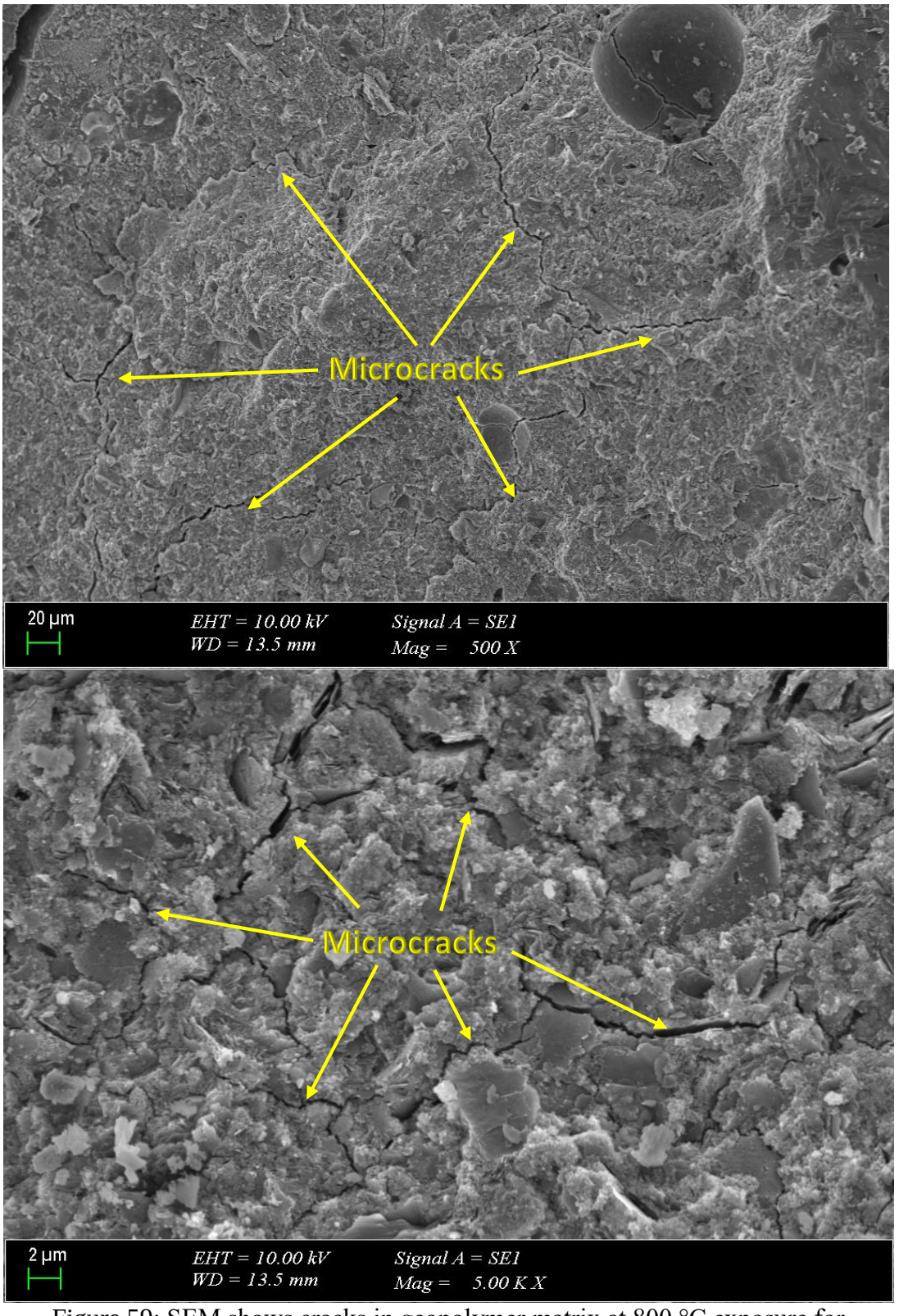

Figure 59: SEM shows cracks in geopolymer matrix at 800 °C exposure for 50MK50RM

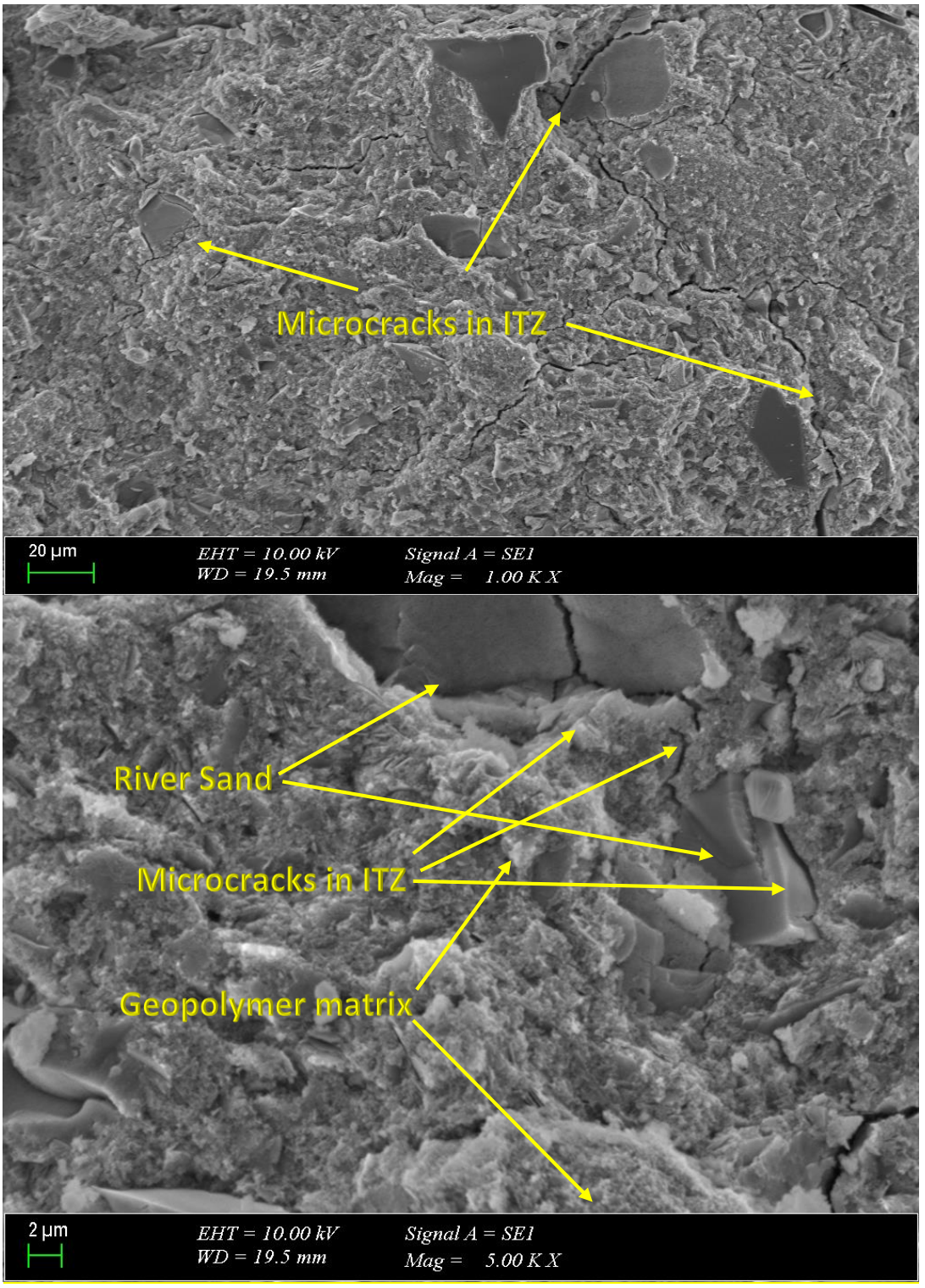

Figure 60: SEM shows microcracks in the ITZ for 50MK50GP after 800 °C exposure

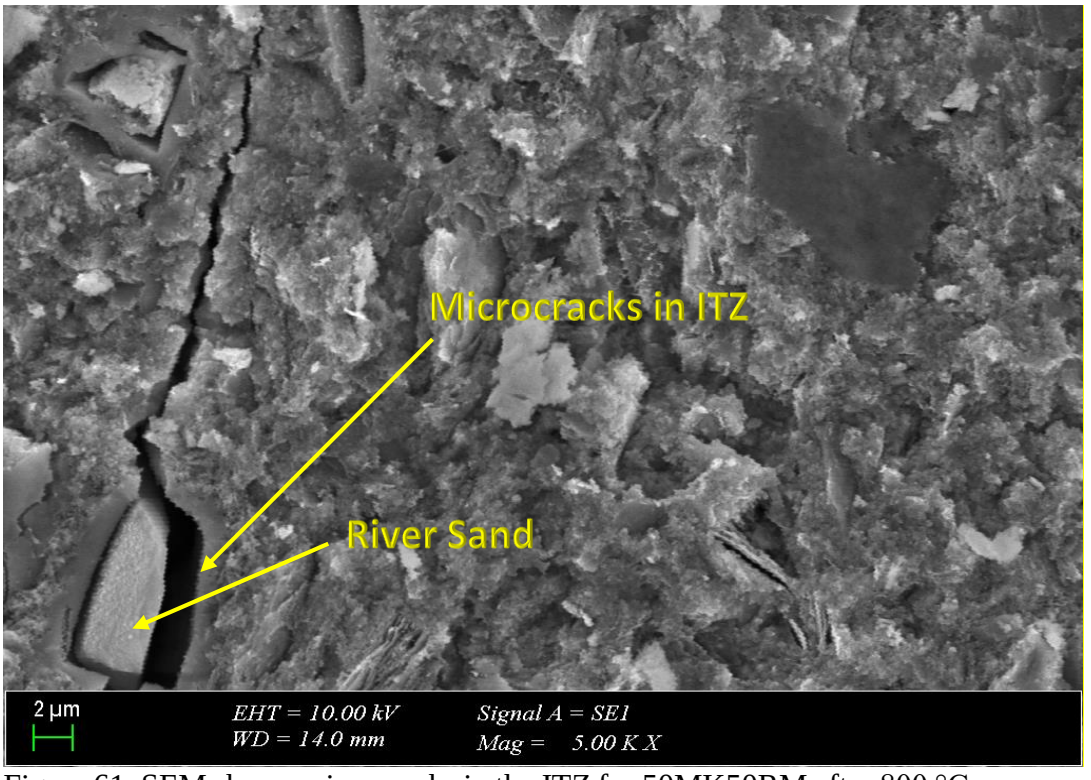

Figure 61: SEM shows microcracks in the ITZ for 50MK50RM after 800 °C exposure

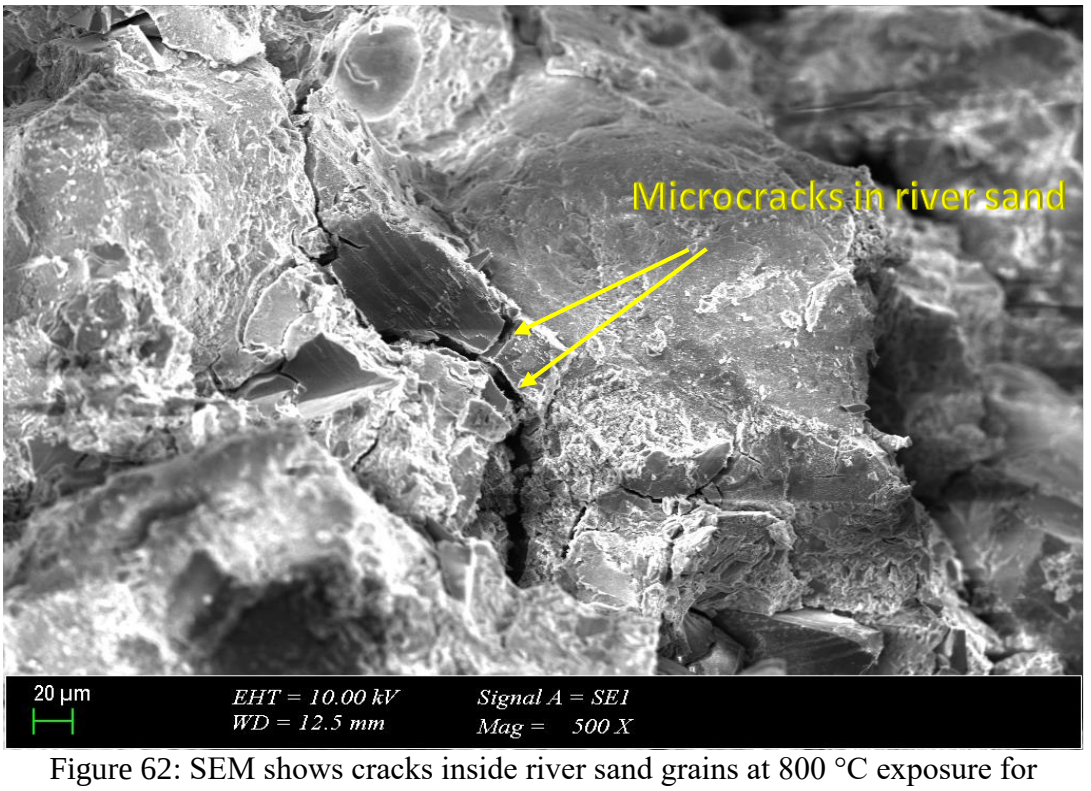

Figure 62: SEM shows cracks inside river sand grains at 800 °C exposure for 50MK50GP

The geopolymer sample after high-temperature exposure had fewer voids and exhibited smoother texture, as shown in the SEM images in Figures 63–72. Figures 63, 64, 68, and 69 show the microcracks in the order of 0.1 mm to 0.2 mm developed on the surface of 100% MK-based specimen and 50%MK and 50% GP-based specimen, whereas there were no clear major surface cracks on other geopolymer mortar specimens.

The SEM images showed that the geopolymer samples microstructure were stable even after 800 °C exposure, which encouraged the usage of the geopolymer heat resistance properties. Further, the S/B ratio had no significant effect on the microstructure.

SEM of samples (S/B ratio = 2.5) after 800 °C temperature exposure:

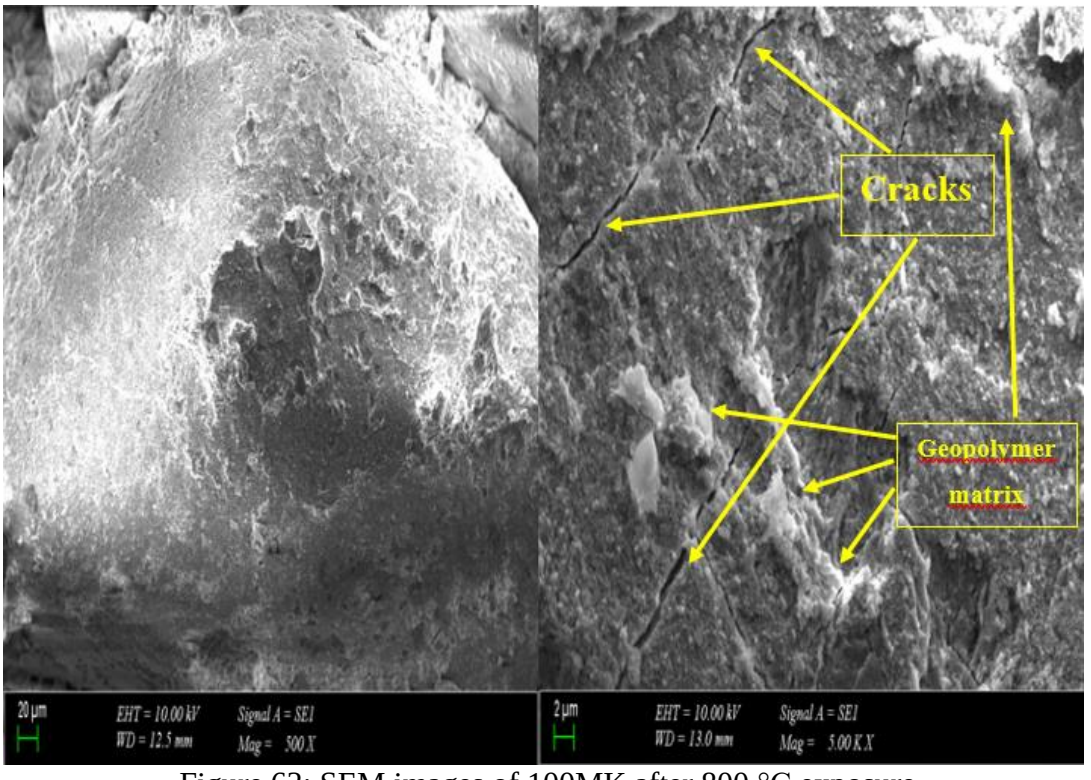

Figure 63: SEM images of 100MK after 800 °C exposure

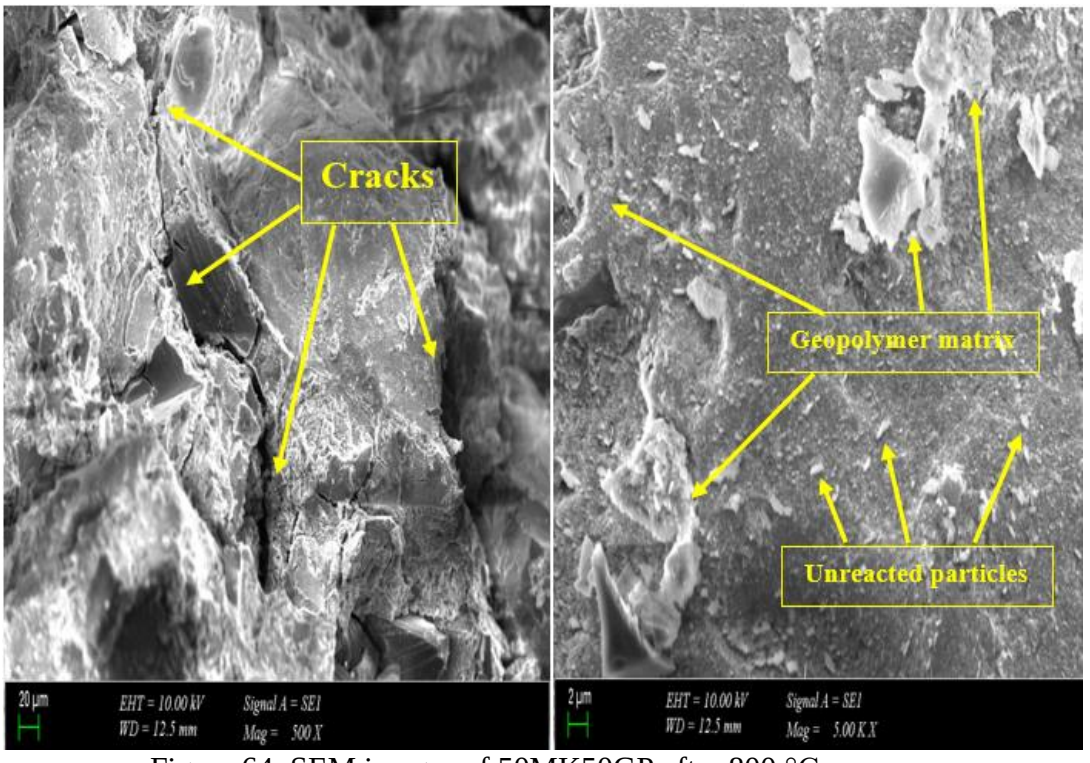

Figure 64: SEM images of 50MK50GP after 800 °C exposure

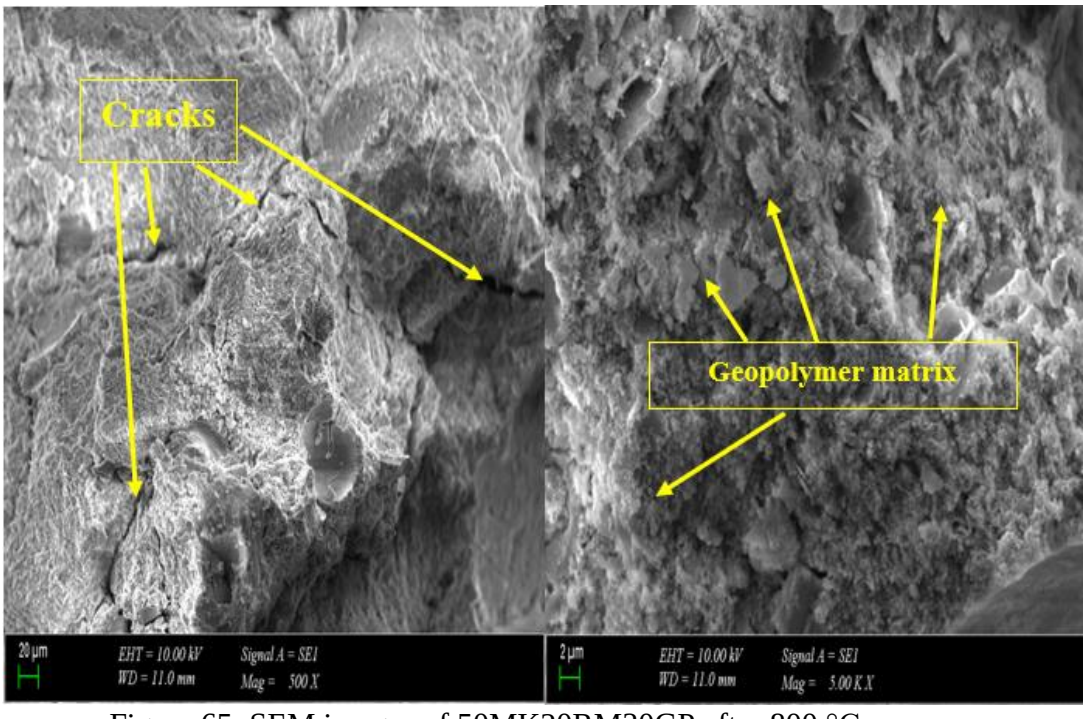

Figure 65: SEM images of 50MK20RM30GP after 800 °C exposure

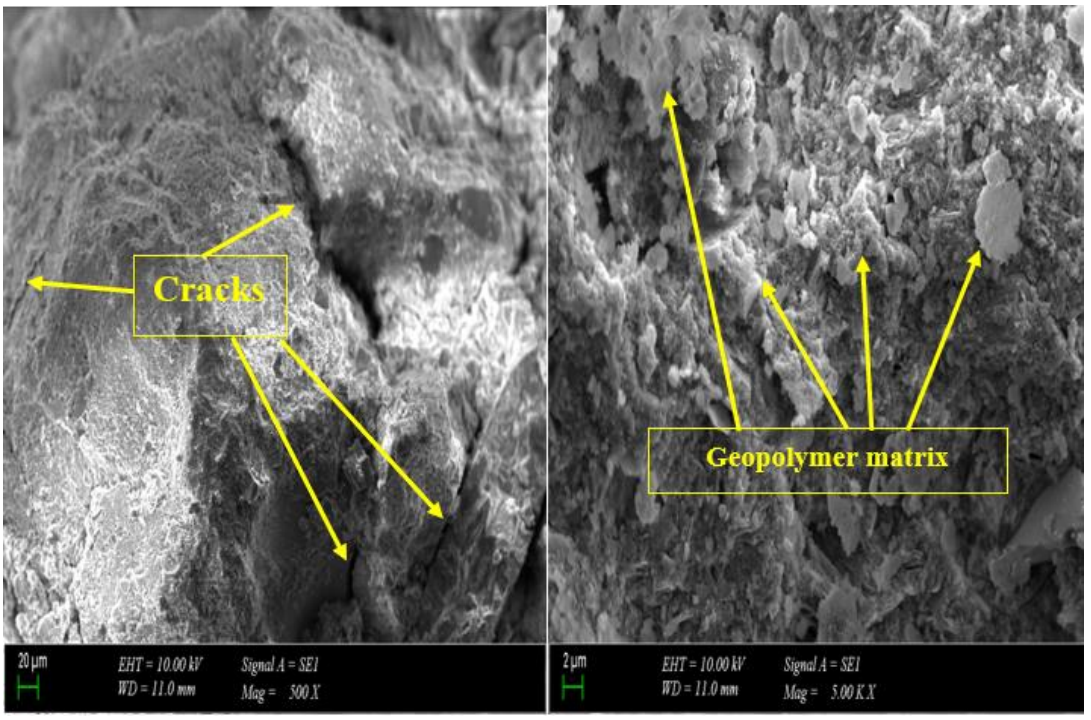

Figure 66: SEM images of 50MK40RM10GP after 800 °C exposure

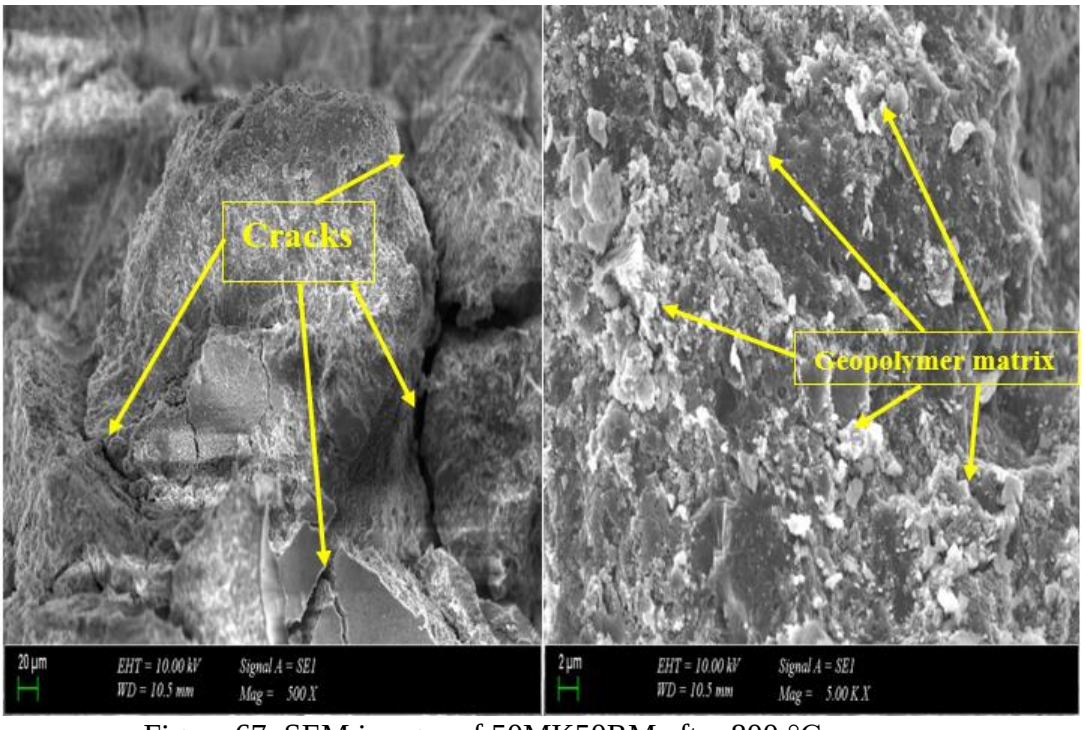

Figure 67: SEM images of 50MK50RM after 800 °C exposure

SEM of samples (S/B ratio = 2.25) after 800 °C exposure:

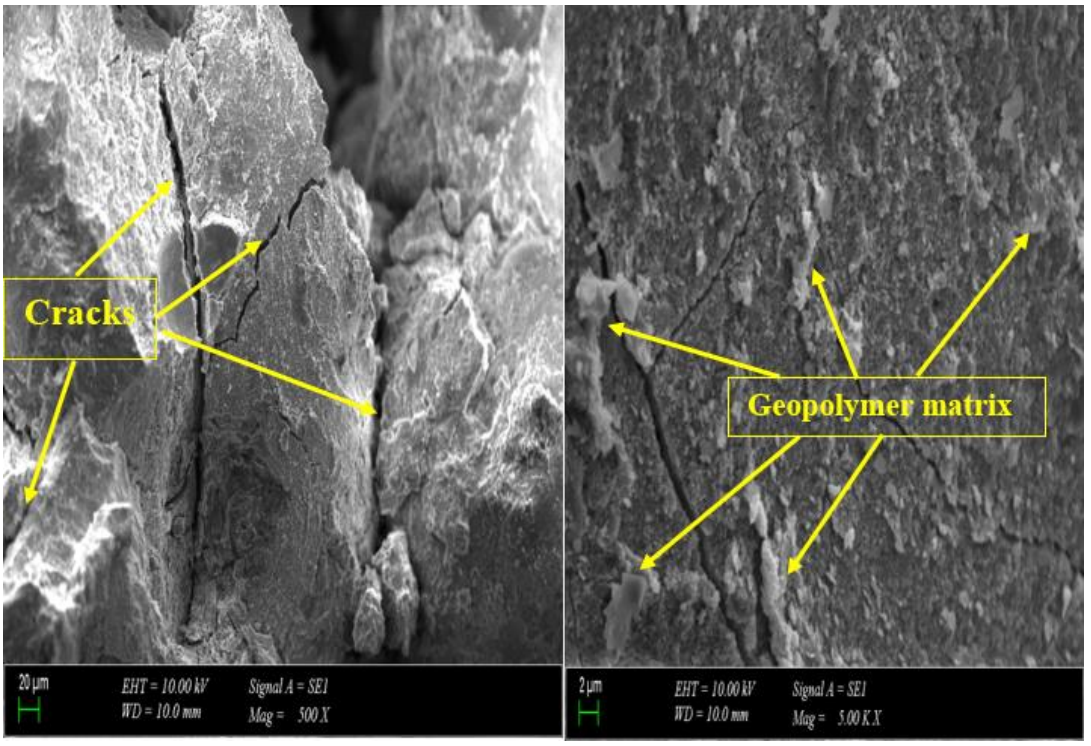

Figure 68: SEM images of 100MK after 800 °C exposure

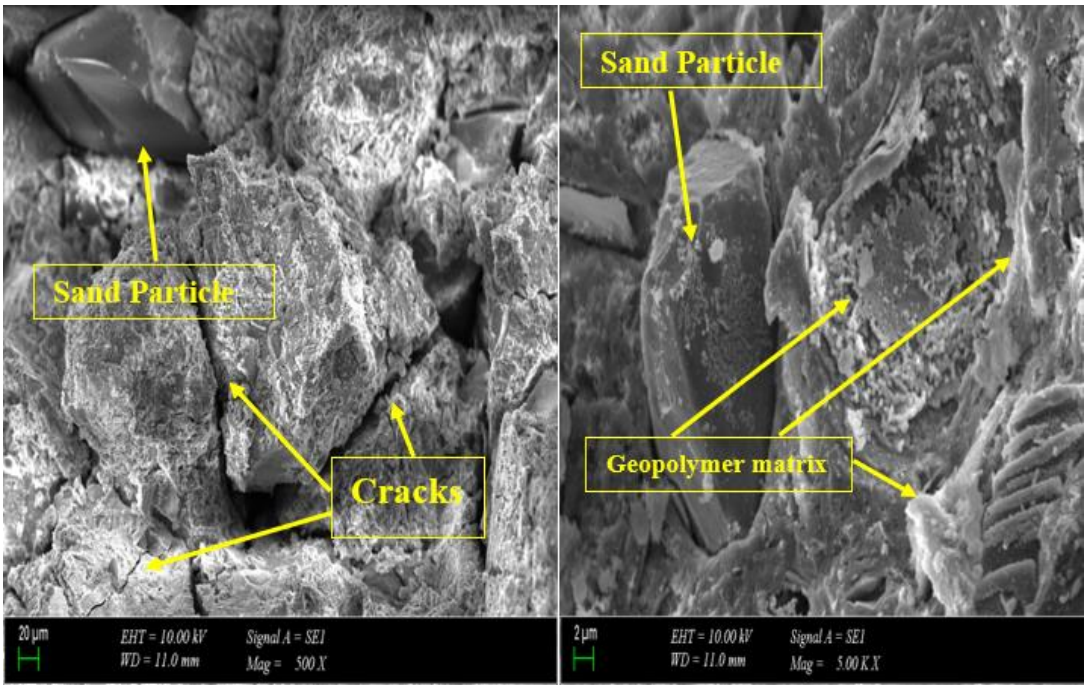

Figure 69: SEM images of 50MK50GP after 800 °C exposure

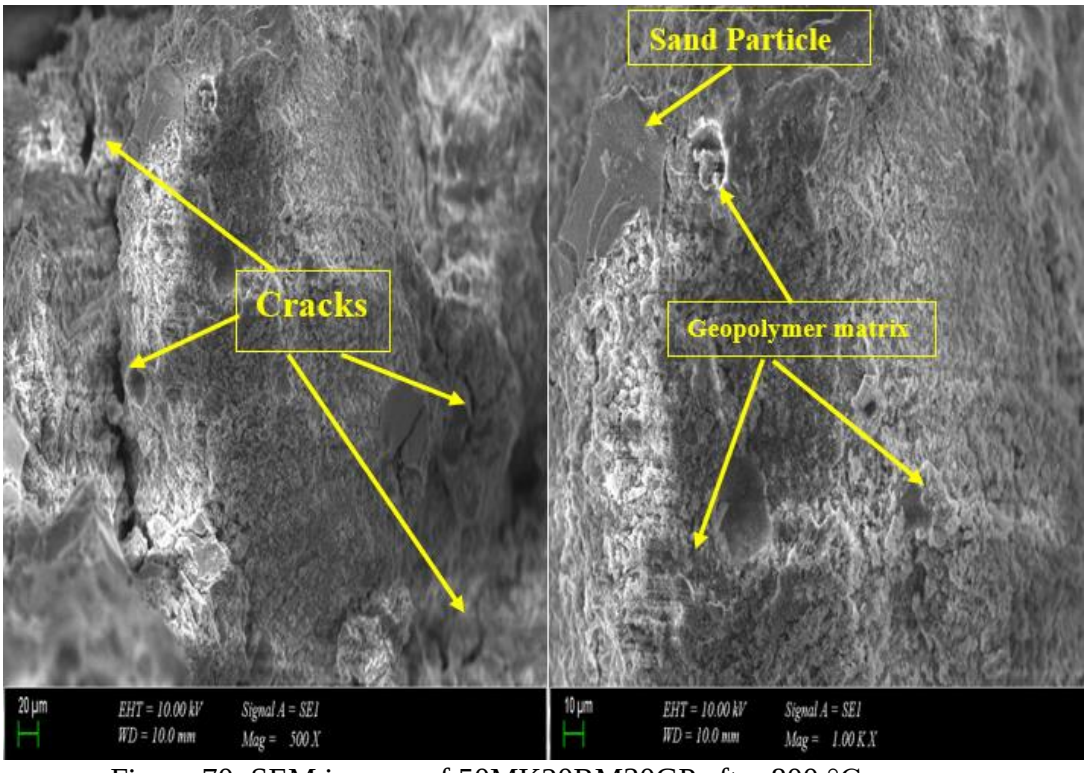

Figure 70: SEM images of 50MK20RM30GP after 800 °C exposure

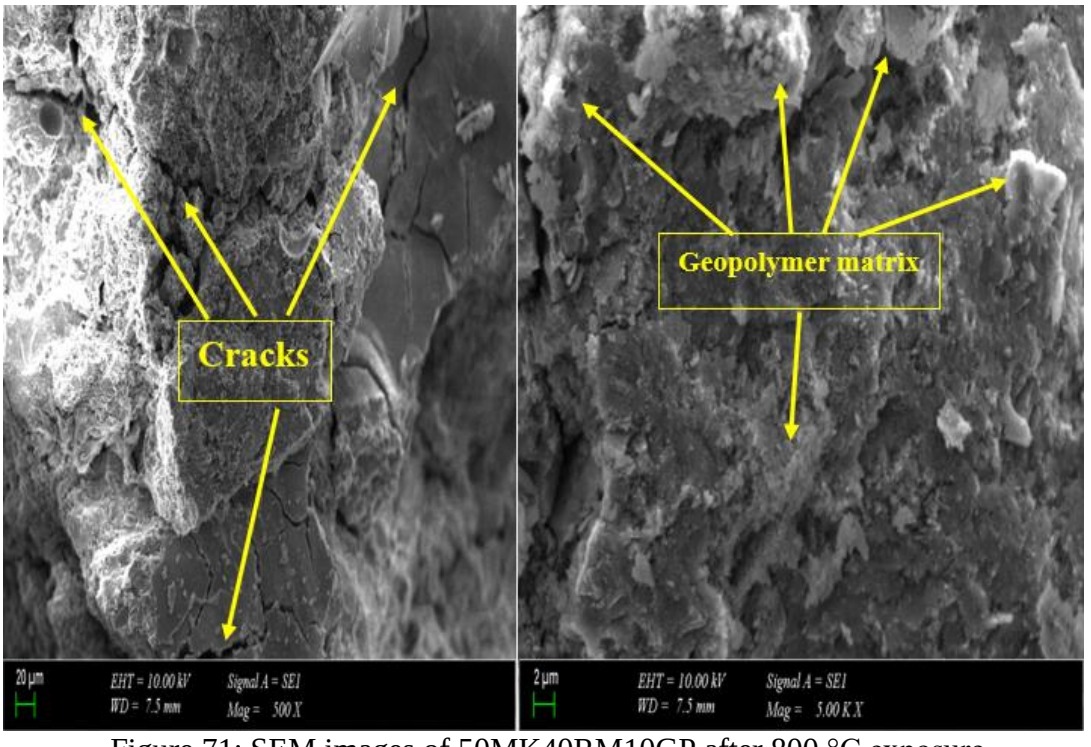

Figure 71: SEM images of 50MK40RM10GP after 800 °C exposure

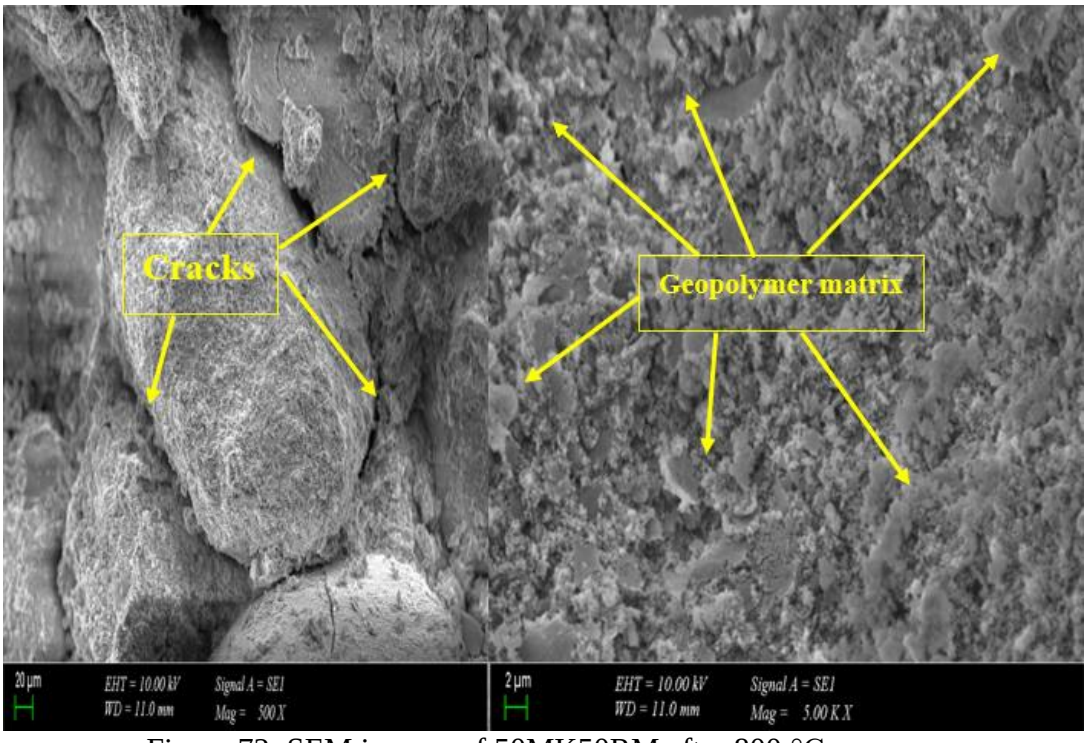

Figure 72: SEM images of 50MK50RM after 800 °C exposure

Chapter 6

CONCLUSIONS

The conclusions of this dissertation are listed below:

1) A geopolymer mortar can be produced using 50% waste materials, and it provides good strength properties. The RM forms an effective chemical combination with MK, but not with GP and RHA; further, MK is good with GP and RM but not with RHA. The compatibility of MK with RM is slightly better than that of GP; 50% MK, and various combinations of GP and RM achieve remarkable compressive and flexural strength.

The incorporation of MK, RM and GP in different percentages in blend combinations improves the strength development of the blend irrespective of the curing age. However, there is no significant difference between 2.5 and 2.25 (S/B) ratio samples in the compressive and flexural strength after 3,7 and 28 days.

2) For various waste materials, the ratio of the activator solution to the binder has noticeable effects on the workability of the geopolymer mortar. A 1:1 ratio achieves good workability for most combinations; RHA requires significantly more chemical solution to react with other materials and be workable. Hence, the cost of the chemical solution makes it impractical to use it even in small proportions.

3) The SiO_2/Al_2O_3 ratio and SiO_2 content affect the f_c value. As far as the SiO_2/Al_2O_3 ratio is below 3, a higher SiO_2 content positively affects the f_c value. Further, the use

of an alkaline activator solution comprising a mixture of sodium silicate and sodium hydroxide solution increases the dissolution of these different waste materials and improves the mechanical properties. The molarity of NaOH significantly affects the mechanical properties of the geopolymer mortar; 12M yields the highest compressive strength compared to 10M and 14M.

4) The addition of GFs slightly improved f_c and f_f. The 12-mm-long GF achieves slightly better results than the 6-mm-long GF. The 50MK20RM30GP geopolymer sample obtained the highest f_c development from 3 to 28 d. The strength development of the 50MK20RM30GP sample without the GF was 11.35%; with the 6-mm-long GF, it increases to 15.31%, and with the 12-mm-long GF, it increases to 20.96%. The addition of the GF affects the f_s of the geopolymer mortar; the GF with the 12 mm length obtained slightly higher results than 6 mm; a 4–6% increase was observed in the mixes when 6- or 12-mm-long GFs were added in the blends.

5) The addition of GFs causes a slight improvement in the length change and weight loss of the geopolymer mortar after high-temperature exposure. The highest reduction of f_c after exposure to 800 °C was 88.85 % for the combination 50MK20RM30GP without the GF; when GFs were added, the reduction rate of f_c decreased to 88.52 % and 86.58 % for the 6-mm and 12-mm- long GFs, respectively. The addition of the GFs serves to limit the thermal damage of the mortar at 800 °C; it is found that the f_c and f_f of all combinations improve at 400 °C. The addition of GFs generally improves the f_c and f_f at 400 °C, 600 °C, and 800 °C compared to the specimens without GFs.

6) The endothermic peaks of DTA curves were observed at about (100–500) °C for all geopolymer mortar samples (470, 324.5, 333.4, 332, and 326.3 °C); this causes

weight loss, and these peaks are a result of pore water evaporation. The XRD analysis shows that all samples are composed of calcite ($CaCO_3$), dolomite ($CaMg(CO_3)_2$), and quartz (SiO_2); this explains the significant strength properties. SEM images show that the microstructure of the geopolymer samples remains stable after 800 °C, which promotes the use of the geopolymer fire resistance properties. Further, the S/B ratio has no significant effect on the microstructural changes for the two S/B ratios used.

7) The compressive strength of samples prepared with an S/B ratio of 2.5 is slightly higher than the specimens with an S/B ratio of 2.25 after 56 d in a sea water environment; the f_c for all samples decreases with time. The flexural strength of the samples prepared with an S/B ratio of 2.5 is slightly higher than that of samples with an S/B ratio of 2.25 after 56 d; further, f_f decreases with time for all samples. The geopolymer mortars showed a tendency to increase in weight and decrease in compressive and flexural strength when immersed in a $MgSO_4$ solution. The S/B ratios have no significant effect on the deterioration of the geopolymer mortar samples when immersed in a $MgSO_4$ solution.

8) All specimens lost weight at 50 and 100 (F–T) cycles; the weight loss increases with time and ranges from 0.74% to 2.24%. The compressive and flexural strength of the specimens decreased after 50 F–T cycles and decreased more after 100 cycles. The S/B ratio has no significant effect under the F–T conditions.

REFERENCES

Abdulkareem, O.A., Abdullah, M. M. A., Kamarudin, H., Nizar, K., Saif, A. (2014). Effects of elevated temperatures on the thermal behavior and mechanical performance of fly ash geopolymer paste, mortar and lightweight concrete. *Construction and Building Materials*, 50, 377-387.

Abousnina, R., Alsalmi, H., Manalo, A., Allister, R., Alajarmeh, O., Ferdous, W., Jlassi, K. (2021). Effect of Short Fibres in the Mechanical Properties of Geopolymer Mortar Containing Oil-Contaminated Sand. *Polymers*, 13, 3008.

Akcaoglu, T., Cubukcuoglu, B., Awad, A. (2019). A critical review of slag and fly-ash based geopolymer concrete. *Computers and Concrete, 24*(5), 453–458.

Ali, N., Canpolat, O., Aygörmez, Y., Al-Mashhadani, M. M. (2020). Evaluation of the 12–24 mm basalt fibers and boron waste on reinforced metakaolin-based geopolymer. *Construction and Building Materials, 251*, 118976.

Allahverdi, A., Abadi, M.M.B.R., Anwar Hossain, K.M., Lachemi, M. (2014). Resistance of chemically-activated high phosphorous slag content cement against freeze–thaw cycles. *Cold Regions Science Technology,* 103, 107–114.

Al-majidi, M., Lampropoulos, A., Cundy, A., Meikle, S. (2016). Development of geopolymer mortar under ambient temperature for in situ applications. *Construction and Building Materials*, 120, 198-211.

Almashhadani, M.M, Canpolat, O., Aygormez, Y., Uysal, M., Erdem, S. (2018). Mechanical and microstructural characterization of fiber reinforced fly ash based geopolymer composites, *Construction Building Materials*, 167, 505–513.

Alnahhal, M. F., Alengaram, U. J., Jumaat, M., Alqedra, M., Mo, K.H., Sumesh, M. (2017). Evaluation of Industrial By-Products as Sustainable Pozzolanic Materials in Recycled Aggregate Concrete. *Sustainability*, 9, 767

Alomayri T., Low, I. M. (2013). Synthesis and characterization of mechanical properties in cotton fiber-reinforced geopolymer composites. *Journal of Asian Ceramic Society*, 1(1), 30-34.

Alonso, S., Palomo, A. (2001). Calorimetric Study of Alkaline Activation of Calcium Hydroxide-Metakaolin Solid Mixtures. *Cement and Concrete Research*, 31, 25-30

American Society for Testing and Materials C1437-20, Standard Test Method for Flow of Hydraulic Cement Mortar, ASTM International, West Conshohocken, PA, 2020, Retrieved from: www.astm.org

American Society for Testing and Materials D1141-98(2013), Standard Practice for the Preparation of Substitute Ocean Water, ASTM International, West Conshohocken, PA, 2013, Retrieved from: www.astm.org

American Society for Testing and Materials E4-21, Standard Practices for Force Calibration and Verification of Testing Machines, ASTM International, West Conshohocken, PA, 2021, Retrieved from: www.astm.org

American Society for Testing and Materials, C. 1012. (2004). Standard Test Method for Length Change of Hydraulic-Cement Mortars Exposed to a Sulfate Solution. *ASTM International*, West Conshohocken, PA, 2004, Retrieved from: www.astm.org

American Society for Testing and Materials, C. 109/109M (2010). Standard Test Method for Compressive Strength of Hydraulic Cement Mortars (Using 2-in. or [50-mm] Cube Specimens). *Chemical Analysis*, (C109/C109M – 11b), 1–9

American Society for Testing and Materials, C. 1365. (2018). Standard Test Method for Determination of the Proportion of Phases in Portland Cement and Portland-Cement Clinker Using X-Ray Powder Diffraction Analysis. *ASTM International*, West Conshohocken, PA, 2018, Retrieved from: www.astm.org

American Society for Testing and Materials, C. 1723. (2016). Standard Guide for Examination of Hardened Concrete Using Scanning Electron Microscopy. *ASTM International*, West Conshohocken, PA, 2016, Retrieved from: www.astm.org

American Society for Testing and Materials, C. 348. (1998). in: Standard Test Method for Flexural Strength of Hydraulic- Cement Mortars ASTM C348. *Annual Book of ASTM Standards*, 1998, 2–7,

American Society for Testing and Materials, C. 496 /496M. (2017). Standard Test Method for Splitting Tensile Strength of Cylindrical Concrete Specimens. *ASTM International*, West Conshohocken, PA, 2017

American Society for Testing and Materials, C. 666 / C666M. (2015). Standard Test Method for Resistance of Concrete to Rapid Freezing and Thawing. *ASTM International*, West Conshohocken, PA, 2015

American Society for Testing and Materials, C. 779/C779M. (2012). Standard Test Method for Abrasion Resistance of Horizontal Concrete Surfaces. *ASTM International*, 2012.

American Society for Testing and Materials, C. 779/C779M. (2012). Standard Test Method for Abrasion Resistance of Horizontal Concrete Surfaces. *ASTM International*, 2012.

American Society for Testing and Materials, E. 794-06. (2018). Standard Test Method for Melting and Crystallization Temperatures by Thermal Analysis. *ASTM International*, West Conshohocken, PA, 2018, Retrieved from: www.astm.org

Arslan, A. A., Uysal, M., Yılmaz, A., Al-mashhadani, M. M., Canpolat, O., Şahin, F., Aygörmez, Y. (2019). Influence of wetting-drying curing system on the performance of fiber reinforced metakaolin-based geopolymer composites. *Construction and Building Materials, 225*, 909-926.

Assi, L., Ghahari, S., Deaver, E., Leaphart, D. & Ziehl, P. (2016). Improvement of the early and final compressive strength of fly ash-based geopolymer concrete at ambient conditions. *Construction and Building Materials*, 123, 806–813.

Astutiningsih, S., Nurjaya, D. M., Ashadi, H. W., Swastika, N. (2010). Durability of geopolymer concretes upon seawater exposure. *In Advances in Science and Technology*, 69, 92-96

Avraamides, J., van Riessen, A., Jamieson, E. (2010). Transforming mining residues into viable by-products. *Energy Generation*., 2010, 1-3

Awad, A., Akcaoglu, T., Cubukcuoglu, B., Canpolat, O. (2021). Experimental investigation of mechanical properties of geopolymer mortars produced with metakaolin, red mud and glass powder. *Computers and Concrete*, *27*(6), 597–606.

Aygörmez, Y. (2021). Evaluation of the red mud and quartz sand on reinforced metazeolite-based geopolymer composites. Journal of Building Engineering, 43, 102528.

Aygörmez, Y., Canpolat, O., Al-mashhadani, M.M., Uysal, M. (2020). Elevated temperature, freezing-thawing and wetting-drying effects on polypropylene fiber reinforced metakaolin based geopolymer composites. *Construction and Building Materials*, 235, 117502.

Ayres, R.U., John, H., Bjorn, A. (2001). Utilisation of the wastes in the new millennium. *MRSI Bull*, 2001, 7, 477–480.

Baerlocher, C., Meier, W.M., Olson, D.H. (2001). *Atlas of zeolite framework types*, 5th revised edition. Elsevier, Amsterdam, 308

Bagherzadeh, R., Pakravan, H., Sadeghi, A., Latifi, M., Merati, A.A. (2012). An Investigation on Adding Polypropylene Fibers to Reinforce Lightweight Cement Composites (LWC). *Journal of engineered fibers and fabrics*, 7, 13-21

Barrer, R.M., Mainwaring, D.E. (1972). Chemistry of soil minerals. Part XIII. Reactions of metakaolinite with single and mixed bases**.** *Journal of the Chemical Society, Dalton Transactions,* 2534-2546

Bascarevic, Z., Komljenović, M., Miladinovic, Z., Nikolic, V., Marjanovic, N., Petrovic, R. (2014). Impact of sodium sulfate solution on mechanical properties and structure of fly ash based geopolymers. *Materials Structure*, 48(3), 683-697.

Basha, N.A., Bharath, B.B. (2018). an experimental study on geopolymer concrete with cement replacement by GBFS and Metakaolin, *International Journal of Research*, 7(9), 1498- 1502

Basheer, L., Kropp, J., Cleland, D.J. (2001). Assessment of the durability of concrete from its permeation properties: a review. *Construction and Building Materials*,15(2), 93–103.

Baskar, P., Shalini, A., Kumar, J.K. (2014). Rice husk ash based geopolymer concrete - A Review. *Chemical Science Review and Letters*, 3, 288-294.

Belmokhtar, N., Ammari, M., Brigui, J., & Ben allal, L. (2017). Comparison of the microstructure and the compressive strength of two geopolymers derived from

metakaolin and an industrial sludge. *Construction and Building Materials*, 146, 621-629

Benhelal, E., Zahedi, G., Shamsaei, E. & Bahadori, A. (2013). Global strategies and potentials to curb CO_2 emissions in cement industry. *Journal of Cleaner Production*, 51, 142–161

Borges, R., Paulo, N., Vitor, P., Schileo, G., Feteira, A. (2016). The Influence of Rice Husk Ash Addition on the Properties of Metakaolin-Based Geopolymers. *The Open Construction and Building Technology Journal*, 10, 406-417

Brinker, C.J., Scherer, G.W. (1990). Sol-Gel science: the chemistry and physics of Sol-Gel processing. Academic, London, 980p

Casci, J., Cundy, C. (1983). R.M. Barrer Hydrothermal Chemistry of Zeolites. Academic Press, London and New York. *Clay Minerals*, 18(2), 223-223

Cengeloglu, Y., Tor, A., Ersoz, M., Arslan, G. (2006). Removal of nitrate from aqueous solution by using red mud. *Separation and Purification Technology*, 51, 374–378

Chakkor, O., Altan, M. (2021). Metakaolin and Red-Mud Based Geopolymer: Resistance to Sodium and Magnesium Sulfate Attack. *Celal Bayar Üniversitesi Fen Bilimleri Dergisi*, 17, 101-113

Chandra Padmakar, K., Sarath, C. K. B. (2017). An Experimental Study on Metakaolin and GBFS Based Geopolymer Concrete. *International Journal of Civil Engineering and Technology (IJCIET)*, 8(1), 544–557

Cheng, T.W., Lee, M.L., Ko, M.S., Ueng, T.H., Yang, S.F. (2012). The heavy metal adsorption characteristics on metakaolin-based geopolymer. *Applied Clay Science*, 56, 90–96.

Chi, M., Chang, J., & Huang, R. (2012). Strength and drying shrinkage of alkali-activated slag paste and mortar. *Advances in Civil Engineering*, 2012(6), 1–7

Davidovits, J. (1991). Geopolymers. *Journal of Thermal Analysis* **37,** 1633–1656, https://doi.org/10.1007/BF01912193

Davidovits, J. (1993). Carbon-Dioxide Greenhouse-Warming: What Future for Portland Cement. *Emerging Technologies Symposium on Cements and Concretes in the Global Environment*.

Davidovits, J. (1994). Geopolymer: Man-made rocks geosynthesis and the resulting development of very early high strength cement. *Journal of Mathematics Teacher Education*, 16, 91-139.

Davidovits, J. (2013). Geopolymer Cement a review, published in Geopolymer Science and Technics, Technical Paper #21, *Geopolymer Institute Library*, www.geopolymer.org.

Davidovits, Joseph. (2008). Geopolymer Chemistry and Applications.

Davidovits. J. (1994). Global warming impact on the cement and aggregates industries. *World Resource Review*, 6, 263-273.

Dezfouli, H.R., Rangaraju, P.R., Kothala, V.S.K. (2018). Influence of selected parameters on compressive strength of geopolymer produced from ground glass fiber. *Construction and Building Materials*, 162, 393–405.

Duan, P., Yan, C., Zhou, W., Ren, D. (2016). Fresh properties, compressive strength and microstructure of fly ash geopolymer paste blended with iron ore tailing under thermal cycle. *Construction and Building Materials*, 118, 76-88.

Duxson, P., Fernandez-Jimenez, A., Provis, J. L., Lukey, G. C., Palom, A. and van Deventer, J. S. J. (2007). Geopolymer technology: the current state of the art. *Journal of Materials Science*, 42, 2917-2933.

Duxson, P., Lukey, G.C., van Deventer, J.S.J. (2006). Physical evolution of Na-geopolymer derived from metakaolin up to 1000 c degrees. *Journal of Materials Science*, 42, 3044–3054.

Duxson, P., Provis, J. L., Lukey, G. C., Mallicoat, S. W., Kriven, W.M. and van Deventer, J. S. J. (2005). Understanding the relationship between geopolymer composition, microstructure and mechanical properties. *Colloids and Surfaces A: Physicochemical and Engineering Aspects*, 269, 47-58

Elson, J., Kevin, M., Chalapuram, P. S., Helna, K.M., Zuman, F. (2016). Geopolymer Concrete Using Red Mud and GBFS, *International Research Journal of Engineering and Technology (IRJET)*, 3(5), 668- 671

Elyamany, H., Abd Elmoaty, A., Elshaboury, A. (2018). Setting time and 7-day strength of geopolymer mortar with various binders. *Construction and Building Materials*, 187, 974-983.

European Standard, EN 1338(2003). Concrete paving blocks – requirements and test, methods

Ganesan, N., Indira, P.V., Santhakumar, A. (2014). Influence of steel fibers on tension stiffening and cracking of reinforced geopolymer concrete. *Magazine of Concrete Research*, 66(6), 268-276.

Geopolymer Institute. (2010). What Is a Geopolymer? Introduction. Institut Géopolymère, SaintQuentin, France. Accessed on January 29, 2010, at http://www.geopolymer.org/science/introduction.

Ghasan, F., Huseien, J. M., Mohammad, I.S.K., Ghoshal, M. A., Mohd, A. (2018). Effect of metakaolin replaced granulated blast furnace slag on fresh and early strength properties of geopolymer mortar. *Ain Shams Engineering Journal*, 9 (2018), 1557–1566.

Global Status Report, (2017). UN Environment and International Energy Agency (2017): Towards a zero-emission, efficient, and resilient buildings and construction sector. *United Nations Environment Programme*, 2017

Gonc¸alves, M. R. F., & Bergmann, C. P. (2007). Thermal insulators made with rice husk ashes: Production and correlation between properties and microstructure. *Construction and Building Materials*, 21(12), 2059– 2065.

Granizo, M.L., Alonso, S., Blanco-Varela, M.T., Palomo, A. (2002). Alkaline activation of metakaolin: effect of calcium hydroxide in the products of reaction. *Journal of the American Ceramic Society*, 85, 225–31.

Grdić, Z., Toplicic-Curcic, G., Ristic, N., Iva, D. (2012). Abrasion resistance of concrete micro-reinforced with polypropylene fibers. *Construction and Building Materials*. 27. 305–312.

Hager, I. (2013). Colour Change in Heated Concrete. *Fire Technology*, 49, 10

Hairi, S. N. M., Jameson, G.N.L., Rogers, J.J., MacKenzie, K.J.D. (2015). Synthesis and properties of inorganic polymers (geopolymers) derived from Bayer process residue (red mud) and bauxite. *Journal of Materials Science*, 50, 7713–7724

He, J. and Zhang, G. (2011). Geopolymerization of Red Mud and Fly Ash for Civil Infrastructure Applications. *Geotechnical Special Publication*, (397)132, 1287-1296

Hind, A.R., Bhargava, S.K., Grocott, S.C. (1999). The surface chemistry of Bayer process solids: A review. Colloids Surf. *A Physicochemical and Engineering Aspects*, 146, 359–374.

Hoa, J., Mccormick, P., Byrne, L. (2002). Investigation of the Synthetic Aluminosilicate Inorganic Polymer. *Journal of Material Science*, 37, 2311-2316.

http://www.fhwa.dot.gov/pavement/pub_details.cfm?id=665, last access on 10/5/2020.

Huseien, G.F., Ismail, M., Tahir, M., Mirza, J., Hussein, A., Khalid, N.H., Sarbini, N.N. (2018). Effect of binder to fine aggregate content on performance of sustainable alkali activated mortars incorporating solid waste materials. *Chemical Engineering Transactions*, 63, 667-672.

Islam, A., Alengaram, U. J., Jumaat, M. Z., & Bashar, I. I. (2014). The development of compressive strength of ground granulated blast furnace slag-palm oil fuel ash-fly ash based geopolymer mortar. *Materials & Design*, 56, 833–841.

Jaarsveld V.J.G.S., Deventer V.J.S.J. (1999). The effect of metal contaminants on the formation and properties of waste-based geopolymers, *Cement and Concrete Research*, 29 (8), 1189-1200

Jiang, X., Xiao, R., Zhang, M., Hu, W., Bai, Y., Huang, B. (2020). A laboratory investigation of steel to fly ash-based geopolymer paste bonding behavior after exposure to elevated temperatures. *Construction and Building Materials*, 254, 119267.

Johannes, H. P. (2012). An Overview of Cement production: How “green” and sustainable is the industry. *Environmental Management and Sustainable Development*, 1, 14 - 37.

Kabay, N. (2014). Abrasion resistance and fracture energy of concretes with basalt fiber, *Construction and Building Materials,* 50, 95–101.

Kalkan, E. (2006). Utilization of red mud as a stabilization material for the preparation of clay liners. *Engineering Geology*, 87, 220–229.

Karim, M.R., Zain, M.F.M., Jamil, M., Lai, F.C. and Islam, M.N. (2012). Strength of Mortar and Concrete as Influenced by Rice Husk Ash: A Review, *World Applied Sciences Journal*, 19 (10), 1501- 1513

Kaya, K., Soyer-Uzun, S. (2016). Evolution of structural characteristics and compressive strength in red mud-metakaolin based geopolymer systems. *Ceramics International*, 42, 7406–7413.

Kchaitanya, D.V.S., Neeharika, P., Kiran K. J. (2017). An Experimental Study on Strength Properties of GBFS and Metakaolin in Addition with Alkaline Solution of Sodium Hydroxide and Sodium Silicate. *International Journal of Advanced Technology and Innovative Research*, 9(5), 719-722

Khale, D., Chaudhary, R. (2007). Mechanism of geopolymerization and factors influencing its development: a review. *Journal of materials science*, 42(3), 729-746.

Khater, H. M., Ezzat Abdeen, M., El Nagar, M. (2016). Alkali Activated Eco-friendly Metakaolin/Slag Geopolymer Building Bricks. *Chemistry and Materials Research*, 8(1), 21- 33

Khatib J.M., Sohl H.S., Sohl, H.S., Chileshe N. (2012). Glass Powder Utilisation in Concrete Production. *European Journal of Applied Sciences*, 4(4), 173-176.

Khoury, G.A. (1992) Compressive strength of concrete at high temperatures: a reassessment. Magazine of Concrete Research, 44, 291–309.

Kong, D., Sanjayan, J., Sagoe-Crentsil, K. (2007). Comparative Performance of Geopolymers Made with Metakaolin and Fly Ash After Exposure to Elevated Temperatures. *Cement and Concrete Research*, 37, 1583-1589.

Korniejenko, K, Frączek, E, Pytlak, E, Adamski, M. (2016). Mechanical properties of geopolymer composites reinforced with natural fibers. *Procedia Engineering*, 151, 388-393.

Kulkarni, S. (2018). Experimental Study on Red Mud, Fly Ash and GBFS based Geopolymer Concrete: A Green Substitute to Conventional Concrete. *International Journal of Engineering Research & Technology (IJERT)*, 7(12), 107-111

Kumar, A., Kumar, S. (2013). Development of paving blocks from synergistic use of red mud and fl y ash using geopolymerization. *Construction and Building Materials*, 38, 865–871.

Kumar, P., Pankar, C., Manish, D., Santhi, A.S. (2018). Study of mechanical and microstructural properties of geopolymer concrete with GBFS and Metakaolin. *Materials Today*, 5(2018), 28127–28135

Kumar, S.M., Varuna, K.D.L., Babu, N. V. K. (2016). A Study on the Strength Properties of Inorganic Polymeric New Materials with GBFS and Metakaolin, *International Journal of Engineering Research-Online*, 4 (3), 558- 565

Lemougna, P., Wang, K., Tang, Q., and Cui, X. (2017). Synthesis and characterization of low temperature (<800 C) ceramics from red mud geopolymer precursor. *Construction and Building Materials*, 131, 564–573

Liao, X., He, Y., Yang, X. (1999). Interfacial behavior of PP fiber reinforced cement composite: study of abrasion resistance. Journal of Building Materials, 2(4), 324–328.

Lin, T., Jia, D., Wang, M., He, P., Liang, D. (2009). Effects of fibre content on mechanical properties and fracture behaviour of short carbon fibre reinforced geopolymer matrix composites. *Bulletin of Materials Science – SCI*, 32, 77-81

Lingyu, T., Dongpo, H., Jianing, Z., Hongguang, W. (2021). Durability of geopolymers and geopolymer concretes: A review. *Reviews on Advanced Materials Science*, 60(1), 1-14.

Lingyu, T., Dongpo, H., Jianing, Z., Hongguang, W. (2021). Durability of geopolymers and geopolymer concretes: A review. *Reviews on Advanced Materials Science*, 60 (1), 1-14.

Luo, R., Cai, Y., Wang, C., Huang, X. (2003), Study of chloride binding and diffusion in GBFS concrete. *Cement and Concrete Research*, 33, 1-7

Lyngdoh, G., Li, H., Zaki, M., Krishnan, N., Anoop, M., Das, S. (2020). Elucidating the Constitutive Relationship of Calcium–Silicate–Hydrate Gel using High Throughput Reactive Molecular Simulations and Machine Learning. *Scientific Reports*, 10, 1038.

Ma, J., Qiu, X., Cheng, L., Wang, Y. (2010). Experimental research on the fundamental mechanical properties of presoaked basalt fiber concrete. *Advances FRP Composites in Civil Engineering*, 85–88.

Malagavelli, V., Rao, P.N. (2010). High performance concrete with GBFS and ROBO sand. *International Journal of Engineering Science and Technology*, 2(10), 5107-5113

Malleswara, R.P., Hamantha, K. R. (2017). Study of The Properties of Metakaolin and GBFS Based Geopolymer Concrete, *International Journal of Civil Engineering and Technology*, 8(1), 565–574.

Marlowe, I., Mansfield, D. (2002), “Toward a Sustainable Cement Industry Substudy 10: Environment, Health & Safety Performance Improvement”, December 2002, *an Independent Study Commissioned by WBCSD*

Mclellan, B., Williams, R., Lay, J., van Riessen, A., Corder, G. (2011). Costs and carbon emissions for geopolymer pastes in comparison to ordinary Portland cement. *Journal of Cleaner Productions*, 19 (9), 1080–1090.

Mishra, S., Siddiqui, N.A. (2014). A Review on Environmental and Health Impacts of Cement Manufacturing Emissions. *International Journal of Geology, Agriculture and Environmental Science*, 2(3), 26- 31

Mitchell, J.K., Soga, K. (2005). Fundamentals of Soil Behaviour, John Wiley & Sons, Hoboken, New Jersey.

Morsy, M., Rashad, A., Shoukry, H, Mokhtar, M. (2019). Potential use of limestone in metakaolin-based geopolymer activated with H3PO4 for thermal insulation. *Construction and Building Materials*, 229, 117088

Motorwala, A., Shah, V., Kammula, R., Nannapaneni, P., & Raijiwala, P.D. (2013). Alkali Activated Fly-Ash Based Geopolymer Concrete. *International Journal of Emerging Technology and Advanced Engineering*: 3(1), 159-167

Mucsi, G., Szabo, R., Racz, A., Kristály, F. & Kumar, S. (2019). Combined Utilization of Red Mud and Mechanically Activated Fly Ash in Geopolymers. *Rudarsko-geološko-naftni zbornik*. 34, 27-36

Mugoni, C., Montorsi, M., Siligardi, C., Andreola, F., Lancellotti, I., Bernardo, E., Barbieri., L. (2015). Design of glass foams with low environmental impact. *Ceramics International*, 41, 3400–3408

Muniz-Villarreal, M.S., Manzano-Ramirez, A., Sampieri-Bulbarela, S., Ramon Gasca-Tirado, J., Reyes-Araiza, J.L., Rubio-Avalos, J.C., Perez-Bueno, J.J., Apatiga, L.M., Zaldivar-Cadena, A., Amigo-Borras, V. (2011). The effect of temperature on the geopolymerization process of a metakaolin-based geopolymer. *Materials Letters*, 65, 995–998.

Novais, R.M., Carvalheiras, J., Capela, M.N., Seabra, M.P., Pullar, R.C., Labrincha J.A. (2018) Incorporation of glass fibre fabrics waste into geopolymer matrices: An eco-friendly solution for off-cuts coming from wind turbine blade production. *Construction and Building Materials*, 187, 876–883.

Oday, H., Daniel, A.G., Susan, A. B., John, L.P. (2018). Lightweight foamed geopolymer. *International Conference on Alkali Activated Materials and Geopolymers: Versatile Materials Offering High Performance and Low Emissions*, ECI Symposium Series.

Oner, A., Akyuz, S. (2007). An experimental study on optimum usage of GBFS for the compressive strength of concrete. *Cement & Concrete Composites*, 29, 505–514.

Ozer, I. and Soyer-Uzun, S. (2015). Relations between the structural characteristics and compressive strength in metakaolin based geopolymers with different molar Si/Al ratios. *Ceramics International*, 41, 10192–10198.

Öztürk, H., Hein, J. R., Hanilçi, N. (2002). Genesis of the Dogankuzu and Mortaş Bauxite Deposits, Taurides, Turkey: Separation of Al, Fe, and Mn and Implications for Passive Margin Metallogeny, *Economic Geology*, 97, 1063–1077.

Palomo, A. and Glasser, F.P. (1992). Chemically-Bonded Cementitious Material Based on Metakaolin. *British Ceramic Transactions*, 91, 107-112.

Patra, R. K., & Mukharjee, B. B. (2017). Influence of incorporation of granulated blast furnace slag as replacement of fine aggregate on properties of concrete. *Journal of Cleaner Production*, 165(2017), 468–476.

Perraki, T., Kakali, G. & Kontori, K. (2005), Characterization and pozzolanic activity of thermally treated zeolite, *Journal of Thermal Analysis and Calorimetry*, 82 (1), 109–113

Pilehvar, S., Szczotok, A.M., Rodríguez, J.F., Valentini, L., Lanzón, M., Pamies, R., Kjøniksen, A.L. (2019). Effect of freeze-thaw cycles on the mechanical behavior of geopolymer concrete and Portland cement concrete containing micro-encapsulated phase change materials. *Construction and Building Materials*, 200, 94–103.

Rai, S., Wasewar, K.L., Lataye, D.H., Mishra, R.S., Puttewar, S.P., Chaddha, M.J., Mahindiran, P., Mukhopadhyay, J. (2012). Neutralization of red mud with pickling waste liquor using Taguchi's design of experimental methodology. *Waste Management Research*, 30(9), 922-930

Rajabipour, F., Maraghechi, H., Fischer, G. (2010). Investigating the alkalisilica reaction of recycled glass aggregates in concrete materials. *Journal of Materials in Civil Engineering*, 22, 1201-1208.

Ranjbar, N., Talebian, S., Mehrali M., Kuenzel, C., Cornelis Metselaar, H.S. (2016). Mechanisms of interfacial bond in steel and polypropylene fiber reinforced geopolymer composites. *Composites Science and Technology*, 122(1), 73-81

Ranjbar, N., Zhang, M.Z. (2020). Fiber-reinforced geopolymer composites: A review, *Cement Concrete Composites*, 107, 103498.

Rashad, A. M., Ouda, A. S., & Sadek, D. M. (2018). Behavior of alkali-activated metakaolin pastes blended with quartz powder exposed to seawater attack. *Journal of Materials in Civil Engineering*, *30*(8), 04018159.

Reddy, Y., Karthi, K.S. (2020). Effect of red mud proportion on the strength and microstructure of ferrosialate based geopolymer mortar. *Indian Journal of Engineering and Materials Sciences*. 27. 554-563.

Rieger, D.; Kovarik, T., Riha, J., Medlin, R., Novotny, P., Belsky, P., Kadlec, J., Holba, P. (2015). Effect of thermal treatment on reactivity and mechanical properties of alkali activated shale-slag binder. *Construction and Building Materials*, 83, 26–33

Roviello, G., Menna, C., Tarallo, O., Ricciotti, L., Ferone, C., Colangelo, F., Asprone, D., di Maggio, R., Cappelletto, E., Prota, A. (2015). Preparation, structure and

properties of hybrid materials based on geopolymers and polysiloxanes. *Materials and Design*, 87, 82–94.

Rovnanik, P. (2010). Effect of curing temperature on the development of hard structure of Metakaolin -based Geopolymer. *Construction and Building Materials*, **24**, 1176–1183

Rowles, M., O'Connor, B. (2003). Chemical Optimization of the Compressive Strength of Aluminosilicate Geopolymers Synthesis by Sodium Silicate Activation of Metakaolinite. *Journal of Materials*, 13. 1161-1165. 10.1039/b212629j.

Şahin, F., Uysal, M., Canpolat, O. (2021). Systematic evaluation of the aggregate types and properties on metakaolin based geopolymer composites. *Construction and Building Materials*, *278*, 122414.

Salami, B.A., Johari, M.A.M., Ahmad, Z.A., Maslehuddin, M. (2017). Durability performance of palm oil fuel ash-based engineered alkaline-activated cementitious composite (POFA-EACC) mortar in sulfate environment. *Construction and Building Materials*, 131, 229-244.

Samson, G., Cyr, M., & Gao, X. X. (2017). Thermomechanical performance of blended metakaolin-GBFS alkali activated foam concrete. *Construction and Building Materials*, 157, 982–993.

Sarath, C. K., Ramesh, K. (2017). Durability studies of GBFS and metakaolin based geopolymer concrete. *International Journal of Civil Engineering and Technology (IJCIET)*, 8(1), 17–28

Sarath, C. K., Ramesh, K. (2017). Experimental Study on Metakaolin and GBFS Based Geopolymer Concrete. *International Journal of Engineering and Technology (IJET)*, 9(2), 341- 349

Sata, V., Sathonsaowaphak, A., Chindaprasirt, P. (2012). Resistance of lignite bottom ash geopolymer mortar to sulfate and sulfuric acid attack. *Cement and Concrete Composites*, 34, 700-708.

Schneider, M., Romer, M., Tschudin, M. & Bolio, H. (2011). Sustainable Cement Production – Present and Future. Cement and Concrete Research. 41. 642-650

Shaikh, F.U.A., Fairchild, A., Zammar, R. (2018). Comparative strain and deflection hard- ening behaviour of polyethylene fibre reinforced ambient air and heat cured geo- polymer composites. *Construction and Building Materials*, 163, 890–900.

Shalwan, A., Yousif, B. (2014). Influence of date palm fibre and graphite filler on mechanical and wear characteristics of epoxy composites. *Materials & Design*. 59. 264–273.

Sharmin, A., Alengaram, U. J., Jumaat, M. Z., Yusuf, M. O., Kabir, S. A., & Bashar, I. I. (2017). Influence of source materials and the role of oxide composition on the

performance of ternary blended sustainable geopolymer mortar. *Construction and Building Materials*, *144*, 608-623.

Siddika, A., Hajimohammadi, A., Mamun, M., Al, A., Alyousef, R., & Ferdous, W. (2021). Waste Glass in Cement and Geopolymer Concretes: A Review on Durability and Challenges. *Polymers*, *13*(13), 2071.

Sikora, P., Cendrowski, K., Abd Elrahman, M., Chung, S. Y., Mijowska, E., Stephan, D. (2020). The effects of seawater on the hydration, microstructure and strength development of Portland cement pastes incorporating colloidal silica. *Applied Nanoscience*, *10*(8), 2627-2638.

Singh, S., Uddappa, A., Ranganath, R.V. (2017). Effect of curing methods on the property of red mud based geopolymer mortar. *International Journal of Civil Engineering and Technology*, 8, 1481-1489.

Sireesha, N., Madhavi, B. (2018). An Experimental Study on Strength Properties Of GBFS And Metakaolin In Addition With Alkaline Solution Of Sodium Hydroxide And Sodium Silicate, *Anveshana's International Journal of Research In Engineering And Applied Sciences*, 3(2), 96- 102

Soleimani, M. A., Naghizadeh, R., Mirhabibi, A. R., Golestanifard, F. (2013). The Influence of Phosphorus Slag Addition on Microstructure and Mechanical Properties of Metakaolin-Based Geopolymer Pastes, *Ceramics – Silikáty*, 57(1), 33-38

Steinerova, M. (2011). Mechanical properties of geopolymer mortars in relation to their porous structure. *Ceramics Silikaty*, 55(4), 362 – 372.

Steinerova, M. (2011). Mechanical properties of geopolymer mortars in relation to their porous structure. *Ceramics Silikaty*, 55.

Tammam, Y., Uysal, M., Canpolat, O. (2021). Effects of alternative ecological fillers on the mechanical, durability, and microstructure of fly ash-based geopolymer mortar. *European Journal of Environmental and Civil Engineering*, 1-24.

Tassew, S.T., Lubell, A. (2014). Mechanical properties of glass fiber reinforced ceramic concrete. *Construction and Building Materials*, 51, 215–224.

Tayeh, B., Bakar, B.H., Megat, J., Megat, A., Voo, Y. (2013). Utilization of Ultra-high Performance Fibre Concrete (UHPFC) for Rehabilitation – A Review. *Procedia Engineering*, 54, 525–538.

Tho-In, T., Sata, V., Boonserm, K., & Chindaprasirt, P. (2018). Compressive strength and microstructure analysis of geopolymer paste using waste glass powder and fly ash. *Journal of Cleaner Production*, 172, 2892-2898.

Tian, L., Feng, W., Ma, H., Zhang, S., & Shi, H. (2017). Investigation on the microstructure and mechanism of geopolymer with different proportion of quartz and K-feldspar. *Construction and Building Materials*, 147, 543-549.

Topcu, B., Canbaz, M. (2004). Properties of concrete containing waste glass. *Cement and concrete research*, 34, 267-274.

Topcu, I.B., Atesin, O., Uygunoglu, T. (2017). Effect of High Dosage Air-Entraining Admixture Usage on Micro Concrete Properties. *European Journal of Engineering and Natural Sciences (EJENS)*, 2(1), 1-11.

Tosheva, L., Valtchev, V. P. (2005). Nanozeolites: Synthesis, crystallization mechanism, and applications. *Chemistry of Materials*, 17 (10), 2494–2513.

Tuyan, M., Andiç-Çakir, Ö., & Ramyar, K. (2018). Effect of alkali activator concentration and curing condition on strength and microstructure of waste clay brick powder-based geopolymer. *Composites Part B: Engineering*, 135, 242-252.

Uysal, M., Al-mashhadani, M. M., Aygörmez, Y., & Canpolat, O. (2018). Effect of using colemanite waste and silica fume as partial replacement on the performance of metakaolin-based geopolymer mortars. *Construction and Building Materials*, *176*, 271-282.

Valeria, F.F., Barbosa, K., Mackenzie, J.D., Clelio, T. (2000). Synthesis and characterisation of materials based on inorganic polymers of alumina and silica: sodium polysialate polymers. *International Journal of Inorganic Materials*, 2(4), 309-317

Vermuelen, Tony, J.W. (1999). Biodiversity and cultural property in the management of limestone resources - lessons from East Asia, Washington D.C.,

Viña, J., García, M., Castrillo, M., Vina, I., Argüelles, A. (2008). Wear Behavior of a Glass Fiber-Reinforced PEI Composite. *Journal of Thermoplastic Composite Materials,* 21, 279-286.

Wan, X.M., Shen, C., Wang, P.G., Zhao, T.J., Lu, Y. (2020) A study on fracture toughness of ultra-high toughness geopolymer composites based on Double-K Criterion. *Construction and Building Materials,* 251, 118851.

Wang, A., Zheng, Y., Zhang, Z., Liu, K., Li, Y., Shi, L., Sun, D. (2020). The Durability of Alkali-Activated Materials in Comparison with Ordinary Portland Cements and Concretes: A Review. *Engineering*, 6(6), 695-706.

Weil, M., Jeske, U., Dombrowski, K., Buchwald, A. (2007). Sustainable Design of Geopolymers - Evaluation of Raw Materials by the Integration of Economic and Environmental Aspects in the Early Phases of Material Development. *Advances in Life Cycle Engineering for Sustainable Manufacturing Businesses. Springer*, 279-283

Winter, G. (1964). Design of Concrete Structures. McGraw Hill Book Company.

Yang, S., Navrotsky, A., Phillips, B. (2000). In Situ Calorimetric, Structural, and Compositional Study of Zeolite Synthesis in the System 5.15Na 2 O−1.00Al 2 O 3 −3.28SiO 2 −165H 2 O. *Journal of Physical Chemistry*, 104(25), 6071–6080

Yanık, G., Esenli, F., Uz, V., Esenli, V., Uz, B., Külah, T. (2010). Ceramic properties of kaolinized tuffaceous rocks in Kesan region, Thrace, NW Turkey. *Applied Clay Science*. 48, 499–505

Ye, J., Zhang, W., Shi, D. (2014). Effect of elevated temperature on the properties of geopolymer synthesized from calcined ore-dressing tailing of bauxite and ground-granulated blast furnace slag. *Construction and Building Materials*, 69, 41-48.

Ye, N., Yang, J., Ke, X., Zhu, J., Li, Y., Xiang, C., Wang, H., Li, L., Xiao, B. (2014). Synthesis and characterization of geopolymer from Bayer red mud with thermal pre-treatment. *Journal of the American Ceramic Society*, 97 (5), 1652-1660

Yip, C., Lukey, G.C.,Van Deventer, J. (2005). The Coexistence of Geopolymeric Gel and Calcium Silicate Hydrate at Early Stage of Alkaline Activation. *Cement and Concrete Research*, 35, 1688-1697.

Zaidi, F. H. A., Ahmad, R., Abdullah, M. M. A. B., Tahir, M. F. M., Yahya, Z., Ibrahim, W. M. W., Sauffi, A. S. (2019). Performance of Geopolymer Concrete when Exposed to Marine Environment. In *IOP Conference Series: Materials Science and Engineering*, 551, 012092

Zhang, G., He, J., Gambrell, R. (2010). Synthesis, Characterization, and Mechanical Properties of Red Mud-Based Geopolymers. *Transportation Research Record (TRR)*, 2167, 1–9.

Zhang, G., He, J., Gambrell, R.P. (2010). Synthesis, characterization, and mechanical properties of red mud–based geopolymers. *Transportation research record*. 2167(1), 1-9.

Zhang, H.Y., Kodur, V., ASCE, P.E., Wu, F., Cao, B., Qi, L., Liang, S. (2016). Comparative Thermal and Mechanical Performance of Geopolymers derived from Metakaolin and Fly Ash. *Journal of Materials in Civil Engineering*, 28(2), 1-12.

Zhao, X., Lim, S. K., Tan, C. S., Li, B., Ling, T. C., Huang, R., & Wang, Q. (2015). Properties of foamed mortar prepared with granulated blast-furnace slag. *Materials*, 8(2), 462–473.

Zhou, W., Yan, C., Duan, P., Liu, Y., Zhang, Z., Qiu, X., Li, D. (2016). A comparative study of high- and low-Al2O3 fly ash based-geopolymers: The role of mix proportion factors and curing temperature. *Materials and Design*, 95, 63–74.